NORTHWESTERN UNIVERSITY

Kinetic Modeling of Acrylate Polymerization at High Temperature

A DISSERTATION

SUBMITTED TO THE GRADUATE SCHOOL

IN PARTIAL FULFILLMENT OF THE REQUIREMENTS

for the degree

DOCTOR OF PHILOSOPHY

Field of Chemical and Biological Engineering

By

Xinrui Yu

EVANSTON, ILLINOIS

June 2008

ABSTRACT

Kinetic Modeling of Acrylate Polymerization at High Temperature

Xinrui Yu

The automobile coating industry is undergoing reformation driven by environmental regulations that demand low content of volatile organic compounds. Traditional solvent-borne acrylic resins consisting of high molecular weight polymers that are produced at low temperatures ($<$ 80 °C) need high levels of organic solvent (70%) to be processed as coatings. Alternatively, novel resin compositions consist of acrylic oligomers with multiple crosslinkable functional groups that can undergo reactions on the metal surface. Polymerization at high temperatures ($>$ 120 °C) is an economical approach to produce such pre-polymers. However, higher reaction temperatures can result in secondary reactions that affect oligomeric quality. Given the potential complexity of resin recipes and the diversity of the reactions that can occur during polymerization at high temperatures, it is desirable to have a method that can predict the characteristics of the final product. In particular, methods for predicting rate coefficients for copolymerization and side reactions such as intramolecular hydrogen transfer and scission would be valuable since these quantities are difficult to access experimentally.

In this research, *ab initio* calculations and transition state theory were employed to predict kinetic parameters of reactions relevant to acrylate polymerization. A methodology was developed that was able to handle the complexity of the large systems required to mimic polymeric systems accurately, which includes optimization of structures with many conformational degrees of freedom, selection of an accurate yet efficient level of theory, and treatment of low frequencies. The methodology was successfully applied to determine the propagation kinetic parameters of the homopolymerization of methyl methacrylate and methyl acrylate. The methodology was also ex-

tended to the copolymerization of methyl methacrylate and methyl acrylate and four secondary reactions in methyl acrylate polymerization. Kinetic Monte Carlo (KMC) was employed to predict the molecular weight distribution (MWD), average molecular weight (M_n, M_w) and average degree of branching with the predicted kinetic parameters for methyl acrylate polymerization. To our knowledge, this methodology is the first demonstration of the prediction of kinetic parameters for acrylate polymerization from first principles.

Contents

List of Tables

List of Figures

Chapter 1

Introduction

1.1 Research Motivation

Solvent-borne acrylate resins have been used in the automobile coating industry since the 1950s for their excellent outdoor application properties. Traditional acrylate resins consist of high molecular weight polymers, which need a high content of volatile organic solvent (VOC) (70%) to be processed as coatings (Grady et al. (2002); Reisch (1993)). The coating mechanism is to evaporate the organic solvent so that a firm coating layer can be formed on the metal surface. EPA regulations require that the VOC should be no more than 30% by the year 2010 in order to decrease the pollution caused by the coating process (Adamsons et al. (1998)). Driven by environmental regulations, novel low molecular weight resins with crosslinkable functional groups (hydroxyl, epoxy, etc.) have been unfurled as the new generation of resin coatings (Adamsons et al. (1998); Grady et al. (2002); Peck et al. (2002)). The required VOC can be decreased to 30% since the resins are mainly composed of low molecular weight oligomers. After the coating process, these crosslinkable oligomers can undergo crosslinking reactions on metal surfaces with an added curing agent, such as melamine, to form a firm coating layer.

Acrylate resins are mainly produced via free radical polymerization. The reactions involved are shown in Figure 1.1. The reaction system starts with the decomposition of initiators, which will generate primary radicals. These radicals can continuously add to an unsaturated carbon atom in monomers to form long chain propagating radicals. Termination by combination or disproportionation can occur between radicals so that dead polymers can be formed. The propagation reaction is the main approach to produce long chain polymers from monomers. Besides propagation, polymeric radicals can abstract a hydrogen atom from another species, such as monomer, solvent, or polymer, to form a dead polymer and another radical which is called intermolecular transfer. The propagating radical can also abstract a hydrogen from itself to undergo an intramolecular transfer reaction. If the abstracted hydrogen is from the backbone of a long chain species, a mid-chain radical can be formed. The mid-chain radical can also undergo propagation, and depending on the position of the mid-chain radical, long chain or short chain branches (LCB or SCB) can be formed. At elevated temperatures, mid-chain radicals can also undergo β-scission reactions to break into a smaller radical and an unsaturated polymer.

Transfer, scission and mid-chain propagation are called secondary reactions. The overall effect of these secondary reactions is to restrict radicals from propagating and decrease the molecular weight. Oligomers can be produced by prompting secondary reactions via different approaches. For example, the addition of a chain transfer agent (CTA) can turn propagating radicals into stable species, which is a method that is frequently used to control molecular weight. In the production of acrylate resins, addition of a CTA is not a feasible approach to control the molecular weight since it will increase the cost and introduce impurities in the coating resins so the transparency and weatherability of the coatings will be affected. For example, sulfur-based chain transfer agents such as thiols will decrease the durability of coating layers; cobalt-based chain transfer agents will give the coating resins a reddish color (Grady et al. (2002)).

Increasing the reaction temperature is an alternative way to produce low molecular weight oligomers. At elevated temperatures, transfer and scission reactions become significant (Ahmad

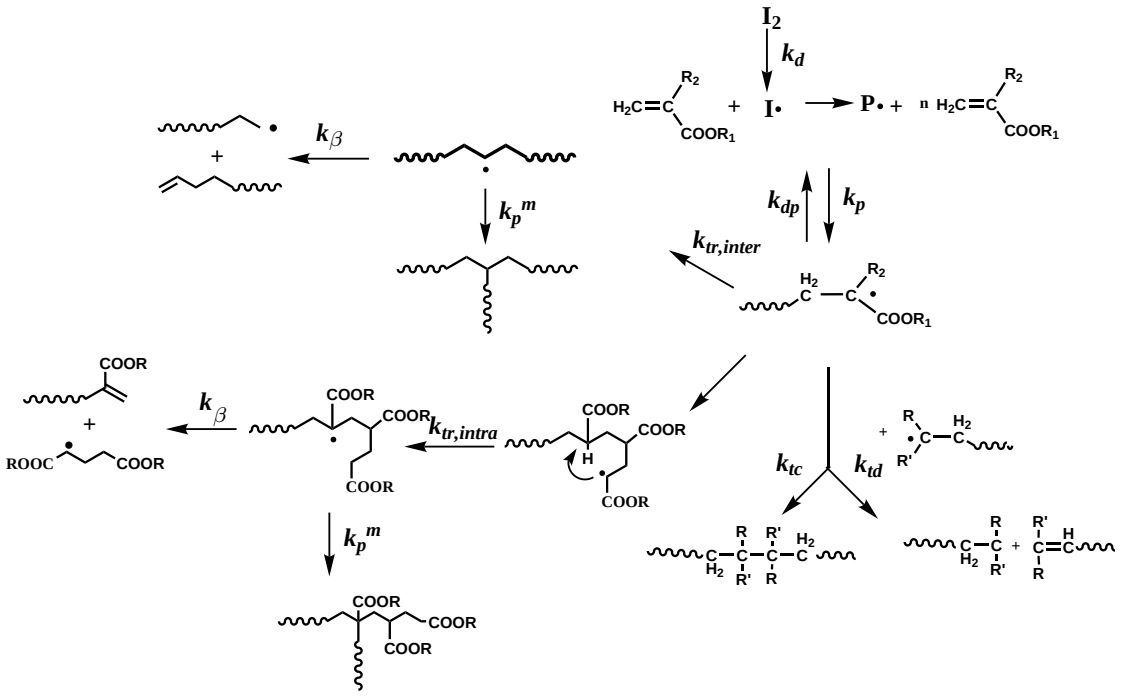

Figure 1.1: Free radical reactions in an acrylate polymerization system, including initiation (k_d), propagation (k_p), termination by combination (k_{tc}), termination by disproportionation (k_{td}), depropagation (k_{dp}), intermolecular transfer ($k_{tr,inter}$), intramolecular transfer ($k_{tr,intra}$), β-scission (k_β) and mid-radical propagation (k_p^m).

et al. (1998); McCord et al. (1997); Plessis et al. (2000)). It requires more accurate process control in order to produce the desired polymer products. For acrylate polymerization, the optimal high temperature range is between 120 °C and 180 °C (Grady et al. (2002)). Producing low molecular weight oligomers using high reaction temperatures can decrease the process cost while minimizing the impurities in the reaction system. However, high temperature makes the reaction system more complex and the process control more difficult. In order to predict the polymer properties, a quantitative description of the polymerization system is important. Accurate modeling of the polymerization system requires both precise kinetic parameters for all the reactions involved and a feasible mathematical algorithm to model the complex reaction system. However, since all these reactions are coupled, measuring kinetic parameters for individual reactions is very difficult. With the advent of some advanced experimental approaches, precise measurement of kinetic parameters becomes practical. Nevertheless, experimental approaches still have restrictions. For example, pulsed laser polymerization in combination with GPC (PLP-SEC) can only measure propagation rate constants (k_p) for limited types of acrylate monomers. PLP-SEC cannot measure the rate coefficients of cross-propagation reactions in copolymerization systems. For secondary reactions, such as transfer and scission, there are no direct experimental measurements available. It is thus critical to have a methodology which can provide accurate kinetic parameters yet not be restricted to certain reaction types.

Because polymerization involves a large number of species, it is infeasible to track the properties of polymers by means of solving ordinary differential equations (ODEs) as done traditionally for small reaction systems. The most frequently used mathematical treatment is the method of moments that lumps variables into manageable subsets. The method of moments can only track average polymer properties, such as average molecular weight and average number of branches per chain. More detailed information, such as the molecular weight distribution, cannot be obtained easily. Although algorithms that have been developed recently, such as the discrete Galerkin finite element method, have afforded some improvements, they are still based on a continuous model.

Thus, it is valuable to have an alternative mathematical algorithm to model the polymerization process. Kinetic Monte Carlo (KMC) is a recent development in the modeling of polymerization processes that is easy to implement and can provide more detailed results.

1.2 Outline of Research

In this research, we have developed a computational approach to calculate the kinetic parameters and thermodynamic properties of the reactions involved in acrylate polymerization. The computational methodology is based on quantum chemistry and transition state theory. The general idea has been used with increasing frequency to determine kinetic parameters, thermodynamic properties and structure-property correlations for small molecules (Irikura (1998), Hehre et al. (1986), Pilar (1990)). The computational methodology is not restricted to any one reaction type and can provide details of reactions which cannot be probed experimentally. The main challenge in applying computational methodology based on quantum chemistry is achieving a balance between computational expense and accuracy. Although higher levels of theory offer more accurate results, it is impractical to apply high-level quantum chemical calculations to all reactions.

Although quantum chemical studies have mostly been applied to small molecule reactions, recent work has extended their application to polymerization reactions. For example, quantum chemistry has been used to investigate propagation of ethylene, vinyl chloride and acrylonitrile (Heuts and Gilbert (1995), Izgorodina and Coote (2006), Van Cauter et al. (2006)). These researchers used similar approaches. For example, relatively low-level methods were used for geometry optimization and several high-level methods were used to calculate the activation energy. For ethylene propagation, Gilbert et al. used HF/3-21G for geometry optimization and QCISD(T)/6-311G(d,p) to determine the activation energy (Heuts and Gilbert (1995)). In another study on ethylene propagation, Van Cauter et al. used density functional theory (B3LYP/6-31G(d)) for geometry optimization and energy evaluation (Van Cauter et al. (2006)). For acrylonitrile and vinyl chloride, Izgorodina

and Coote used B3LYP/6-31G(d) for geometry optimization and various DFT methods (BLYP, B3LYP, MPWB195, BB1K and MPWB1K) and an ONIOM-based method (G3(MP2)-RAD for core, ROMP2/6-311+G(3df,2p) for substituents) were used to calculate activation energies. In the calculation of frequency factors, they all went beyond the rigid-rotor, harmonic oscillator (HO) approximation and treated low frequency modes as internal rotations. In their internal rotation model, the partition functions were all based on energy levels obtained by solving a Schrödinger equation. However, their approaches were also different in some respects. For example, the long chain was modelled as a heavy atom by Gilbert and coworkers. Note that all of these methodologies were applied to small monomers, and there are additional issues that need to be addressed in order to apply a computational approach to acrylate and methyl acrylate polymerization reactions. Nevertheless, the body of previous work provides guidance about the different choices that must be made when quantitatively accurate values of rate coefficients in polymerization are sought. In order to apply a computational methodology to quantify acrylate and methyl acrylate polymerization reactions, there are three problems that need to be solved: geometry optimization, quantum chemistry method/basis set selection and low frequency treatment.

Multiple conformations exist for reactants and products involved in polymerizatoin because of the large number of degrees of freedom. Conventional optimization algorithms typically locate stable conformations based on the change in the energy gradient, which means they can only be used to locate the local minimum corresponding to the initial input. In order to overcome the energy barriers between multiple minima to locate the global minimum, which corresponds to the most stable conformation, the combination of conventional optimization and relaxed potential energy scans for individual rotors defined by all single bonds was performed. Although such a combined method cannot guarantee that the conformation is the global minimum since it neglects interactions between rotations, lower conformations than those located using conventional optimization were indeed found using this approach.

Application of the highest levels of theory is restricted to only small systems with a limited number of electrons. To overcome these limitations, density functional theory (DFT) has been used. DFT has shown to provide a compromise between accuracy and computational expense in various studies of radical reactions (Coote and Davis (1999); Van Cauter et al. (2006); Wong and Radom (1998)). In the work described in this thesis, the B3LYP functional and 6-31G(d) basis set were used for geometry optimization and potential energy scans. However, it was found that the deviation between the calculated and the experimental values of the activation energy was 17 $kJ{\cdot}mol^{-1}$ for methyl methacrylate propagation, which turns into a factor of 500 at 50 °C. Increasing the size of the basis set did not improve the agreement with the experimental data. It was concluded that although B3LYP yielded good results for other polymerization systems such as ethylene, it is not suitable for acrylate and methyl acrylate. Therefore, two new hybrid DFT methods (MPWB1K/6-31G(d,p) and BB1K/6-31G(d,p)) were used to calculate the activation energy. It was found that MPWB1K/6-31G(d,p) yielded activation energy data which were closest to the experimental data for both methyl methacrylate and methyl acrylate propagation.

In the calculation of rate constants and thermodynamic properties, all the motions other than translation and external rotation are traditionally modelled as harmonic oscillators, which has been shown to be a poor assumption for low frequencies which are mainly composed of rotational motions (Coote (2005); Coote and Davis (1999); Heuts and Gilbert (1995); Huang et al. (1998); Izgorodina and Coote (2006)). For large systems such as the ones studied here, there are many low frequencies that are better treated as hindered rotations. In this research, the rotational motions were modelled using a one-dimensional internal rotor model. The energy levels were calculated by solving a one-dimensional Schrödinger equation based on calculated rotational potential functions. The rotational low frequencies were taken out of the partition functions which are based on the harmonic oscillator model and replaced by those calculated with the internal rotor model. Results for methyl methacrylate and methyl acrylate propagation show that treating low frequencies

using a one-dimensional internal rotor model makes the calculated results more consistent with experimental values.

Once the computational methodology was developed, kinetic parameters and thermodynamic properties for the following reactions were calculated: homopolymerization propagation of methyl methacrylate and methyl acrylate, copolymerization reactions of methyl methacrylate-methyl acrylate, and depropagation, 1,5-hydrogen transfer, β-scission, and mid-chain propagation of methyl acrylate.

The homopolymerization propagation reactions of methyl methacrylate and methyl acrylate were chosen as the first research objective because the availability of accurate experimental kinetic parameters measured using PLP-SEC allowed validation of our methodology. The size of the propagating radicals was systematically increased to investigate the dependence of the kinetic parameters on radical chain length. The addition of monomeric, dimeric and trimeric radicals to monomer was studied as shown in Figure 1.2. Rate coefficients were calculated from 298.15 K to 800 K. Kinetic parameters A and E_a were regressed from a plot of ln$k$ versus 1/T. Multiple DFT methods were compared to identify a suitable method/basis combination for obtaining quantitatively accurate results. Potential energy scans were performed for all the rotors defined by single bonds (and the bond defining the transition state for transition state structures). The calculated kinetic parameters were compared with those measured from PLP-SEC. The chain length, quantum chemistry calculation method/basis set and low frequency treatment that best reflected the macroscopic reaction properties were selected. A solvation model (PCM) was also used to evaluate the difference between results calculated in the gas phase and those in the bulk, and it was found that the solvation model only had a slight influence on the calculated kinetic parameters.

Methyl methacrylate-methyl acrylate copolymerization reactions were also studied. Twenty eight reactions with all possible combinations of methyl methacrylate and methyl acrylate units for radical chain length increasing from one to three were investigated as shown in Figure 1.3 (A: methyl methacrylate, B: methyl acrylate). Frequency factors (A) and activation energies (E_a) were

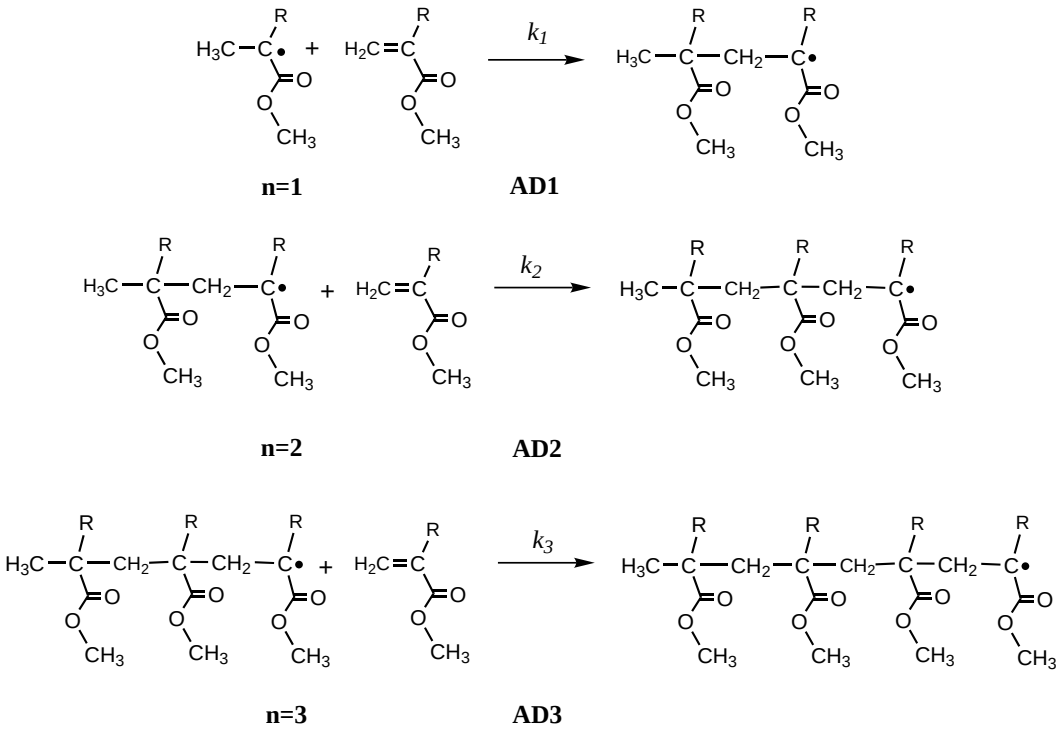

Figure 1.2: Methyl methacrylate and methyl acrylate addition reactions were studied as a function of chain length. ADn is used to denote the different calculations performed, where n is the number of monomeric units in the radical reactant. For methyl methacrylate, R is a CH_3 group, and for methyl acrylate, R is a hydrogen atom.

calculated over a temperature range of 298.15 K to 800 K for these reactions. Heat of reactions (ΔH_r) were also calculated. The monomer reactivity ratios (r_{11}, r_{12}, r_{21}, r_{22} for penultimate model and r_1, r_2 for terminal model) and radical reactivity ratios (s_1 and s_2) were compared with those fitted based on experimental measurements at 23 °C and 1000 bar. The calculated rate constants and ratios were used to predict the composition and overall rate constants at different compositions and compared with experimental data. Furthermore, the quantum chemical calculations allowed the reactivity of methyl methacrylate and methyl acrylate to be explained using frontier orbital theory. It was found that the activation energy correlated with the energy gap between the singly occupied molecular orbital (SOMO) of the radical and the highest occupied molecular orbital (HOMO) of the monomer. In addition, the ability of the classic Evans-Polanyi relationship to capture the activation energy as a function of heat of reaction was assessed.

Four secondary reactions for methyl acrylate polymerization, depropagation, 1,5-hydrogen transfer, mid-chain radical propagation and β-scission, were studied. It was found that local minima must be accessed first to effect the 1,5-hydrogen transfer, and these conformations, which are obtained through facile rotations, were assumed to be in equilibrium with the global minimum. The chain length dependence of the calculated value of the rate coefficient for 1,5-hydrogen transfer was also investigated. Tunneling coefficients, which are important for hydrogen transfer reactions, were calculated using four approximations including small curvature tunneling (SCT), zero curvature tunneling (ZCT), Eckart and Wigner. Mid-chain radical propagation and two possible β-scission paths were also investigated.

Using all of the calculated values of the rate coefficients, polymerization of methyl acrylate was simulated using kinetic Monte Carlo (KMC). Initiation, propagation, termination, depropagation, 1,5-hydrogen transfer, mid-chain radical propagation and β-scission of methyl acrylate were included. The average molecular weight (M_n, M_w), the full molecular weight distribution (MWD) and the degree of branching were tracked.

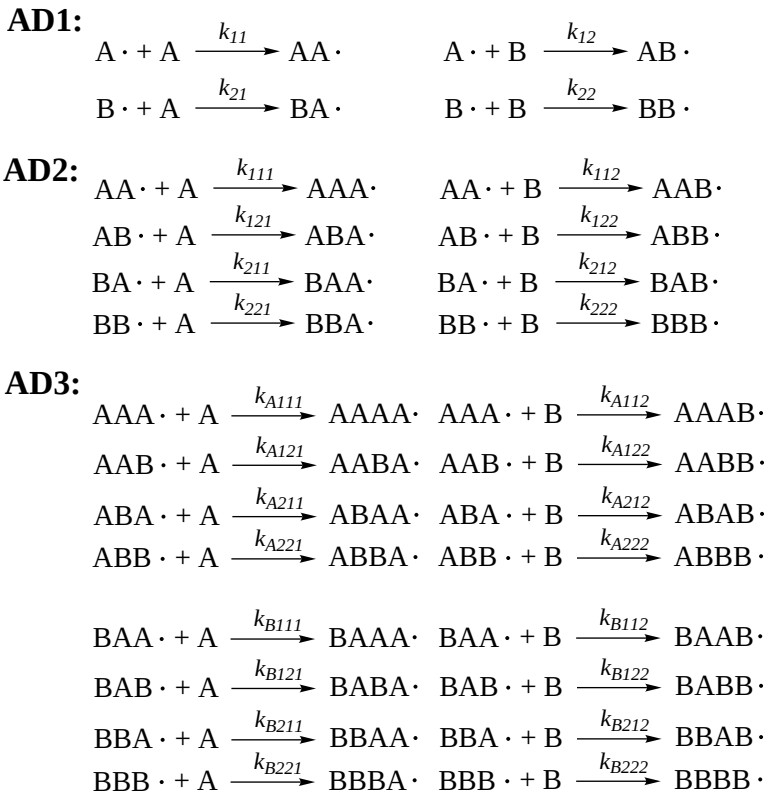

Figure 1.3: Methyl methacrylate and methyl acrylate copolymerization reactions, A: methyl methacrylate, B: methyl acrylate.

Chapter 2

Background

Acrylate resins have been used in the automobile coating industry since the 1950s for their transparency and weatherability. The general formula of an acrylate monomer is shown in Figure 2.1. Acrylate resins have undergone a transition in terms of their desired structures and the mechanism by which coating is carried out. Initially, the resin products were mainly composed of high molecular weight polymers (molecular weight $>$ 100,000). The polymerization was carried out at low temperature ($<$ 80 °C). High levels of organic solvent (70%) are needed to be used to keep the solution viscosity low enough for the coating process. The coating layer was formed by evaporating the organic solvent. In order to reduce the pollution caused by organic solvents, North American regulations on volatile organic content (VOC) of coatings requires the VOC to be no more than 30% by the year 2010. Thus, the development of a new generation of resins has been driven by environmental regulations. In the application of new acrylate resins, polymerization happens in two steps: the production of polymer resins and the formation of the coating layer. Acrylate resins are mainly composed of low molecular weight oligomers ($<$ 10,000). Crosslinkable functional groups, such as hydroxyl and epoxy groups, are introduced to the polymer chains. The oligomeric resins need low solvent content ($<$ 30%) to decrease the viscosity. After the coating process, with an added multi-functional curing agent, such as melamine, the oligomer chains can undergo conden-

sation polymerization reactions to form a firm polymer coating layer on metal surfaces (Adamsons et al. (1998); Grady et al. (2002)). Such polymers which need two polymerization steps are called prepolymers.

The production of oligomeric acrylate resins is mainly via free radical polymerization, as shown in Figure 1.1. The molecular weight of polymers can be controlled by means of termination and transfer. Termination reactions offer few handles for control since the reaction rate is high and typically diffusion controlled. Transfer reactions are frequently used in several ways to control the molecular weight; for example, increasing the content of initiator, addition of chain transfer agents and increasing the reaction temperature all favor transfer reactions (Odian (2004)). However, increasing the initiator content and using chain transfer agents will increase the product cost, and the use of chain transfer agents will introduce impurities into the resins which will affect the coating quality (Grady et al. (2002)). The most economical way to control molecular weight is to polymerize at elevated temperature ($> 120\ ^{\circ}$C), which prompts secondary reactions such as transfer and scission. This method also has drawbacks in that it increases the energy consumption and the promotion of secondary reactions makes the product control more difficult, which requires more elaborate process design and safety controls. Nevertheless, polymerization at high temperature is the most attractive approach to produce low molecular weight polymers. The practical high temperature range for acrylate polymerization is 120-180 $^{\circ}$C (Grady et al. (2002)).

Polymerization at high temperature results in a more complex reaction system, and thus quality control is more difficult. Modeling can thus play a crucial role. In order to model the polymerization system properly to predict the polymer properties, such as average molecular weight (M_n, M_w), molecular weight distribution and compositions of copolymers, understanding the reaction mechanism and specification of accurate kinetic parameters are critical. However, coupling of the polymerization reactions makes the measurement of rate constants for individual reactions very difficult. The measurement of accurate values of propagation rate coefficients was not achieved until the advent of advanced experimental technologies, such as pulsed laser polymerization in

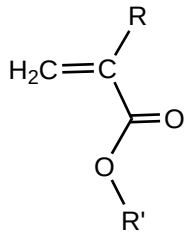

Figure 2.1: Acrylate monomer general formula.

combination with size exclusion chromatography (PLP-SEC). PLP-SEC provides accurate kinetic parameters and has been recommended by IUPAC as the standard measurement for free radical propagation rate constants. PLP-SEC requires that transfer reactions are negligible on the time scale of the pulse interval, which makes it feasible only for a limited number of acrylate monomers. Although the existence of secondary reactions, such as transfer and mid-chain radical propagation, has been verified with electron spin resonance (ESR) and nuclear magnetic resonance (NMR), measuring accurate rate constants for these reactions experimentally is still infeasible. Determination of kinetic parameters for polymerization reactions has become a bottleneck for the advancement of polymerization modeling research. In this research, quantum chemistry and transition state theory have been used to determine kinetic parameters for homopolymerization of methyl methacrylate and methyl acrylate, propagation rate constants for methyl methacrylate-methyl acrylate copolymerization, and depropagation, intramolecular transfer, β-scission and mid-chain radical propagation for methyl acrylate.

The following sections will introduce the relevant background knowledge for this research, including the mechanism of free radical polymerization, copolymerization, experimental measurements, mathematical models for free radical polymerization, quantum chemistry and transition state theory and microscopic factors that influence the activation energy.

2.1 Free Radical Polymerization

Free radical polymerization is one of the most important processes to produce high molecular weight polymers. It can be used for almost all vinyl-based monomers to produce both homopolymers and copolymers. In free radical polymerization, the chain starts with the primary radicals generated from the initiator and grows rapidly by continuously reacting with monomers to form high molecular weight polymers at low monomer conversion.

Initiation

The primary radicals are generated by thermal or photochemical cleavage of covalent bonds. The most commonly used initiators include azo and peroxy compounds, such as 2,2-azobisisobutyronitrile (AIBN) and benzoyl peroxide (BPO). The initiation rate is shown in Equation 2.1:

$$r_d = 2fk_d[I_2] \tag{2.1}$$

in which f is the decomposition efficiency which is normally in the range of $0.4-0.9$. Initiation is typically a first-order reaction. Activation energies for the thermal homolysis of peroxide and azo initiators are in the range of 100-150 kJ·mol^{-1} and representative initiation rate coefficients (k_d (s^{-1})) at normal polymerization conditions are in the range of $10^{-6} - 10^{-4}$ (Meyer and Keurentjes (2005)). Initiation is the only reaction in which initiator participates so the measurement of the reaction rate constant is relatively easy. The concentration of initiator can be monitored with equipment such as infrared spectroscopy. AIBN and BPO can decompose under both thermal and photo irradiation conditions. Some special initiators which are only sensitive to photo irradiation at a specific wave length need to be used in PLP-SEC experiments, such as 2,2-dimethoxy-2-phenylacetophenone (DMPA).

Propagation

The primary radical generated from initiation adds to unsaturated monomer to form a propagating radical, which can continuously add to monomers so that long chain radicals can be formed, as

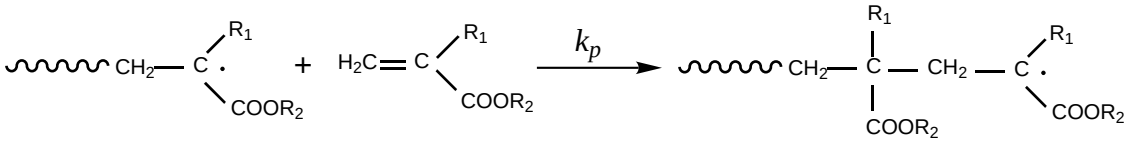

Figure 2.2: Acrylate propagation.

shown in Figure 2.2. Propagation is a second order reaction, and the rate is expressed as in Equation 2.2.

$$R_p = k_p[P\cdot][M] \tag{2.2}$$

The measurement of accurate propagation kinetic parameters (A, E_a) is feasible with the advent of PLP-SEC. It is also known that the propagation rate coefficient is pressure-dependent with a negative activation volume ($\Delta V^{\#}$). Pressure increases cause an increase in the k_p values. The relationship between the rate coefficient and pressure is expressed in Equation 2.3.

$$\frac{dlnk_p}{dp} = -\frac{\Delta V^{\#}}{RT} \tag{2.3}$$

Kinetic parameters for acrylate and methacrylate monomers are listed in Table 2.1. It can be seen that all methacrylate monomers have similar activation energies (21.0 $-$ 23.4 kJ·mol^{-1}) and frequency factors (2.67 $-$ 8.89$\times 10^6$ L·mol^{-1}·s^{-1}). Acrylate monomers also have similar activation energies (17.0 $-$ 17.7 kJ·mol^{-1}) and frequency factors (1.66 $-$ 1.81$\times 10^7$ L·mol^{-1}·s^{-1}). The activation volumes for methacrylate monomers vary from -16.0 $-$ -16.7 cm^3·mol^{-1}, and the activation volumes for acrylate monomers center around -11.7 cm^3·mol^{-1}. Comparison of activation energies shows that the substituent on the α- carbon has much more influence than that on the ester group; for example, for the same ester substituent, the methacrylate has an activation energy that is 4 kJ·mol^{-1} higher than the corresponding acrylate.

Table 2.1: Kinetic parameters for acrylate monomers determined by PLP-SEC (Brandrup et al. (1999); Meyer and Keurentjes (2005)).

Monomer	E_a (kJ·mol^{-1})	$\Delta V^{\#}$ (cm^3·mol^{-1})	A (L·mol^{-1}·s^{-1})
Methyl methacrylate	22.4	-16.7	2.67×10^6
Ethyl methacrylate	23.4		4.07×10^6
Butyl methacrylate	22.9	-16.5	3.78×10^6
Dodecyl methacrylate	21.0	-16.0	2.50×10^6
2-Hydroxyethyl methacrylate	21.9		8.89×10^6
Methyl acrylate	17.7	-11.7	1.66×10^7
Butyl acrylate	17.4		1.81×10^7
Dodecyl acrylate	17.0	-11.7	1.79×10^7

The influence of solvents on the propagation rate coefficients has been examined through extensive studies, and it is concluded that there is little influence of solvent on propagation rate coefficients. Thus, propagation is often treated as chemically controlled up to high conversion values (80%) in typical polymerization modeling (Brandrup et al. (1999)). However, there are not exact cut-off conversion values for the transition from chemical control to diffusion control for different polymeric structures and operating conditions.

The addition reaction of a radical to a monomer is a reversible reaction. Depropagation becomes significant at elevated temperatures. The temperature at which the propagation and depropagation rates are equal is called the ceiling temperature T_c. For a given monomer concentration, $[M]$, T_c is calculated as in Equation 2.4:

$$T_c = \frac{\Delta H_p}{\Delta S_p + Rln[M]} \tag{2.4}$$

The typical heat of polymerization ΔH_p for acrylate monomers is in the range of -50 $-$ -80 kJ·mol^{-1} (Meyer and Keurentjes (2005)). ΔS_p is hard to measure, but a representative value is -120 J·mol^{-1}·K^{-1}. The ceiling temperature for methyl methacrylate (ΔH_p=-56 kJ·mol^{-1}) at a concentration of 1 mol·L^{-1} is 194 °C. The ceiling temperature for methyl acrylate (ΔH_p=-80 kJ·mol^{-1}) at a concentration of 1 mol·L^{-1} is 394 °C.

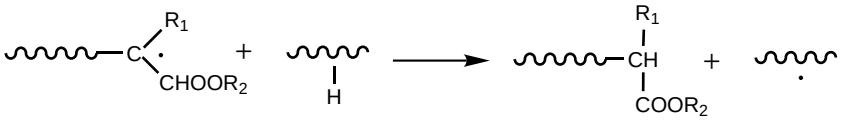

Figure 2.3: Acrylate intermolecular transfer reaction.

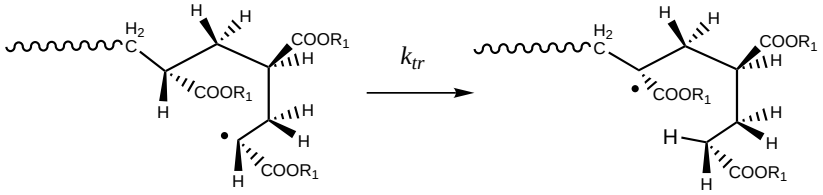

Figure 2.4: Acrylate intramolecular transfer reaction.

Transfer

The propagating radical can abstract a hydrogen or halogen atom from any another species, including monomer, solvent, long chain radicals or dead polymers to transfer the radical center. The transfer constant (C_{tr}), which is the ratio of the transfer rate constant and the propagation rate constant (k_{tr}/k_p), is used to indicate the relative extent of transfer reactions.

Transfer occurring between radicals and other species is called intermolecular transfer which is shown in Figure 2.3. The transfer products are dead polymer and a new radical. Transfer reactions can also happen within polymeric radicals which is called intramolecular transfer. The most common intramolecular transfer in acrylate polymerization is 1,5-hydrogen transfer, which is shown in Figure 2.4.

The mid-chain radical produced by transfer to the middle of a polymer chain can undergo propagation with monomers, which is called mid-chain radical propagation. The first addition step, which is the transition from a tertiary carbon radical to a secondary carbon radical, has a lower propagation rate coefficient than that for the end-chain radicals. In this research, the first addition reaction of mid-chain radical propagation is thus treated separately. The secondary radical that is

generated is treated the same as an end-chain radical. Depending on the position of the radical, mid-chain propagation yields short-chain branching (SCB) or long-chain branching (LCB).

The activation energies for transfer reactions (E_{tr}) are usually higher than the activation energies (E_p) for propagation; for example, the typical ($E_{tr}^{mon} - E_p$) is in the range of $10 - 40$ kJ·mol^{-1} (Meyer and Keurentjes (2005)). Thus, transfer reactions can be suppressed by decreasing the reaction temperature. PLP-SEC is usually carried out at low temperatures, thereby eliminating interference from transfer reactions. Transfer reactions can be used to control molecular weight. For example, a small amount of chain transfer agent (CTA) can be added to control the molecular weight of polymers.

Scission

Besides mid-chain propagation, mid-chain radicals formed by intra- or intermolecular transfer to polymer can undergo $\beta-$scission as shown in Figure 2.6 to yield short chain radicals and unsaturated dead polymer. Besides lowering polymer molecular weight, β-scission can also produce unsaturated long chains. β-scission is more strongly activated by temperature than hydrogen transfer so it becomes important only at high temperatures. For example, β-scission for butyl acrylate becomes significant when temperature is higher than 140 °C (Chiefari et al. (1999); Grady et al. (2002)). Kinetic coefficients for scission reactions can only be determined based on modeling in concert with the measurement of quaternary carbons and unsaturated terminal groups by NMR.

Termination

Termination between two radicals can proceed by combination or disproportionation. The termination form directly influences the polymer molecular weight and polydispersity index (PDI). Termination by combination results in a narrower PDI. If all termination reactions involve combination of two radicals, the PDI equals 1.5; if all termination reactions are in the form of disproportionation, the PDI equals 2.0. The ratio of the disproportionation rate to the total termination rate is

Table 2.2: Kinetic parameters for acrylate termination reactions (Brandrup et al. (1999)).

Monomer	E_t (kJ·mol^{-1})	A (L·mol^{-1}·s^{-1})	k_t at 50 °C, 1 atm (L·mol^{-1}·s^{-1})
Methyl methacrylate	4.1	4.3×10^{8}	9.4×10^{7}
Butyl methacrylate	4.1	8.5×10^{7}	1.9×10^{7}
Dodecyl methacrylate	4.1	2.8×10^{7}	6.2×10^{6}
Methyl acrylate	6.7	6.0×10^{9}	5.1×10^{8}
Butyl acrylate	4.0	5.1×10^{8}	1.2×10^{8}
Dodecyl acrylate	1.7	2.1×10^{7}	1.1×10^{7}

expressed in Equation 2.5:

$$\delta = \frac{k_{td}}{k_{td} + k_{tc}} \tag{2.5}$$

For methacrylate monomers, δ is within the range of $0.5 - 0.8$; for acrylate monomers, δ is within the range of $0.05 - 0.2$ (Moad and Solomon (1995)).

The single-pulse-pulsed laser polymerization (SP-PLP) can be used to measure termination rate coefficients (k_t). SP-PLP measurement is used in combination with infrared or near-infrared spectroscopic measurements of monomer conversion induced by a single laser pulse. Kinetic parameters for acrylate and methacrylate termination reactions are shown in Table 2.2. The termination rate constant is usually higher than 10^7 L·mol^{-1}·s^{-1} and is often treated as diffusion controlled. Thus, termination is not only influenced by the reaction conditions, but also by the viscosity of the reaction system. Diffusion control depends on both chain diffusion and segment diffusion. The dependence of k_t on system viscosity is very complex, especially for systems including branching reactions. The rate constant can decrease by several orders of magnitude with monomer conversion. In kinetic modeling, only at very low conversion values (20%), k_t can be treated as a constant.

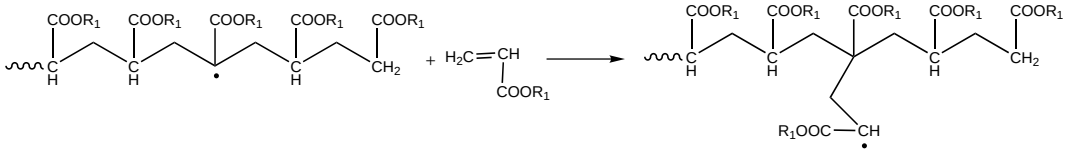

Figure 2.5: Propagation of acrylate mid-chain radical.

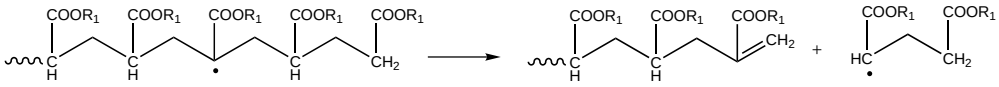

Figure 2.6: β-scission of acrylate mid-chain radical.

2.2 Copolymerization

Copolymerization is one of the most commonly used approaches to produce polymers which combine the application properties from their parent polymers. Diverse application properties can be achieved in the form of copolymers. For example, the adhesive and cohesive properties of acrylate coating resins can be balanced by controlling the proportions of monomers in the recipe (Meyer and Keurentjes (2005)). Different monomers in the reaction system have different reactivities, which makes the chain growth dependent on both the monomer and radical species. The propagation rate determines both the conversion rate of monomers and composition of polymer products.

In order to model the polymerization process and predict the product properties, accurate kinetic parameters for these reactions are critical. The rate constant depends on the reactive units in both the radical and the monomer. However, PLP-SEC can only be used to measure the overall propagation rate constant ($k_{p,copo}$). No experimental measurements are available for the rate constants of all the reactions between various radicals and monomers.

Extracting quantitative information about copolymerization kinetics is largely based on modeling. Modeling is used to investigate two basic aspects of copolymerization: the overall rate constant ($k_{p,copo}$) and polymer composition (F) at different monomer compositions (f). Depending on

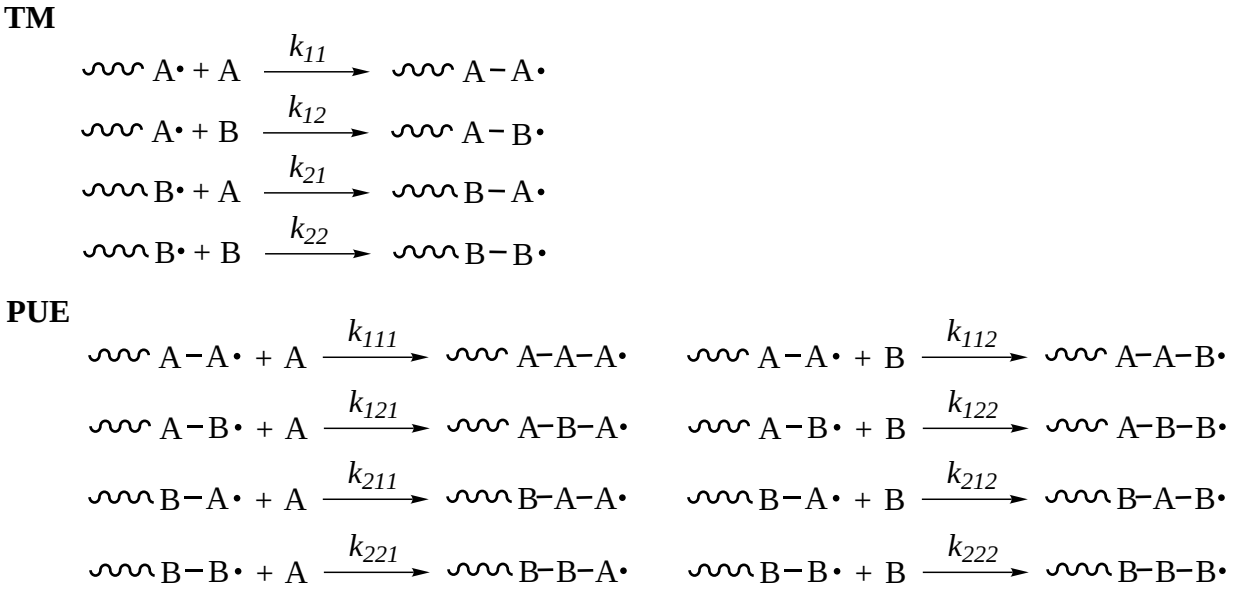

Figure 2.7: Terminal model (TM) and penultimate effect (PUE) model of binary copolymerization.

the active units of the propagating radicals, copolymerization has been modelled according to the terminal unit model (TM), in which the radicals are divided into two types based on the terminal unit, and the penultimate unit model (PUE), in which radicals are divided into four types based on both the terminal and penultimate units. Four addition reactions are included in the terminal model as shown in Figure 2.7. Two reactivity ratios are defined as shown below:

$$r_1 = \frac{k_{11}}{k_{12}} \quad r_2 = \frac{k_{22}}{k_{21}}$$

With these two ratios and the homopolymerization rate constants (k_{11} and k_{22}), the overall rate constant ($k_{p,copo}$) at different monomer compositions (f) is expressed in Equation 2.6.

$$k_{p,copo} = \frac{r_1 f_1^2 + 2 f_1 f_2 + r_2 f_2^2}{(r_1 f_1 / k_{11}) + (r_2 f_2 / k_{22})} \tag{2.6}$$

The instantaneous component fraction in the polymer product at different monomer compositions can be calculated via the Mayo-Lewis equation as shown in Equation 2.7:

$$F_1 = \frac{r_1 f_1^2 + f_1 f_2}{r_1 f_1^2 + 2 f_1 f_2 + r_2 f_2^2} \tag{2.7}$$

Fukuda et al. found that in some cases, the reactivity ratios fitted from $k_{p,copo}$ and composition do not match, which was attributed to the neglect of effects of the penultimate units on the reactivity of the propagating radicals (Fukuda et al. (1985)). The penultimate unit effect (PUE) model, which includes the influence of both the terminal and the penultimate units on the radical chains, was thus proposed. The relevant reactions and rate coefficients increase to eight, which are shown in Figure 2.7. Four monomer reactivity ratios (r_{ij}) and two radical reactivity ratios (s_i) are defined:

$$r_{11} = \frac{k_{111}}{k_{112}}, \quad r_{12} = \frac{k_{122}}{k_{121}}, \quad r_{22} = \frac{k_{222}}{k_{221}}, \quad r_{21} = \frac{k_{211}}{k_{212}}, \quad s_1 = \frac{k_{211}}{k_{111}}, \quad s_2 = \frac{k_{122}}{k_{222}}$$

The overall propagation rate constant $k_{p,copo}$ and polymer composition (F) are expressed as in Equations 2.8 and 2.9, respectively.

$$k_{p,copo} = \frac{\bar{r}_1 f_1^2 + 2 f_1 f_2 + \bar{r}_2 f_2^2}{(\bar{r}_1 f_1 / \bar{k}_{11}) + (\bar{r}_2 f_2 / \bar{k}_{22})} \tag{2.8}$$

$$F_1 = \frac{\bar{r}_1 f_1^2 + f_1 f_2}{\bar{r}_1 f_1^2 + 2 f_1 f_2 + \bar{r}_2 f_2^2} \tag{2.9}$$

The average reactivity ratios and rate constants are defined in Equation 2.10.

$$\bar{r}_i = r_{ji} \frac{r_{ii} f_i + f_j}{r_{ji} f_i + f_j} \quad \bar{k}_{ii} = k_{iii} \frac{r_{ii} f_i + f_i}{r_{ii} f_i + f_j / s_i} \tag{2.10}$$

The PUE model including six ratios (r_{11}, r_{12}, r_{22}, r_{21}, s_1 and s_2) is called the explicit penultimate unit effect (EPUE) model. A simplified PUE model with four ratios (r_1, r_2, s_1 and s_2) is called the implicit penultimate effect (IPUE) model. In the IPUE model, it is assumed that $r_{11} \approx r_{21} \approx r_1$ and $r_{22} \approx r_{12} \approx r_2$ (Buback and Müller (2007); Fukuda et al. (1985)). In most cases, the IPUE model yields satisfactory results for both the rate constant and composition (Coote and Davis (1999); Hutchinson et al. (1997); Madruga and Fernandez-Garcia (1996)), and the EPUE model does not provide significantly better results than the IPUE model.

Buback et al. measured the rate coefficients ($k_{p,copo}$) for methyl methacrylate (MMA)-methyl acrylate (MA), dodecyl methacrylate (DMA)-MA, MMA-dodecyl acrylate (DA) and DMA-DA

bulk copolymerization via PLP-SEC at ambient temperature and 1000 bar. The monomer conversion was monitored via NIR spectroscopy in the 6000 $-$ 6300 cm^{-1} range. Both the TM and PUE models were used to fit the reactivity ratios. For MMA-MA copolymerization, the following results were provided (Buback and Müller (2007)):

(A) TM based on $F_{MMA} - f_{MMA}$ data: r_{MMA}=3.03, r_{MA}=0.20

(B) TM based on $k_{p,copo}$ measurements: r_{MMA}=1.95, r_{MA}=0.21

(C) IPUE fit: r_{MMA}=2.40, r_{MA} =0.18, s_{MMA} =1.46, s_{MA} =0.38, $k_{p,MMA}$ =702 L·mol^{-1}·s^{-1}, $k_{p,MA}$ =18,088 L·mol^{-1}·s^{-1}

Although the TM and PUE models have been widely used in the study of copolymerization, these two models are both based on the ratios of rate constants and the derivations are based on the steady state assumption. Neither of them can be used to determine the kinetic parameters (E_a and A) for an individual reaction. In PLP-SEC measurements, secondary reactions like transfer need to be suppressed, so PLP-SEC experiments can only be carried out at low temperatures. To measure the required parameters over a wide temperature range is infeasible.

2.3 Experimental Measurements for Kinetic Parameters

Direct measurement of kinetic parameters for free radical polymerization reactions is very limited. The most frequently used experimental approach to measure propagation rate constants is pulsed laser polymerization in combination with size exclusive chromatography (PLP-SEC). Under the irradiation of a pulsed laser, photoinitiators decompose to generate radicals, which can undergo propagation. Most of the propagating radicals are terminated with the newly generated radicals at the successive irradiation. The probability for a propagating radical to survive decreases with the irradiation time. Thus, the chain length of the polymer produced is discretized. The majority of

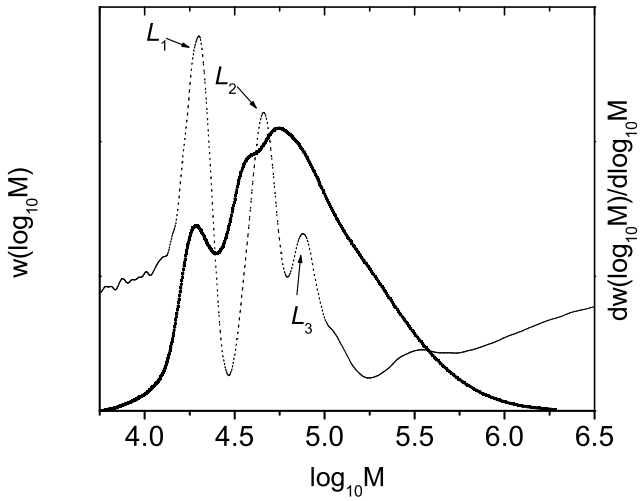

Figure 2.8: Experimental MWD (solid line) of p-acetoxystyrene produced at 40 °C, 1 atm using a pulse repetition rate of 20 Hz. The first derivative of the MWD is given as the dashed line. The inflection points (L_1, L_2 and L_3) correspond to the polymer chains growing within one, two and three pulse intervals.

polymers are derived from those radicals that existed for one time interval between laser pulses. The polymer chain length can be measured with SEC, and the chain length is determined by the peaks of the first derivative of the distribution curve, as shown in Figure 2.8. The propagation rate coefficient (k_p) can be determined using Equation 2.11. PLP-SEC is carried out at very low conversions of monomer ($< 5\%$) so $[M]$ can be treated as a constant.

$$L_2 - L_1 = k_p \cdot [M] \cdot t_0 \tag{2.11}$$

In order to eliminate thermal initiation, photoinitiators which are only sensitive to irradiation, such as 2,2-dimethoxy-2-phenylacetophenone (DMPA), are used. PLP-SEC requires that the chain termination only be controlled by pulses, so for those systems in which transfer reactions are significant, PLP-SEC cannot be used. In order to suppress transfer reactions, PLP-SEC is usually carried out at low temperature. For example, PLP-SEC for methyl acrylate can only be carried out lower than 30 °C. Another approach is to increase the laser frequency so that the pulse interval is

shorter than the time scale for transfer reactions. If neither of these two approaches eliminates the influence of transfer reactions, PLP-SEC cannot be used. Because the measurement is reliable, k_p measured by PLP-SEC is used as a benchmark to verify other methodologies.

In copolymerization systems, PLP-SEC can also be used. Only the overall propagation rate coefficients ($k_{p,copo}$) can be measured. By tracking the monomer concentration changes using measurements which are sensitive to a specific functional group or carbon structure, such as infrared (IR), near infrared (NIR) and NMR, the composition in the polymer product (F) at different monomer compositions (f) can be obtained. The monomer reactivity ratios and radical reactivity ratios can be fitted based on the Mayo-Lewis plot and overall rate constants.

Because quaternary carbons can be generated via transfer and mid-chain radical propagation, ^{13}C NMR is frequently used to monitor branching based on the resonance at $47.6 - 48.6$ ppm arising from the quaternary carbon of the branch point (Ahmad et al. (1998)). The concentration of branch points can be determined, which can be used in combination with models to estimate transfer rate constants.

Small fragments produced by β-scission reactions can be captured by mass spectroscopy so that scission reaction paths can be investigated. Hutchinson et al. studied β-scission of n-butyl acrylate by monitoring the intramolecular transfer product using electrospray ionization-Fourier transform mass spectrometry (ESI-FTMS) (Grady et al. (2002); Peck et al. (2002)).

In general, NMR, ESI/FTMS and other measurements such as ESR can validate the existence of secondary reactions and provide quantitative data for modeling analysis. However, none of these measurements can be used to determine kinetic parameters independently.

2.4 Mathematical Modeling of Polymerization Processes

Mathematical modeling can be used to help to understand the polymerization process and predict the polymer properties at different operating conditions, which can be used to optimize the poly-

merization process. Because of the complexity of the polymerization system, it is challenging to develop detailed models of the polymerization process. Nonetheless, the sophistication of mathematical models is increasing, and they are becoming more and more important in the study of polymerization. Because of the large number of chain lengths and functionalities that are relevant in polymerization modeling, it is infeasible to develop explicit continuum models. The method of moments, discrete Galerkin finite element models and kinetic Monte Carlo (KMC) offer attractive and manageable alternatives. In this research, kinetic Monte Carlo was used to model homopolymerization of methyl acrylate, which includes initiation, propagation, intramolecular transfer, mid-chain radical propagation and $\beta-$scission reactions. The average molecular weight (M_n, M_w), molecular weight distribution and average number of branches per chain were tracked.

Method of Moments

The method of moments decreases the dimensionality of a mathematical model of polymerization by reducing the number of equations through definition of the principal moments of the various distributions. The moments can be related to measurable quantities. For example, the zeroth moment of dead polymer is the total concentration of polymers; the first moment of dead polymer is the concentration of monomer units in all dead polymers (Dotson et al. (1996)). The k-th order moments are expressed as follows:

$$\mu_k = \sum_{n=1}^{\infty} n^k D_n \tag{2.12}$$

where D_n is the concentration of dead polymer of chain length n. The number average molecular weight and weight average molecular weight are calculated as follows:

$$M_n = \frac{\mu_1}{\mu_0} \tag{2.13}$$

$$M_w = \frac{\mu_2}{\mu_1} \tag{2.14}$$

The equations for the moments are derived from the population balance equations of radicals and dead polymer. For a system including initiation, propagation, termination (combination and

disproportionation) and transfer to polymer, the radical (P_n) and dead polymer (D_n) balance equations are written as (Meyer and Keurentjes (2005)):

$$\frac{dP_n}{dt} = 2fk_dI\delta(n-1) + k_pM(P_{n-1} - P_n) + k_{tr}^{pol}nD_n\sum_{j=1}^{\infty}P_j - k_{tr}^{pol}P_n\sum_{j=1}^{\infty}jD_j - (k_{tc}+k_{td})\sum_{j=1}^{\infty}P_jP_n$$

$$\frac{dD_n}{dt} = k_{td}\sum_{j=1}^{\infty}P_jP_n + \frac{1}{2}k_{tc}\sum_{j=1}^{n-1}P_jP_{n-j} - k_{tr}^{pol}nD_n\sum_{j=1}^{\infty}P_j + k_{tr}^{pol}P_n\sum_{j=1}^{\infty}jD_j$$

The rates of change of the zeroth, first and second moments of the radicals are derived as follows:

$$\frac{d\mu^P}{dt} = 2fk_dI - (k_{td}+k_{tc})(\mu^P)^2$$
$$\frac{d\mu^P}{dt} = 2fk_dI + k_pM\mu_0^P - (k_{td}+k_{tc})\mu_0^P\mu_1^P + k_{tr}^{pol}(\mu_0^P\mu_2^D - \mu_1^P\mu_1^D)$$
$$\frac{d\mu^P}{dt} = 2fk_dI + k_pM(\mu_0^R + 2\mu_1^P) - (k_{td}+k_{tc})\mu_0^P\mu_2^P + k_{tr}^{pol}(\mu_0^P\mu_3^D - \mu_2^P\mu_1^D)$$

The rates of change of the zeroth, first and second moments of dead polymer are derived as follows:

$$\frac{d\mu_0^D}{dt} = k_{td}(\mu_0^P)^2 + \frac{1}{2}k_{tc}\mu_0^P$$
$$\frac{d\mu_1^D}{dt} = (k_{td}+k_{tc})\mu_0^P\mu_1^P + k_{tr}^{pol}(\mu_1^P\mu_1^D - \mu_0^P\mu_2^D)$$
$$\frac{d\mu_2^D}{dt} = (k_{td}+k_{tc})\mu_0^P\mu_2^P + k_{tc}(\mu_1^P)^2 + k_{tr}^{pol}(\mu_2^P\mu_1^D - \mu_0^P\mu_3^D)$$

The third moment, μ_3^D, can be represented by a truncated series of Laguerre polynomials (Hulburt and Katz (1964)).

$$\mu_3^D = \frac{\mu_2^D}{\mu_0^D\mu_1^D}(2\mu_0^D\mu_2^D - (\mu_1^D)^2)$$

The major limitation of the method of moments is that it can only be used to track average quantities. More detailed information such as molecular weight distribution cannot be provided, unless a form of the distribution, such as the Schultz or Wesslau distribution, is assumed (Kruse et al. (2003)).

Kinetic Monte Carlo

Kinetic Monte Carlo is the stochastic simulation of a reaction system based on the probability for a reaction to happen (Gillespie (1977)). This method has been used in polymerization research to a limited extent and has primarily been used to predict relative branch contents rather than actual kinetics (Al-Harthi et al. (2006); Tobita (1996, 2006)).

In KMC modeling, a control volume (V) which contains a manageable number of reactant particles is used as the calculation basis. The number of particles in the control volume is calculated as Equation 2.15:

$$X_m = [M] N_A V \tag{2.15}$$

where N_A is Avogadro's number and $[M]$ is the concentration. Larger control volumes mean longer computational times while providing more accurate results. As the control volume is increased, an asymptotic limit is reached, and thus, it is imperative that the minimum control volume at which the calculated values are converged be identified. Rate constants, which are based on the continuum variable of concentration, need to be converted to be based on the change of particle number. For example, for initiation, propagation and termination rate constants, the corresponding KMC rate constants are shown in Equations 2.16, 2.17 and 2.18.

$$k_d^{KMC} = k_d \tag{2.16}$$

$$k_p^{KMC} = \frac{k_p}{N_A V} \tag{2.17}$$

$$k_t^{KMC} = \frac{2k_t}{N_A V} \tag{2.18}$$

The probability for a reaction i to happen at a given time is calculated as the ratio of the rate of reaction i to the total reaction rate.

$$p_i = \frac{R_i}{\sum R_i} \tag{2.19}$$

In KMC, at each time, only one reaction is selected to proceed. The choice of the reaction is based on a random number which falls into a region set by the reaction probability of reaction m:

$$\sum_{i=1}^{m-1} p_i < r_1 < \sum_{i=1}^{m} p_i \tag{2.20}$$

Once the reaction is complete, the time interval for the reaction to proceed is determined using another random number, r_2, in the interval of [0,1]. The time interval τ is calculated as:

$$\tau = \frac{1}{\sum R_i} ln(\frac{1}{r_2}) \tag{2.21}$$

The advantage of KMC is that each species is constructed explicitly. Thus, the complex structure of polymer chains, such as multiple degrees of branching, can be represented seamlessly. The full molecular weight distribution can be tracked without any assumptions about its form.

2.5 Quantum Chemistry and Transition State Theory

Quantum chemistry has become a powerful tool for the study of kinetics to discover the reaction mechanism and predict kinetic parameters as a substitute for experimental approaches. Quantum chemistry can provide details about reactions which are difficult if not impossible to isolate using experimental approaches. In quantum chemistry, the energy levels are determined by solving the Schrödinger equation based on the atomic coordinates. The Schrödinger equation, $\hat{H}\Psi = E\Psi$, is a numerical eigenvalue problem for which multiple solutions can be found, in which $\hat{H}$ is the

Hamiltonian operator, E is the electronic energy and Ψ is the wave function, which depends on the coordinates of all the atoms in the system (Leach (2001)). Conformation optimization is done by probing the energy surface as a function of the atomic coordinates until the lowest energy conformation is obtained. Typically, gradient-based algorithms are used to search for low energy geometries. Once the optimized conformation is obtained, the electronic energy, frequencies and thermodynamics properties can be obtained. Commercial software is widely available to carry out these calculations. In this study, *Gaussian 03* on a 64-bit Linux cluster was used for all the quantum chemistry calculations (Frisch et al. (2004); Gaussian Inc. (1990)).

Transition state theory characterizes a reaction as proceeding via a transition state structure between the reactants and the products, which is characterized as a maximum along the reaction coordinate and a minimum in all other dimensions and thus possesses one imaginary frequency (McQuarrie and Simon (1999)). The imaginary frequency corresponds to the motion along the reaction coordinate. Two classes are provided in Gaussian 03 for locating transition states: *QSTN* and conventional optimization. Once a transition state structure is identified, it needs to be further verified with intrinsic reaction coordinate (IRC) following, which starts from the transition state and probes the conformations along the "*forward*" and "*reverse*" directions. Although IRC following can automatically search conformations in both directions, it was found in this research that including the "*phase*" keyword and specifying the bond length or angle which increases during the transition is helpful. In this research, IRC following was used not only for the verification of transition states but also for the energy topologies required for semi-classical calculations of tunneling coefficients (κ). The default step size in Gaussian 03 is 0.1 amu$^{1/2}$·Bohr, and six points are mapped in each direction. By default, the reaction coordinate can be mapped 0.6 amu$^{1/2}$·Bohr in each direction. In the tunneling coefficient calculation, it is required to reach 1.0 amu$^{1/2}$·Bohr in both directions. Thus, the step size was adjusted by "*IRC(stepsize=N)*", where a step size of 10 corresponds to 0.1 amu$^{1/2}$·Bohr. It was found that for large reaction systems, small step sizes (for example, *stepsize=2*) were necessary to converge the IRC calculations.

Transition state theory also provides the method to calculate the reaction rate constant as shown in Equation 2.22 (Pfaendtner et al. (2006)):

$$k(T) = \kappa(T)\frac{k_B T}{h}(c^o)^{1-m}\frac{Q^{\ddagger}}{Q_{mon}Q_{rad}}e^{-\Delta E_0/RT} \tag{2.22}$$

in which $\kappa(T)$ is the tunneling factor, which is important for reactions involving light atoms such as hydrogen transfer. The tunneling effect for propagation reactions can be neglected so $\kappa(T)$ was approximated as one. k_B is Boltzmann's constant (1.3806×10^{-23} J·mol^{-1}· K^{-1}), h is Planck's constant (6.6261×10^{-34} J·s), m is the number of reactants, which is two for propagation and one for unimolecular reactions, such as intramolecular hydrogen transfer, c° is the standard state concentration (mol·L^{-1}) to which the quantum chemical calculations are referenced, $\frac{P}{RT}$, where P is 1 atm, and ΔE_0 is the difference between E_0 of the transition state and the reactants, which is defined as the summation of the electronic energy (E_e) and the zero-point vibrational energy (ZPVE):

$$E_0 = E_e + ZPVE \tag{2.23}$$

ZPVE is the contribution to the energy from vibration at 0 K as defined in Equation 2.24 (McQuarrie and Simon (1999)):

$$ZPVE = \frac{1}{2}\sum_{i}^{3N-6} h\nu_i \tag{2.24}$$

in which N is the number of atoms, and ν_i represents the frequencies. For transition states, $3N-7$ frequencies are included in the ZPVE.

All the necessary energy levels and partition functions in Equation 2.22 are calculated using quantum chemistry. However, the exact solution to the Schrödinger equation is only feasible for very simple species such as the hydrogen atom. Approaches to solve the Schrödinger equation approximately are classified into two categories: *ab initio* and semi-empirical methods (Leach (2001)). *ab initio* means "from the beginning", which uses the full Hartree-Fock/Roothaan-Hall

equations, without ignoring any of the integrals in the Hamiltonian. Semi-empirical methods simplify the calculations using empirical parameters and ignoring some of the Hamiltonian terms. Semi-empirical methods, such as CNDO, INDO, AM1 and PM3, are less computational demanding. However, their performance is heavily dependent on the applications. Even the best performing semi-empirical methods such as PM3 and AM1 failed in describing radical reactions (Wong and Radom (1995)). Therefore, in this research, semi-empirical methods were only used in the potential energy scans for comparison with *ab initio* methods.

A reference *ab initio* method is Hartree-Fock (HF), in which the wave function (Ψ) is expressed as a linear combination of molecular orbitals, and these molecular orbitals are expanded linearly in terms of atomic orbitals with fixed coefficients (Leach (2001)). The solution is carried out via a self-consistent field (SCF) approach, in which the coefficients for the molecular orbital combinations are optimized until the minimum electronic energy is obtained. Hartree-Fock does not consider the detailed interactions between the electrons. Two different ways of introducing electron correlations have been used: configuration interaction and perturbation theory. Configuration interaction methods include CIS, CID, CCSD and QCISD which differ in the manner in which the configuration interaction is taken into account. Perturbation theory includes Møller-Plesset theory at second order (MP2) and higher order theories (MP3, MP4...). Configuration interaction methods have been used to quantify radical reactions. However, perturbation theory performs poorly for radical reactions (Wong and Radom (1995, 1998)).

The functions used to describe molecular orbitals are called basis functions. A basis set is a set of such functions used to create the molecular orbitals. The most common minimal basis set is STO-nG, where the integer n represents the number of Gaussian primitive functions comprising a single basis function (Leach (2001)). In these basis sets, the same number of Gaussian primitives comprise core and valence orbitals. The more Gaussian primitive functions used, the more accurate results that can be obtained at the expense of higher computational time. Pople and coworkers developed the concept of “split-valence” basis sets, in which the valence orbitals are composed of

two or more basis functions. For example, 3-21G denotes three primitive Gaussian functions with the valence orbitals consisting of two parts: the first part is composed of a linear combination of two primitive Gaussian functions and the other part is composed of a linear combination of one primitive Gaussian function. Split-valence triple basis sets are also used such as 6-311G. Diffuse functions can be added to the basis set in order to describe the long-range behavior, such as 6-31G(d) (Leach (2001)).

Density functional theory (DFT) is an alternative way to solve the Schrödinger equation. DFT solves for the properties such as total electronic energy based on the total electron density of the system instead of the wave function. DFT has been used successfully in the study of many-electron systems which are too complicated to treat with conventional *ab initio* methods. DFT solutions are mostly based on the Kohn-Sham equations. Like the Hartree-Fock equations, approximations need to be used to solve the Kohn-Sham equations. Hybrid DFT methods, in which part of the energy is calculated using Hartree-Fock, have shown great improvement over conventional Hartree-Fock methods since DFT naturally includes electron correlation. BLYP and B3LYP are the most widely used hybrid DFT methods which have shown similar or even better performance than high level *ab initio* methods (Becke (1998)). Unrestricted B3LYP/6-31G(d) is used in this research for geometry optimization, potential energy scans and frequency calculations.

A new generation of hybrid DFT methods has been developed to enhance accuracy, such as MPW1K, MPWB1K, BB1K and M05 and M06-L (Lynch et al. (2000); Zhao et al. (2004, 2006); Zhao and Truhlar (2004)). The hybrid Fock-Kohn-Sham operator is written as follows:

$$F = F^{H} + (X/100)F^{HFE} + (1 - (X/100)](F^{SE} + F^{GCE}) + F^{Cor} \tag{2.25}$$

where F^{H} is the Hartree-Fock operator, X is the percentage of Hartree-Fock exchange, F^{SE} is the Dirac-Slater local density functional for exchange, F^{GCE} is the gradient-corrected of the exchange functional and F^{Cor} is the total correlation functional including both local and gradient-corrected parts of the kinetic energy density. In MPW1B95 and MPWB1K, Adamo and Barone's mPW

exchange functionals are used for F^{GCE} and the Becke95 functional is used for F^{Cor} (Zhao et al. (2004); Zhao and Truhlar (2004)). The parameter X is optimized to minimize the root-mean-square error compared with experimental data. In the MPWB1K model, X was optimized based on the activation energy of nine elementary reactions (Zhao and Truhlar (2004)). X is set to 44% for the MPWB1K model. *Gaussian 03* does not support the direct calculation of MPWB1K. Instead, it needs to be carried out based on the available methods with the adjustment of the overlay parameter (IOp). The overlay parameter IOp(3/76) needs to be specified with the optimized HF and DFT coefficients. The keyword required in Gaussian 03 to carry out MPWB1K/6-31G(d,p) calculations is "MPWB95/6-31G(d,p) IOp(3/76=0690003100)" (Zhao and Truhlar (2004)).

2.6 Tunneling Effects

Tunneling effects are important when small atoms are involved in the reactions, for example, hydrogen transfer. The tunneling effect is expressed as a temperature-dependent tunneling coefficient $\kappa(T)$ in the calculation of the rate constant as shown in Equation 2.22. Tunneling effects account for the situation when the reaction can happen for some small atoms even though the reaction system does not have enough energy to overcome the reaction barrier, i.e., it is as if the small atoms go through the barrier instead of overcoming it (Masel (2001); Renaud and Sibi (2001)). Thus, the actual reaction rate constant is higher than predicted.

Detailed approaches and algorithms for calculating the transmission coefficient have been put forth. Different approximations have been developed, including classical and semi-classical approximations. The most widely used classical approximation is the Wigner tunneling correction which is given as Equation 2.26 (Wigner (1932)):

$$\kappa(T) = 1 - \frac{1}{24}(\frac{ih\nu^{\ddagger}}{k_B T})^2 \tag{2.26}$$

in which $\nu^{\ddagger}$ is the imaginary frequency in the transition state which represents the motion along the reaction coordinate. The Wigner approximation is frequently used; however, it is known to underestimate the tunneling effect since it only accounts for the contributions near the barrier top (Gonzalez-Lafont et al. (1991); Truong et al. (1999)). Semi-classical approximations calculate the tunneling coefficient in terms of the probability for a wave function to go through the energy barrier, which is called the path integral formulation. Three semi-classical approximations were used in this research, including the small curvature tunneling (SCT), the zero curvature tunneling (ZCT) and the Eckart models.

In the SCT method, the tunneling coefficient is approximated as the ratio of the thermally averaged multidimensional semiclassical transmission probability ($P(E)$) to the thermally averaged classical transmission probability for scattering by the effective potential as shown in Equation 2.27 (Gonzalez-Lafont et al. (1991); Truong et al. (1999)):

$$\kappa(T) = \frac{\int_0^\infty P(E) e^{-E/k_B T} dE}{\int_{E^*(T)}^\infty e^{-E/k_B T} dE} \tag{2.27}$$

where $E^*(T)$ represents the total energy ($V_{MEP} + \sum_{i=1}^{3N-7} \frac{1}{2} h\nu$) at the bottleneck. The probability ($P(E)$) is calculated as Equation 2.28.

$$P(E) = \frac{1}{1 + e^{2\theta(E)}} \tag{2.28}$$

$\theta(E)$ is the imaginary action integral along the tunneling path shown as Equation 2.29:

$$\theta(E) = \frac{2\pi}{h} \int_{s1}^{s2} \sqrt{2\mu_{eff}(s)|E - V^G(s)|} ds \tag{2.29}$$

where s_1 and s_2 represent the reaction turning point and μ_{eff} is the reduced mass.

The Eckart approximation assumes the effective reduced mass, which accounts for the reaction path curvature, is constant. The tunneling is thus assumed to proceed along the minimum energy path (MEP) and the reaction path curvature is neglected. The potential width is obtained from

fitting the potential for the MEP going from the reactants through the transition state to the products. In this research, CSEO software (*www.cseo.net*) was used for the calculation of tunneling coefficients.

2.7 Factors Influencing the Activation Energy

The major factors that influence the reaction activation energy include: (1) steric effects of the substituent in the radical and the monomer, (2) reaction enthalpy and (3) polar effects (Fischer and Radom (2001)). Steric effects account for the decrease of rate constants caused by the repulsion between radicals and monomers caused by substituents. This explains, for example, the addition to methyl acrylate happening predominantly at the unsubstituted carbon atom. Polar effects account for the electron donating effect of substituents, which can be explained in terms of frontier orbital theory. For example, radical addition reactions are the interaction of the singly occupied molecular orbital (SOMO) of the radical and the highest occupied molecular orbital (HOMO) of the monomer or the interaction of the SOMO of the radical with the lowest unoccupied molecular orbital (LUMO) of the monomer depending on the energy gap between the SOMO-HOMO and the LUMO-SOMO as shown in Figure 2.9. Reactions proceed according to the lower energy gap procedure: if the energy gap between the LUMO and the SOMO is lower, interaction of these two orbitals includes the partial electron transfer from the radical to the monomer, which is nucleophilic for the radical; on the other hand, if the energy gap between the SOMO and the HOMO is lower, interaction of these two orbitals includes the partial electron transfer from the monomer to the radical, which is electrophilic for the radical (Lozano et al. (1999)). The most frequently used approach to account for enthalpic effects is to correlate activation energy (E_a) and heat of reaction (ΔH_r) linearly, which is known as the Evans-Polanyi equation shown as Equation 2.30:

$$E_a = E_0 + \alpha \Delta H_r \tag{2.30}$$

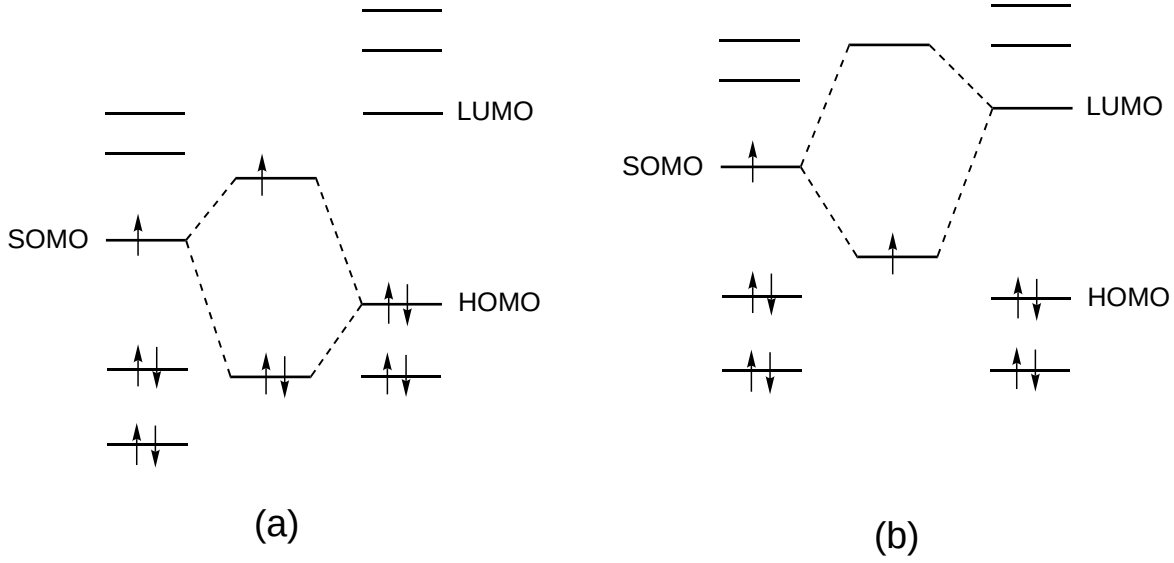

Figure 2.9: Interactions between the SOMO of the radical with the (a) HOMO or (b) LUMO of the monomer.

in which E_0 and α are constant for the same reaction family. Radical addition reactions are all exothermic reactions; higher exothermicity is related to a lower activation energy and an earlier transition state. For radical addition to alkenes, a general number for α of 0.25 was proposed, which means about one quarter of the variation in ΔH_r is translated to the transition state structure (Fischer and Radom (2001)). The strict application of the Evans-Polanyi relationship requires that the other factors are minor.

Besides steric, polar and enthalpic effects, other factors governing radical addition reactions have also been suggested. For example, the state correlation diagram (SCD) includes the triplet excitation state and ionization energy (Gomez-Balderas et al. (2003)). SCD can predict the influence of various energy parameters on the activation energy, while more complex models which include triplet excitation energy, ionization energy, Coulomb attraction parameter (C) and interaction strength parameter (γ) have also been used (Gomez-Balderas et al. (2003)). In the present research, the molecules (methyl methacrylate and methyl acrylate) have similar structures and re-

action mechanisms (for example, all the addition reactions undergo electrophilic addition); it will be shown that the reaction enthalpy is the dominating factor in determining the activation energy.

Chapter 3

The One-dimensional Internal Rotor Model

3.1 Introduction

Computational chemistry is under continuous development and has been used widely in various fields of chemical research. The accuracy has been continually improved with the development of new computational methods and levels of theory. However, there are still advances that need to be made to extract the most accurate results from quantum chemical calculations, particularly for reaction systems involving large molecules. For example, motions within a molecule are expressed in terms of frequencies, which encompasses stretching, bending and torsional motions. Traditionally, all of these motions are modeled using a harmonic oscillator (HO) model, which captures pure stretching motions. However, for the other motions, a HO description may not be appropriate. Because the energy levels calculated based on the HO model are used in the calculation of partition functions and related calculations, such as the rate constant and thermodynamic properties, a HO treatment may result in deviations between calculated and experimental properties, particularly if the number of torsional motions is large. Even though this issue is well known, the HO model is still widely used. Recently, significant attention has begun to focus on more accurate treatment of vibrational motions. As early as the 1940s, alternative models were developed which

can better model torsional motions and yield more accurate data (Pitzer and Gwinn (1942)), but activity in this field has dramatically heightened in recent years (Ayala and Schlegel (1998); Chuang and Truhlar (2000); Heuts and Gilbert (1995); Izgorodina and Coote (2006); Pitzer (1946); Speybroeck et al. (2002, 2001, 2005); Vansteenkiste et al. (2005)). This research has provided general guidelines for implementing a quantitatively accurate treatment of internal rotation; however, all treatments that are suggested still require substantial manual effort for two main reasons. First, these treatments were designed to solve a specific problem which might not be generally translated to other research. For example, in the study of some simple molecular structures, such as ethane, the rotational profile can be fitted using a single cosine function; however, this is not suitable for molecular structures which have more complex rotational profiles (McClurg et al. (1997)). The second reason is that no commercial software is available to perform such treatments. Although the algorithm developed by Schlegel et al. (Ayala and Schlegel (1998)) has been incorporated into *Gaussian 03*, its performance is quantitatively poor. The following sections introduce the detailed methodology we developed and implemented in which low frequencies characterizing torsional motions were treated using a one-dimensional internal rotor in the calculation of rate constants and thermodynamic properties.

3.2 Partition Functions

The calculation of rate constants and thermodynamic properties are all based on the partition function. The partition function is calculated based on the energies of various forms. The traditional classification includes four different types of energies: electronic energy, and energies from translational, rotational and vibrational motions. The energy (ε) is written as the summation of these four energies:

$$\varepsilon = \varepsilon_e + \varepsilon_{trans} + \varepsilon_{rot} + \varepsilon_{vib} \tag{3.1}$$

and the partition function is expressed as the product of the partition functions of these four energy forms as shown in Equation 3.2 (McQuarrie and Simon (1999)).

$$Q = Q_e Q_{trans} Q_{rot} Q_{vib} \tag{3.2}$$

The electronic partition function is written as Equation 3.3:

$$Q_e = \omega_0 e^{-\epsilon_0/k_B T} + \omega_1 e^{-\epsilon_1/k_B T} + \omega_2 e^{-\epsilon_2/k_B T} + \cdots \tag{3.3}$$

where ω_n is the degeneracy of the n-th energy level and ϵ_n is the n-th energy level. For the molecule at the ground state, only the ground state energy is considered and the higher levels of energy are much greater than $k_B T$, which simplifies the electronic partition function to:

$$Q_e = \omega_0 \tag{3.4}$$

The translational partition function is based on the assumption that there are no interactions between particles, which is written as Equation 3.5:

$$Q_{trans} = (\frac{2\pi m k_B T}{h^2})^{3/2} V \tag{3.5}$$

The reference volume V can be calculated based on the ideal gas law, $V = k_B T/P$, so the translational partition function is written as:

$$Q_{trans} = (\frac{2\pi m k_B T}{h^2})^{3/2} \frac{k_B T}{P} \tag{3.6}$$

The rotational partition function Q_{rot} is dependent on the molecular structure. For linear molecules, Q_{rot} is a function of temperature, moment of inertia and symmetry number, which is shown in Equation 3.7:

$$Q_{rot,linear} = \frac{1}{\sigma_r}(\frac{T}{\Theta_r}) \tag{3.7}$$

where Θ_r is defined as follows:

$$\Theta_r = \frac{h^2}{8\pi^2 I k_B} \tag{3.8}$$

I is the moment of inertia, which is defined as the summation of the product of the mass of an atom and the square of its distance to the rotation center: $I = \sum md^2$. For nonlinear molecules, Q_{rot} is written as Equation 3.9:

$$Q_{rot,nonlinear} = \frac{\pi^{1/2}}{\sigma_r}(\frac{T^{3/2}}{(\Theta_{r,x}\Theta_{r,y}\Theta_{r,z})^{1/2}}) \tag{3.9}$$

$\Theta_{r,x}$, $\Theta_{r,y}$ and $\Theta_{r,z}$ are defined similarly to Equation 3.8 with the moment of inertia defined with respect to the distance to the x, y and z axes.

The motions other than the three mentioned above are classified as vibrational modes, which are the "*internal*" motions of the atoms including stretching, bending and torsional forms. For a molecule having N atoms, $3N - 6$ frequencies are calculated based on the combinations of these different motions. For a transition state, the motion along the reaction coordinate is labelled as an imaginary frequency which is ignored in the calculation of the zero-point vibrational energy. The vibrational frequencies are calculated based on the vibrational temperature, which for the i-th vibrational frequency, ν_i, is defined as follows:

$$\Theta_i = \frac{h\nu_i}{k_B} \tag{3.10}$$

The energy contributions from the vibrational motions are typically calculated by treating the modes using the harmonic oscillator (HO) model. The vibrational partition function is calculated as the product of the partition functions of all the vibrational modes using Equation 3.11:

$$Q_v = \prod_i \frac{e^{-\Theta_{v,i}/2T}}{1 - e^{-\Theta_{v,i}/T}} \tag{3.11}$$

The total partition function (Q) is the product of these four partition functions as in Equation 3.12:

$$Q = Q_e Q_{trans} Q_{rot} Q_{vib} \tag{3.12}$$

Thermodynamic properties (entropy, enthalpy, internal energy and heat capacity) can be calculated based on the partition function. The entropy value (S) is calculated using Equation 3.13:

$$S = R + RlnQ + RT(\frac{\partial lnQ}{\partial T})_V \tag{3.13}$$

Internal energy is calculated using Equation 3.14:

$$U = RT^2(\frac{\partial lnQ}{\partial T})_V \tag{3.14}$$

Enthalpy is calculated using Equation 3.15:

$$H = U + RT = RT^2(\frac{\partial lnQ}{\partial T})_V + RT \tag{3.15}$$

The heat capacity (C_V) is calculated using Equation 3.16:

$$C_V = (\frac{\partial U}{\partial T})_{N,V} \tag{3.16}$$

The calculation of thermodynamic properties using the rigid rotor, harmonic oscillator approximation has been implemented into quantum chemistry software such as *Gaussian 03* (Frisch et al. (2004)). Although partition functions have been used widely in the determination of rate constants and thermodynamic properties, they are typically calculated using the default treatment based on the harmonic oscillator model. However, many low frequency modes are better described as rotations than as vibrations. These rotational modes should be separated from the harmonic oscillator description and treated using a more appropriate model to describe them. Although the deviation caused by modeling the rotational modes using a harmonic oscillator model has been realized since the 1940s (Kilpatrick and Pitzer (1949); Pitzer (1946); Pitzer and Gwinn (1942)), accurate treatment of rotational modes has not been implemented in commercial quantum chemistry software. With increasing molecular size, the deviation caused by treating rotational modes using a harmonic oscillator model becomes significant, so development of an appropriate approach to model the internal rotations and thereby enhance the accuracy of the kinetic parameters and thermodynamic properties calculated was one of the most important challenges that this research met.

3.3 Internal Rotor Model

Depending on the degree of coupling of various rotations, the internal rotor model can be classified into two types. If all the rotations (including all internal rotations and external rotation) are considered as a whole, it is called a multi-dimensional rotor model. If individual rotations are treated separately, and the overall rotational partition function is calculated as the product of the partition functions of all the rotors, the method is called an uncoupled rotation model or a one-dimensional internal rotor model.

In a multi-dimensional model, the overall rotational kinetic energy is written as Equation 3.17 (Van Cauter et al. (2006)):

$$T = \frac{1}{2}(\omega_0, \omega_1, \cdots, \omega_n)A \begin{pmatrix} \omega_0 \\ \omega_1 \\ \cdots \\ \omega_n \end{pmatrix} \tag{3.17}$$

in which A is defined as in Equation 3.18:

$$A = \begin{pmatrix} I & \Lambda_{01} & \Lambda_{02} & \cdots \\ \Lambda_{01}^T & I_1 & \Lambda_{12} & \cdots \\ \Lambda_{02}^T & \Lambda_{12}^T & I_2 & \cdots \\ \cdots & & & \end{pmatrix} \tag{3.18}$$

where n is the number of internal rotations in the molecule. ω_i are the instantaneous angular velocities of the external and internal rotations. I is the inertia tensor, which is defined as in Equation 3.19:

$$I = \begin{pmatrix} I_{xx} & I_{xy} & I_{xz} \\ I_{yx} & I_{yy} & I_{yz} \\ I_{zx} & I_{zy} & I_{zz} \end{pmatrix} \tag{3.19}$$

and I_{ij} is defined as follows:

$$\begin{aligned} I_{xx} &= \sum_i m_i(y_i^2 + z_i^2) \\ I_{yy} &= \sum_i m_i(x_i^2 + z_i^2) \\ I_{zz} &= \sum_i m_i(x_i^2 + y_i^2) \\ I_{xy} &= I_{yx} = -\sum_i m_i x_i y_i \\ I_{xz} &= I_{zx} = -\sum_i m_i x_i z_i \\ I_{yz} &= I_{zy} = -\sum_i m_i y_i z_i \end{aligned}$$

I_i in Equation 3.18 represents the moment of inertia of the i-th rotation top. The total rotational partition function is written as Equation 3.20.

$$Q_{rot} = \frac{1}{\sigma}\frac{1}{h^{(3+n)}}(\frac{2\pi}{\beta})^{(3+n)/2}8\pi^2\int_0^{\frac{2\pi}{\sigma_1}} d\phi_1 \cdots \int_0^{\frac{2\pi}{\sigma_n}} d\phi_n \times \sqrt{detA(\phi_1, \cdots, \phi_n)}e^{-\beta V(\phi_1,\cdots,\phi_n)} \tag{3.20}$$

The advantage of a multi-dimensional rotor model is that it includes the interactions between various rotations. However, multi-dimensional treatment requires simultaneous potential energy scans from 0 to 360° for all the rotors, which is very computationally expensive. For example, methyl methacrylate dimeric radical has nine internal rotors. With a scan interval of 30°, a multi-dimensional treatment would require 12^9 scan points. Obviously, a multi-dimensional rotor model is not tractable for a reaction system with as many degrees of freedom as methyl methacrylate and methyl acrylate.

In the one-dimensional rotor model, the interactions between various rotors are neglected. The rotational energy levels caused by each rotation are calculated separately, and the partition function

for each rotation is calculated based on these energies. The overall partition function is calculated as the product of all these partition functions. Because the number of scan points is greatly decreased compared with a multi-dimensional model, the one-dimensional treatment is frequently used. The one-dimensional model has shown good performance when compared with the results based on higher dimensional treatments (Speybroeck et al. (2001)).

There are several methods to implement the one-dimensional rotor model. The partition function for a single rotor can be calculated explicitly with the energy levels which are obtained by solving a one-dimensional Schrödinger equation constructed based on the reduced moment of inertia (I_r) and potential energy scan ($V(\theta)$) for this rotor. The rotation can also be classified into three types according to the height of the rotation barrier. If the energy barrier is very high ($>> k_BT$), the full rotation cannot be achieved, and the rotor can only oscillate near the equilibrium position. In this case, the rotor can be modelled using a harmonic oscillator model. If the energy barrier is very low ($< k_BT$), the full rotation can be achieved at a constant angular velocity, and thus the rotor can be treated as a free rotor. If the rotation barrier height is of intermediate height, the full rotation can still be achieved, but the angular velocity is not constant, and such a rotation is called a hindered rotation. The hindered rotor partition function should asymptote to the harmonic oscillator partition function at low temperatures and match the free rotor partition function at high temperatures (Chuang and Truhlar (2000)). The partition functions based on a harmonic oscillator and a free rotor are easy to calculate, so the hindered rotor partition function can be expressed in terms of asymptotes which approach the harmonic oscillator partition function at the low temperature limit while approaching the free rotor partition function at the high temperature limit. McClurg et al. put forth one approach for specifying the hindered rotor partition function in which they constructed an interpolation function in terms of a zeroth-order Bessel function (I_0) (McClurg et al. (1997)). An asymptotic factor (f) for specifying the partition function value $Q_{int,rot}$ which converges to that for a free rotor at high temperature and to that for a harmonic oscillator at low

temperature is shown in Equation 3.21.

$$Q_m^{IR} = f_m \cdot Q_m^{HO} \tag{3.21}$$

Truhlar (1991) also used such an interpolating factor (f) to address the hindered rotor partition function. The interpolating factor is expressed in terms of hyperbolic functions. Both of these two methods are applicable to rotations in which the potential energy can be expressed in the form shown in Equation 3.22:

$$V_m = V_0 + \frac{1}{2} W_m (1 - cosn\theta) \tag{3.22}$$

where V_0 is the energy at a torsion angle (θ) equaling zero, and W_m is the height of the rotation energy barrier. Such potential energy profiles can only be used for symmetric tops such as methyl groups; for asymmetric tops such as methoxy groups and hydroxyl groups, these two methods cannot be used.

Another approach to calculate the one-dimensional partition function is based on the definition of the partition function shown in Equation 3.23 for the m-th rotation (Heuts and Gilbert (1995); Pitzer (1946); Speybroeck et al. (2001)).

$$Q_{int,rot,m} = \frac{1}{\sigma_m} \sum_i exp(-\frac{\epsilon_i}{k_B T}) \tag{3.23}$$

where σ_m is the symmetry number. The rotational energy levels (ϵ_i) are calculated by solving the one-dimensional Schrödinger equation as shown in Equation 3.24.

$$-\frac{\hbar^2}{2I_r}\frac{d^2}{d\theta^2}\Psi + V(\theta)\Psi = \epsilon\Psi \tag{3.24}$$

where $\hbar$ is Planck's constant divided by 2π, Ψ is the wave function, θ is the torsional angle, $V(\theta)$ is the potential energy as a function of torsional angle and I_r is the reduced moment of inertia. The one-dimensional internal rotor treatment of rotational modes is computationally economical, and it has been shown to have quantitative accuracy in previous research (Speybroeck et al. (2005)). However, codes for treating rotational modes are not available. Thus, we developed software to calculate the necessary variables and partition functions in a generalized way.

3.4 Reduced Moment of Inertia

The reduced moment of inertia (I_r) in Equation 3.24 is required for the solution of the Schrödinger equation. All of the coordinates of the atoms in the molecule should be referenced to the center of mass of the molecule. The center of mass of a multi-atom molecule is calculated as shown in Equations 3.25, 3.26 and 3.27 (McQuarrie and Simon (1999)).

$$x_0 = \frac{\sum_i m_i \cdot x}{\sum_i m_i} \tag{3.25}$$

$$y_0 = \frac{\sum_i m_i \cdot y}{\sum_i m_i} \tag{3.26}$$

$$z_0 = \frac{\sum_i m_i \cdot z}{\sum_i m_i} \tag{3.27}$$

There are different approaches to calculate the reduced moment of inertia. Pitzer and Gwinn defined the reduced moment of inertia for a symmetric top as shown in Equation 3.28 (Pitzer and Gwinn (1942)).

$$I_r = I - I^2(\frac{cos^2\alpha}{I_x} + \frac{cos^2\beta}{I_y} + \frac{cos^2\gamma}{I_z}) \tag{3.28}$$

I is the moment of inertia of the rotation top, which is the summation of the products of the mass of each atom and the square of its distance to the rotation axis as shown in Equation 3.29.

$$I = \sum_i m_i \cdot d_i^2 \tag{3.29}$$

α, β and γ are the angles between the axis of the top and and the three principal axes of the whole molecule. The principal axes are defined as the eigenvectors of the inertia tensor as shown in Equation 3.19. The cosines of the angles between the rotation axis ($\overrightarrow{R}$) and the principal axes ($\overrightarrow{P}$) are calculated as the ratio of the dot product of the rotation axes and principal axes and the product of the two modes of the rotation axes and principal axes as shown in Equation 3.30.

$$cos\theta = \frac{\overrightarrow{R} \cdot \overrightarrow{P}}{|\overrightarrow{R}| \times |\overrightarrow{P}|} \tag{3.30}$$

For asymmetric tops, Pitzer defined a method to calculate I_x, I_y and I_z (Pitzer (1946)). For each top, the rotation axis is defined as the z axis; the x axis is perpendicular to the z axis and passes through the center of gravity of the rotation top; the y axis is the cross product of the z axis and the x axis. The following four variables are defined:

$$\begin{aligned} A_m &= \sum_i m_i(x_i^2 + y_i^2) \\ B_m &= \sum_i m_i x_i z_i \\ C_m &= \sum_i y_i z_i \\ U_m &= \sum_i x_i \end{aligned}$$

The cosines between the axes (x, y, z) of the m-th top and the axes of the whole molecule $(1, 2, 3)$ are defined as follows:

$$\begin{pmatrix} \alpha_m^{1x} & \alpha_m^{2x} & \alpha_m^{3x} \\ \alpha_m^{1y} & \alpha_m^{2y} & \alpha_m^{3y} \\ \alpha_m^{1z} & \alpha_m^{2z} & \alpha_m^{3z} \end{pmatrix} \tag{3.31}$$

For a one-dimensional rotor, the reduced moment inertia is calculated as shown in Equation 3.32.

$$I_r = A_m - \sum_i \{ \frac{\alpha_m^{iy} U_m)^2}{M} + \frac{(\beta_m^i)^2}{I_i} \} \tag{3.32}$$

in which i equals 1,2 or 3 and β_m^i is defined as shown in Equation 3.33.

$$\beta_m^i = \alpha_m^{iz} A_m - \alpha_m^{ix} B_m - \alpha_m^{iy} C_m + Um(\alpha_m^{i-1,y} r_m^{i+1} - \alpha_m^{i+1,y} r_m^{i-1}) \tag{3.33}$$

i is taken as a cyclic shift of the axes, i.e., if $i = 1$, $i - 1 = 3$ and if $i = 3$, $i + 1 = 1$. The reduced moment of inertia for symmetric and asymmetric tops defined by Pitzer has been used in several literature accounts (Speybroeck et al. (2001); Van Cauter et al. (2006)). However, we found that such a definition for asymmetric tops resulted in negative reduced moments of inertia for some rotations which have high mass rotors, such as the backbone rotation of a trimeric radical.

Another method to calculate the reduced moment of inertia was defined by East and coworkers (East and Radom (1997)). $I^{(m,n)}$ was introduced based on different rotation axes and different levels of approximation of the coupling between external and other internal rotors. n defines three different possible rotation axes: if $n = 1$, the rotation axis is the single bond; if $n = 2$, the rotation axis is defined as parallel to the single bond but passing through the center of mass of the rotation top; if $n = 3$, the rotation axis passes through the centers of gravity of the rotation top and the remaining part of the molecule. m indicates the level of reduction. If $m = 1$, the moment of inertia is not reduced; if $m = 2$, the reduced moment of inertia due to the coupling with overall molecular rotation is calculated as Equation 3.34.

$$\frac{1}{I^{2,n}} = \frac{1}{I_L^{1,n}} + \frac{1}{I_R^{1,n}} \tag{3.34}$$

in which I_L and I_R are the moment of inertia of the left and right sides, which are arbitrarily labeled. Since $I^{2,n}$ includes the coupling of both the rotation and the remainder of the molecule, it is independent of the selection of the rotation top. Higher orders of reduction (i.e., $m = 3, 4$) are similar to the reduced moment of inertia for symmetric and asymmetric tops defined by Pitzer (Pitzer (1946); Pitzer and Gwinn (1942)). In this research, the method for $I^{2,3}$ was used, in which the rotation axis is parallel to the single bond and passing through the center of mass of the rotation top and the coupling of the rotation and the rest of molecule is taken into consideration.

3.5 Potential Energy Scan for a Single Rotor

Potential energy scans are required for two purposes: geometry optimization and obtaining the potential energy function $V(\theta)$. Rigid potential energy scans, although computationally economical, overestimate the rotation barrier. In addition, the symmetry number inferred from a rigid potential energy scan is not true to the definition of symmetry number which is the number of identical conformations through a whole rotation. Therefore, more computationally expensive relaxed po-

tential energy scans were used instead. The term "*relaxed*" means that geometry optimization of the remaining atoms was performed at each scan point. In *Gaussian 03*, such relaxed optimizations were performed with "*opt(modredundant)*" as a keyword and definition of the dihedral being scanned, the scan step and the number of scan points. For example, the dihedral defined as the methoxy group of methyl methacrylate monomer shown as D3 in Figure 3.1 is composed of atoms 4, 5, 11 and 12 with the rotation axis consisting of atoms 5 and 11. The dihedral and scan interval are defined as "4 5 11 12 S 12 30.0" at the bottom of the Gaussian 03 input file which means the dihedral is scanned in intervals of 30.0° for a total of 12 different scan points.

The potential energy profile is then expressed as a function of the torsional angle (θ). Since methyl methacrylate and methyl acrylate have both symmetric and asymmetric tops, the expression needs to be able to describe both of these types. In this research, the potential energy was expressed using a full Fourier expansion as shown in Equation 3.35.

$$V(\theta) = \sum_{i=1}^{n} [a_i(1 - cosi\theta) + b_i sini\theta] \tag{3.35}$$

With finer scans, more precise potential energy profiles can be obtained, but the computational cost increases. Potential energy scans were the most time consuming task in this research. For example, the tetrameric methyl methacrylate radical has 23 rotors. If all of these rotors are scanned at an interval of 10°, a total of 805 constrained optimizations will be performed. It was found that the scans with an interval of 30° provided almost identical profiles when compared with those based on an interval of 10°, as shown in Figure 3.2. Therefore, an interval of 30° was used for all the potential energy scans.

The coefficients a_i and b_i can be obtained from the discrete electronic energy values ($V(\theta)$). The Fourier expansion in Equation 3.35 can be written as the product of matrices as shown in Equation

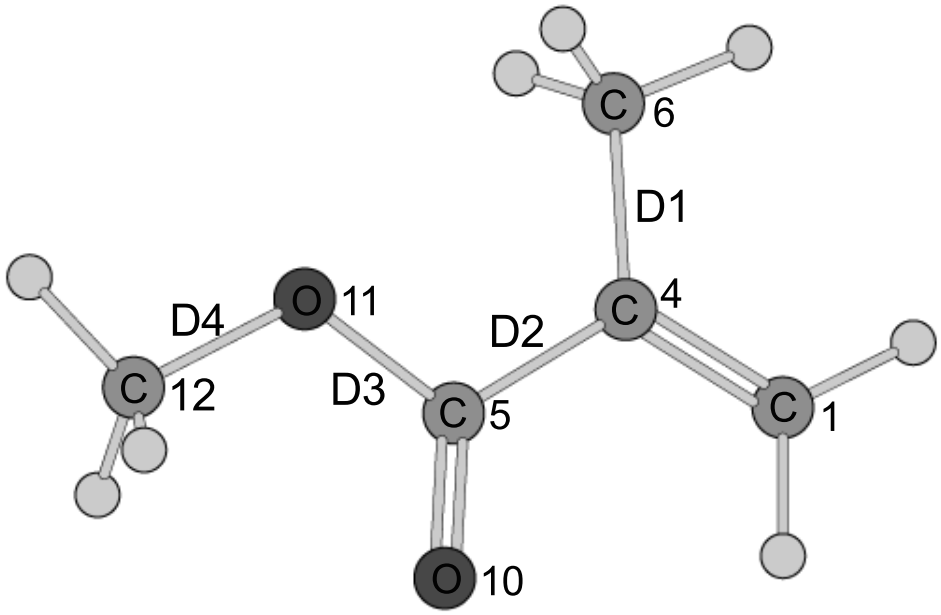

Figure 3.1: Potential energy scans were carried out for the four dihedral axes of methyl methacrylate monomer: D1 (C4,C6), D2 (C4,C5), D3 (C5,O11) and D4 (O11,C12).

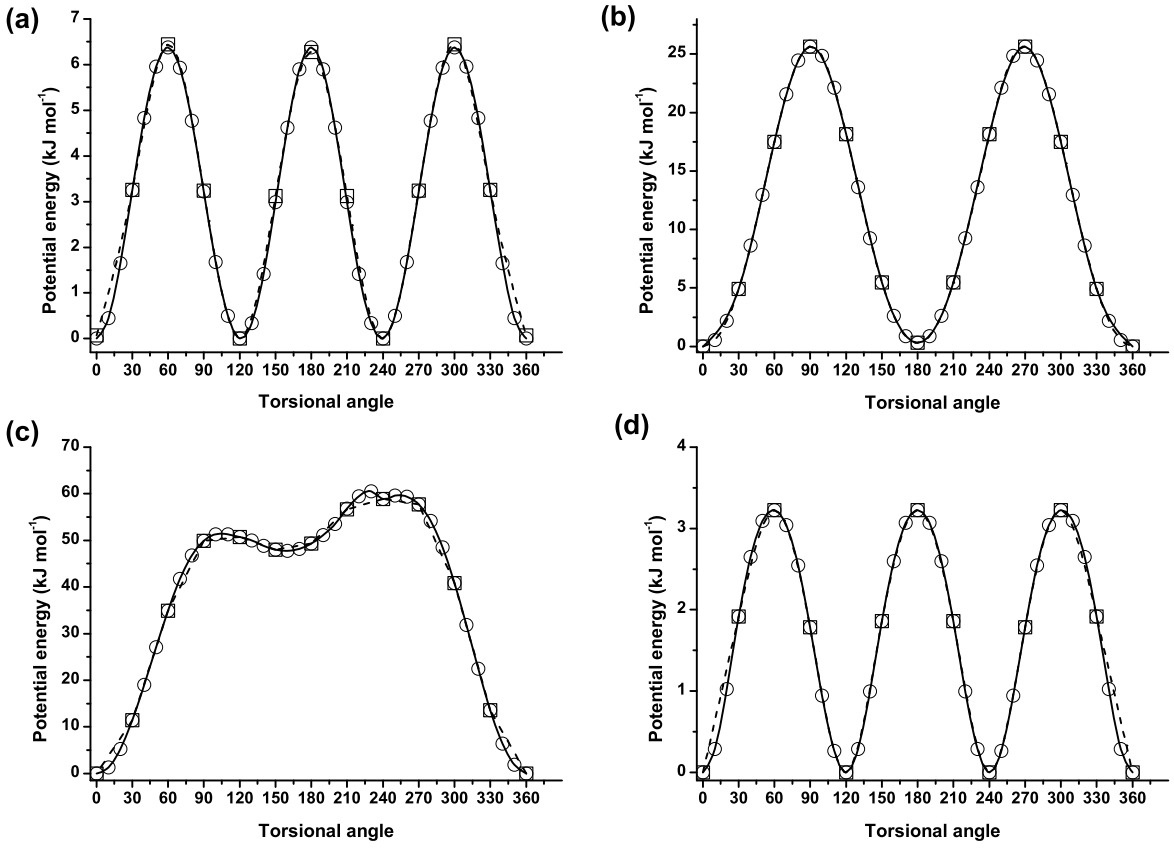

Figure 3.2: Potential energy scans for all the dihedrals defined for methyl methacrylate monomer in Figure 3.1: (a) D1, (b) D2, (c) D3 and (d) D4 at intervals of 10° (circles, solid line) and 30° (squares, dashed line) using unrestricted B3LYP/6-31G(d).

3.36.

$$\begin{bmatrix} 1-cos\theta_1 & sin\theta_1 & \cdots & 1-cosn\theta_1 & sinn\theta_1 \\ 1-cos\theta_2 & sin\theta_2 & \cdots & 1-cosn\theta_2 & sinn\theta_2 \\ 1-cos\theta_3 & sin\theta_3 & \cdots & 1-cosn\theta_3 & sinn\theta_3 \\ & & \cdots & & \\ 1-cos\theta_{m-2} & sin\theta_{m-2} & \cdots & 1-cosn\theta_{m-2} & sinn\theta_{m-2} \\ 1-cos\theta_{m-1} & sin\theta_{m-1} & \cdots & 1-cosn\theta_{m-1} & sinn\theta_{m-1} \\ 1-cos\theta_m & sin\theta_m & \cdots & 1-cosn\theta_m & sinn\theta_m \end{bmatrix} \begin{bmatrix} a_1 \\ b_1 \\ . \\ a_n \\ b_n \end{bmatrix} = \begin{bmatrix} \varepsilon_1 \\ \varepsilon_2 \\ \varepsilon_3 \\ \cdots \\ \varepsilon_{m-2} \\ \varepsilon_{m-1} \\ \varepsilon_m \end{bmatrix} \quad (3.36)$$

The dimensions of the three matrices, denoted as A, x and E from left to right, are $m \times 2n$, $2n \times 1$ and $m \times 1$, where n is the number of coefficient pairs and m is the number of energy points in the potential energy scan. The coefficient matrix x can be determined by solving an overdetermined function as shown in Equation 3.37.

$$x = (A^T A)^{-1} A^T E \quad (3.37)$$

In order to keep the matrix overdetermined, the number of coefficient pairs must be lower than the number of energy points. In this research, three coefficient pairs were used to fit the potential energy profile which consists of 12 energy points. For example, the potential energy scan points and the fitted curves for the four rotors in methyl methacrylate monomer are shown in Figure 3.3. It is obvious that three coefficient pairs (a_i, b_i, $i = 1, 2, 3$) are sufficient to describe the profiles for both symmetric and asymmetric tops.

Since the conformation at each scan point needs to be optimized, the potential energy scan is the most time consuming task. In order to probe the influence of quantum chemistry method and basis set on the potential energy scan, three *ab initio* methods (unrestricted B3LYP/6-31G(d), HF/6-31G(d) and HF/3-21G) and two semi-empirical methods (AM1 and PM3) were used to carry out potential energy scans, and the results were compared. Potential energy scans of methyl methacrylate monomer based on these five methods are shown in Figure 3.4. For symmetric tops, these

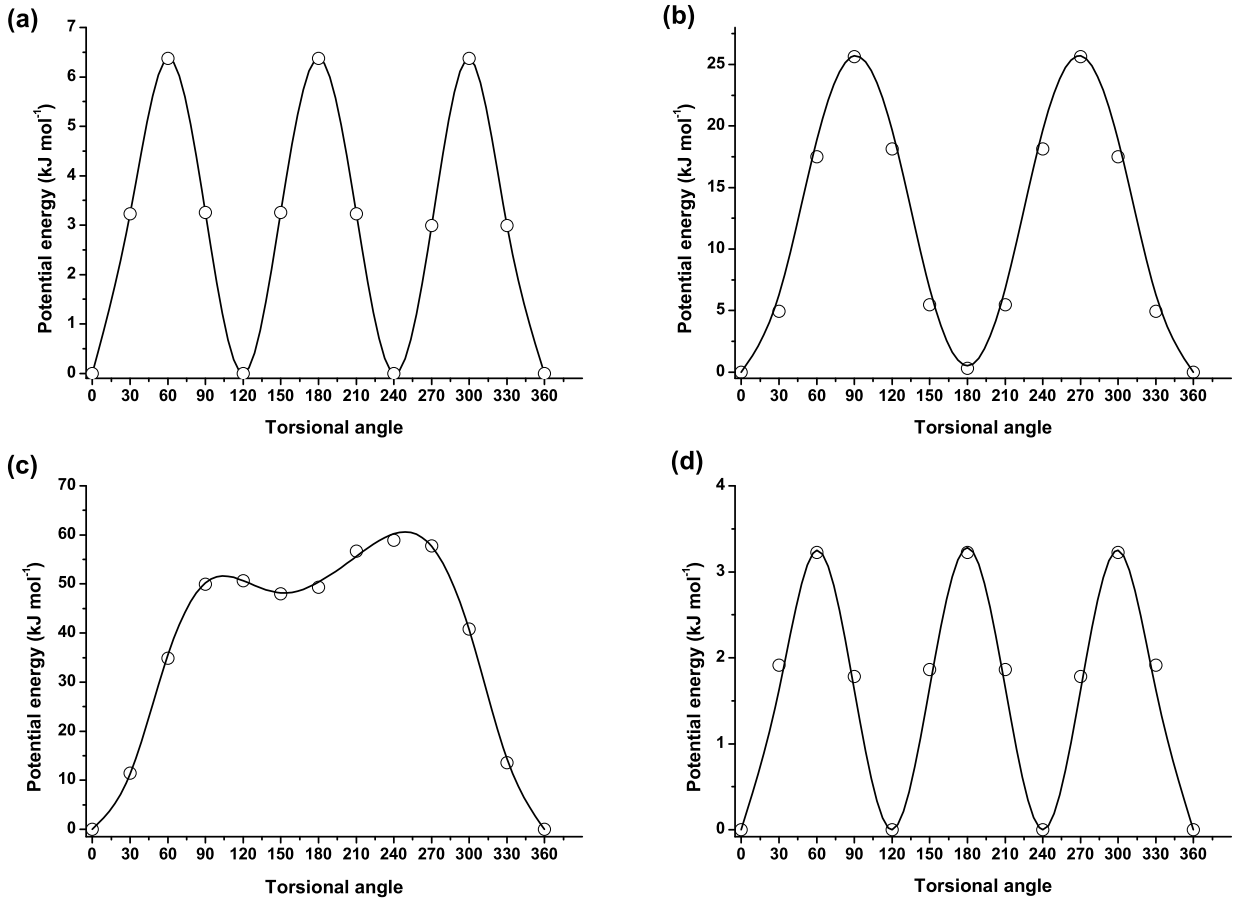

Figure 3.3: Potential energy scans for all the dihedrals defined for methyl methacrylate monomer in Figure 3.1: (a) D1, (b) D2, (c) D3 and (d) D4. The potential energy scans carried out in 30° increments using unrestricted B3LYP/6-31G(d) are shown as points, and the Fourier fits are shown as lines.

methods afford similar potential energy shapes, but the barrier heights are different by as much as 30 kJ· mol^{-1}. For asymmetric tops as shown in Figure 3.4 (c), B3LYP/6-31G(d) and HF/6-31G(d) have similar shapes and barrier heights, but the other three methods are different in both shape and barrier height. These results show that smaller basis sets and semi-empirical methods are not a viable option for investigating methyl methacrylate polymerization. Therefore, all of the internal rotor partition functions in this research were calculated based on potential energy scans with unrestricted B3LYP/6-31G(d). It is also interesting to note that the barrier height is not only determined by the type of rotating group, but it also depends on the environment where the group is located. For example, the barrier height of the CH_3 group defined as D4 in Figure 3.1 is about 3 kJ·mol^{-1} lower than that defined as D1. It is attractive to have a "general" barrier height for a type of group because of the prevalence of repeating groups in polymerization chemistry, so that the treatment of internal rotations can be greatly simplified. However, analysis of each of the rotating tops in the monomer, radicals and transition states showed that it is not quantitatively accurate for methyl methacrylate and methyl acrylate polymerization to assign a single barrier height for a type of rotating top since the rotation is inevitably influenced by its surrounding groups.

3.6 Obtaining the Energy Levels

The energy levels of the m-th rotor are obtained by solving the one-dimensional Schrödinger equation as shown in Equation 3.24. The Fourier Grid Hamiltonian (FGH) method developed by Marston and Balint-Kurti (Balint-Kurti et al. (1992)) is a common approach to solve the time-independent Schrödinger equation by discretizing the Hamiltonian operator over the rotation range into a sparse matrix. The energy levels (eigenvalues) are determined by diagonalizing the matrix. The detailed algorithm is described by Marston and coworkers (Balint-Kurti et al. (1992)). Our program *calck* was developed to solve the Schrödinger equation using the FGH algorithm, in which the Hamiltonian operator was discretized as a 1000$\times$1000 matrix. For comparison, the Hamilto-

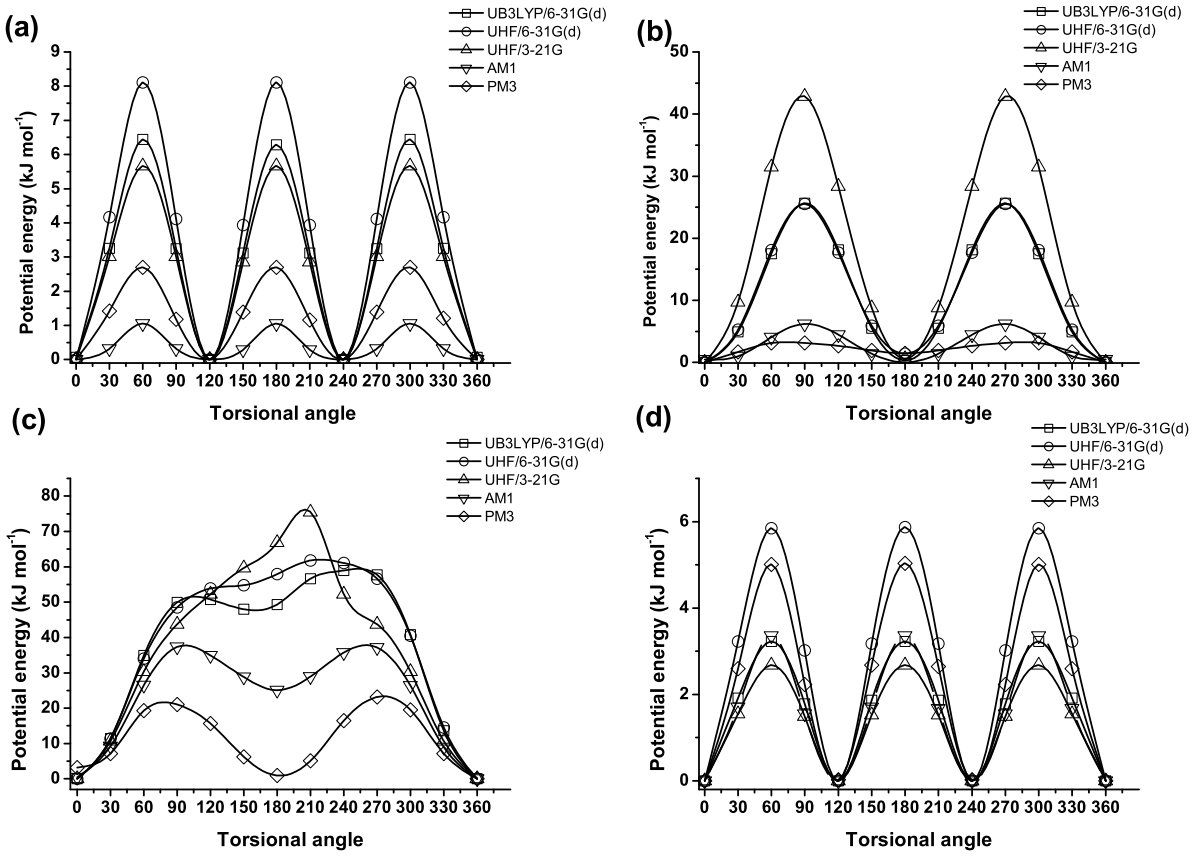

Figure 3.4: Comparison of potential energy scans for the dihedral angles of methyl methacrylate monomer using various methods. The dihedrals are defined as in Figure 3.1: (a) D1, (b) D2, (c) D3 and (d) D4.

nian operator was discretized as a 5000×5000 matrix. Comparison of partition functions calculated for methyl methacrylate monomer showed that 1000 points gave results that were consistent with finer grids containing 5000 points; the maximum deviation was less than 1.2%, and the deviation decreased with increasing temperature, as shown in Table 3.1. Therefore, the coarse mesh size was used, and the Hamiltonian operator was represented using a 1000×1000 matrix.

3.7 Correction to Q_{HO}

The energy levels (ε_i) obtained from the one-dimensional Schrödinger equation were used in Equation 3.23 to calculate the partition function for the m-th rotation. The next issue to address was how to correct the partition functions based on the harmonic oscillator model. That is, it was necessary to determine which frequencies' contributions should be removed and replaced by $Q_{int,rot}$. For very simple molecules, identification of internal rotations is easy. For example, the lowest frequency (314 cm^{-1}) in ethane mainly consists of the rotation about the carbon-carbon single bond. Correction can thus be performed by simply substituting the HO partition function based on the lowest frequency with the one calculated based on the one-dimensional internal rotor model. However, identification of such one-to-one correspondences becomes difficult with increasing molecular size. A given rotational motion disperses into more than one frequency as the molecule becomes more complicated. Van Cauter et al. used a method to calculate the frequency corresponding to the "*pure*" rotation and identified the frequency that most closely corresponded to a given rotation so that the partition function can be cleanly substituted (Van Cauter et al. (2006)). However, this method could not be used for larger molecules since the calculated "*pure*" frequency based on the rotation was not necessarily close to a frequency identified by the HO analysis. Another approach is "*bulk*" replacement. In some reports, 200 cm^{-1} was used as the upper limit to define low frequencies by some researchers (Heuts and Gilbert (1995)), while 300 cm^{-1} was used in other examples (Izgorodina and Coote (2006)). The frequencies lower than the cutoff value were taken

out of Q_{vib} and replaced by $Q_{int,rot}$, which was calculated as the product of the partition functions for each rotor.

In the present approach, we did not apply an arbitrary upper bound to define what was classified as a low frequency, and we used a method for calculating $Q_{int,rot}$ that was general for rotations of any symmetry. The number of low frequencies that were removed was set as the number of rotors, which included rotations about σ bonds and the bond defining the transition state. Although the bond defining the transition state is not a real bond, it is treated as a hindered rotor since the lowest positive frequency in the transition state mainly consists of torsional motion about this bond. Rather than simply removing the contribution of the N lowest frequencies from Q_{vib}, where N is the number of rotors, the low frequencies were examined to make sure they consisted of rotational components. Interestingly, all vibrational motions that were removed for all species had frequencies less than 200 cm^{-1}. For the reactants (monomer and radical) and the radical product, the lowest N frequencies all had rotational components. However, the transition states were different since some low frequencies are essentially a bending motion involving the monomer and the radical. For example, as shown in Figure 3.5, frequency ν-2 (45.3 cm^{-1}) in the methyl methacrylate AD1 transition state involves the bending motion of the monomer and the radical. Frequencies that did not consist of torsional motions were not treated as hindered rotations and thus remained as part of the harmonic oscillator portion of Q_{vib}. For those frequencies removed from Q_{vib}, their contributions to ZPVE were also removed.

3.8 Automatic Treatment of 1-D Internal Rotation

The algorithm described above has been implemented in our software to facilitate the treatment of hindered rotations (Pfaendtner et al. (2007)). The reduced moment of inertia is calculated, the potential energy profile is fit, the one-dimensional Schrödinger equation is solved, and the partition functions are corrected. The process is summarized in Figure 3.6.

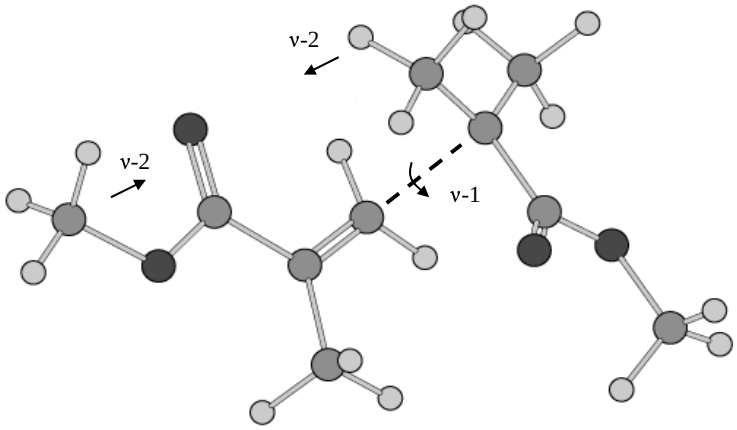

Figure 3.5: The transition state for the AD1 reaction of methyl methacrylate and characteristic motions of two of its frequencies. ν-1 (20.3 cm^{-1}) is the lowest positive frequency, and it corresponds to the torsional motion about the bond defining the transition state. ν-2 (45.3 cm^{-1}) is the second lowest frequency, and it has no torsional component.

Calck and *calctherm* were developed for the calculation of kinetic parameters and thermodynamic properties, respectively. *Calck* requires input files for the reactants, transition state and products. Rate constants for a series of temperatures defined in the array "@T" are calculated, and the frequency factor and activation energy are determined from regression of ln$k$ versus 1/T. In *calck*, the following options can be specified:

- *nr*: number of reactants
- *np*: number of products
- *rpd*: Forward reaction path degeneracy
- *rpd_r*: Reverse reaction path degeneracy
- Eo: Forward reaction zero-point energy corrected electronic energy difference
- Eo_r: Reverse reaction zero-point energy corrected electronic energy difference
- *zpe*: Scale factor for frequencies for zero-point vibrational energy (default factor is 0.9806)

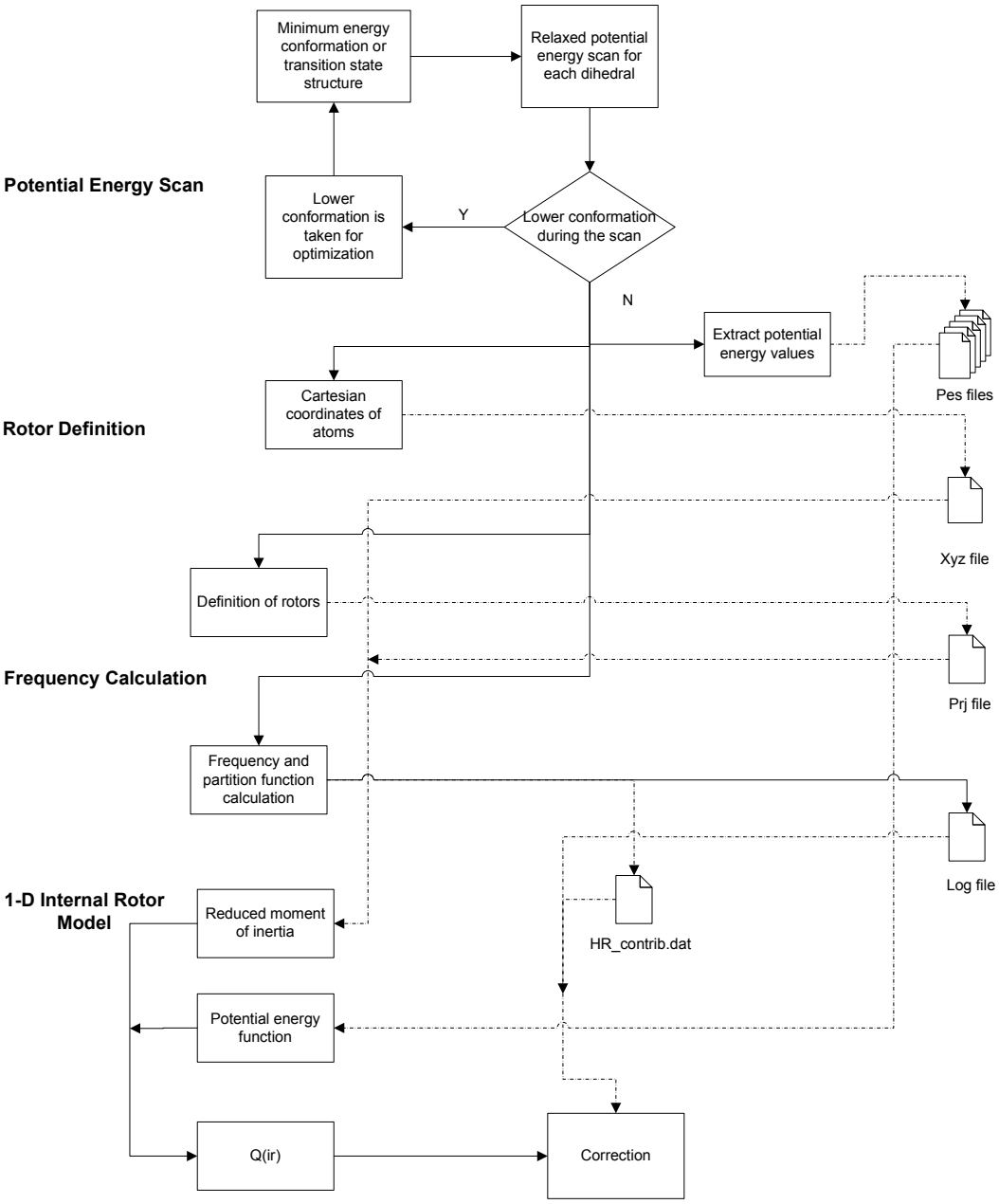

Figure 3.6: Flowsheet showing the process of one-dimensional treatment of hindered rotations. The process begins with an optimized structure or transition state, and the outputs are the corrected partition functions for subsequent calculation of kinetic parameters and thermodynamic properties.

- *qsf*: Scale factor for frequencies for partition function
- *irf*: Flag to treat torsional modes using one-dimensional partition functions

Calctherm is designed to calculate the thermodynamic properties including entropy (S), enthalpy (H) and heat capacity (C_v) with low frequencies treated using the one-dimensional internal rotor model for a single molecule. The required input files (atomic coordinates, definition of rotors, output files from *Gaussian 03* and potential energy scan files) are identical to those required for *calck*. The following options are provided by *calck*:

- *qsf*: Frequency scale factor for partition function
- *ssf*: Scale factor for the calculation of S_{vib} (default factor is 1.0015)
- *hsf*: Scale factor for the calculation of H_{vib} (default factor is 1.0015)
- *irf*: Flag to treat torsional modes using one-dimensional partition functions
- *Solvent*: The total energy is based on PCM calculation from *Gaussian 03*

3.9 Future Work

In this research, low frequencies were treated using a one-dimensional internal rotor model. As will be shown in subsequent chapters, treating low frequency torsional motions as hindered rotations influences both frequency factors and activation energies, with a more dramatic impact on the frequency factor. The general result is that the calculated values are in better agreement with experimental values than the results based on a harmonic oscillator treatment.

While substantial advances were made to make the one-dimensional internal rotor model applicable to more complex molecules in a general way, some issues remain targets for future work. The influence of the reduction degree in calculating the reduced moment of inertia on the energy

levels and partition functions was not discussed. In the solution of the energy levels, the reduced moment of inertia was treated as a constant. The change of the reduced moment of inertia as a function of the rotation angle was not considered. Furthermore, the current substitution methodology involves "*bulk*" replacement, which is based on the assumption that dispersing the rotational motion of a rotor among various frequencies and a pure rotation have the same resulting partition function. It was found that with increasing molecular size, highly mixed motions make the identification of torsional motions more difficult, which is one of the reasons this substitution method may not be applicable for larger systems. Schlegel et al. developed an identification method based on the displacement of atoms in terms of an identification matrix (Ayala and Schlegel (1998)), but this method has not been widely used. Efforts should be targeted to advance the development of a more quantitative identification treatment. Finally, the coupling of various internal rotors with each other and with external rotation was neglected in the treatment because of the high computational expense. A simplified treatment which is less computationally demanding but can incorporate coupling among various rotations needs to be developed.

Table 3.1: $Q_{int,rot}$ of the four rotors of methyl methacrylate monomer defined in Figure 3.1 based on a one-dimensional internal rotor model as a function of the number of grid points used to solve the one-dimensional Schrödinger equation and temperature.

	$Q_{int,rot,D1}$			$Q_{int,rot,D2}$			$Q_{int,rot,D3}$			$Q_{int,rot,D4}$		
T(K)	**1000**	**5000**	**%Dev.**	**1000**	**5000**	**%Dev.**	**1000**	**5000**	**%Dev.**	**1000**	**5000**	**%Dev.**
298.15	1.402	1.400	0.12	3.116	3.105	0.33	1.084	1.071	1.16	1.980	1.979	0.06
300	1.412	1.410	0.12	3.136	3.126	0.33	1.091	1.078	1.16	1.993	1.991	0.06
350	1.676	1.674	0.10	3.701	3.690	0.29	1.284	1.270	1.06	2.314	2.313	0.05
400	1.936	1.934	0.09	4.269	4.258	0.27	1.476	1.462	0.98	2.619	2.618	0.05
450	2.190	2.188	0.08	4.841	4.829	0.24	1.669	1.653	0.92	2.907	2.906	0.04
500	2.437	2.435	0.07	5.418	5.406	0.23	1.861	1.845	0.86	3.182	3.180	0.04
550	2.678	2.676	0.06	5.999	5.987	0.21	2.054	2.037	0.82	3.443	3.442	0.03
600	2.912	2.910	0.06	6.586	6.573	0.20	2.248	2.230	0.77	3.692	3.691	0.03
700	3.360	3.358	0.05	7.772	7.759	0.17	2.638	2.619	0.71	4.161	4.160	0.03
800	3.783	3.781	0.04	8.974	8.960	0.15	3.035	3.015	0.65	4.595	4.594	0.02

Chapter 4

Homopolymerization Propagation of Methyl Methacrylate and Methyl Acrylate

4.1 Introduction

In free radical polymerization, propagation is the reaction to increase chain length, as illustrated in Figure 4.1 for methyl methacrylate and methyl acrylate. With the advent of pulsed laser polymerization in combination with size exclusion chromatography (PLP-SEC), direct measurement of propagation rate constants (k_p) is feasible (Beuermann et al. (1997, 2000, 1996); Buback et al. (1998)). However, measurement of k_p for polymerization reactions is confounded when transfer or other reactions are significant between laser pulses (Beuermann et al. (1996); Buback et al. (1998)). For cross-propagation in copolymerization, PLP-SEC needs to be used in combination with modeling to determine reactivity ratios (Buback et al. (2001); Hutchinson et al. (1998)).

It is thus valuable to have alternative methods for specifying rate coefficients of the elementary steps composing polymerization. In particular, the use of quantum chemistry to calculate rate coefficients in free radical polymerization systems is particularly attractive (Fischer and Radom (2001)). Computational chemistry can be applied to any reaction type, and extracting quantitative

values of rate coefficients does not rely on assuming a model such as the terminal or penultimate models commonly used in copolymerization. With the development of computational quantum chemistry, obtaining accurate kinetic parameters via a computational approach is feasible, especially for reactions of small molecules (Hehre et al. (1986); Irikura (1998); Pilar (1990)). Recently, this approach has been extended to the determination of polymerization reactions. However, these studies have focused on small monomers such as ethylene, vinyl chloride and acrylonitrile (Heuts and Gilbert (1995); Huang et al. (1998); Izgorodina and Coote (2006); Van Cauter et al. (2006)). Nevertheless, this body of work provides guidance about the different choices that must be made when quantitatively accurate values of rate coefficients in polymerization are sought. Heuts and Gilbert and Van Cauter et al. both studied radical addition reactions of ethlyene using quantum chemical calculations (Heuts and Gilbert (1995); Van Cauter et al. (2006)). Heuts and Gilbert used a relatively low level method, HF/3-21G, to optimize geometries based on the conclusion that geometry is not sensitive to the method and basis set. A high level method, QCISD(T)/6-311G(d,p) was used to calculate the activation energy (Heuts and Gilbert (1995)), and an artificial heavy atom was used on the chain end to simulate the presence of a long chain. Van Cauter et al. used B3LYP/6-31G(d) for both geometry optimization and calculation of the energies. The influence of chain length was studied by increasing the radical chain length to 15 (Van Cauter et al. (2006)). Both sets of researchers went beyond the rigid-rotor, harmonic oscillator (HO) approximation and treated low frequency modes as internal rotations. Van Cauter and coworkers analyzed the difference between the results obtained when one-dimensional and two-dimensional hindered rotor models were used and found that these two treatments only differed slightly. Izgorodina and Coote studied the homopolymerization of acrylonitrile and vinyl chloride (Izgorodina and Coote (2006)). Geometry optimization was performed using B3LYP/6-31G(d), and the influence of the calculation method on the activation energy for k_p was probed for various methods, including density functional theory (B-LYP, B3LYP, MPWB1B95, BB1K, MPWB1K), ROMP2 with a basis set of

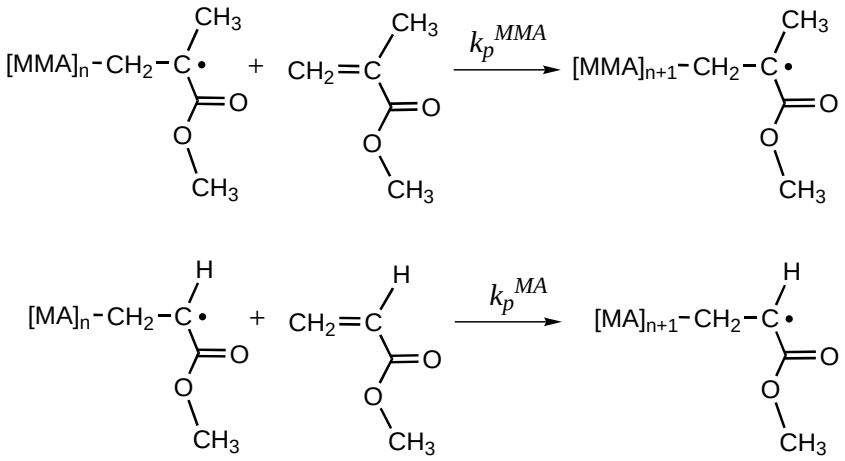

Figure 4.1: Methyl methacrylate and methyl acrylate propagation reactions.

6-311+G(3df,3p), and the hybrid ONIOM method. Polymeric radicals only as large as three units long were studied, and low frequencies were treated using a one-dimensional internal rotor model.

In the present work, we extended this general approach to calculate k_p for larger monomers, methyl methacrylate and methyl acrylate. Because of the size of the reaction systems, density functional theory (DFT) was used for all calculations, which has been shown to provide a compromise between computational time and accuracy in previous research (Coote (2005); Fischer and Radom (2001); Izgorodina and Coote (2006); Van Cauter et al. (2006); Wong and Radom (1998)). Geometry optimization, location of transition states and potential energy scans for treatment of internal rotations were all based on unrestricted B3LYP/6-31G(d). B3LYP with three different basis sets (6-31G(d), 6-31G(d,p) and 6-311G(d,p)), MPWB1K/6-31G(d,p) and B1B95/6-31G(d,p) were used to calculate the electronic energy (E_e). The results from the harmonic oscillator model and internal rotation treatment were contrasted. Activation energies and frequency factors were regressed from ln$k$ versus 1/T over a temperature range of 298.15 to 800 K, and the calculated data were benchmarked against the experimental data of Buback et al., who measured k_p for methyl

methacrylate between -1 °C and 90 °C using PLP-SEC as reported in Equation 4.1 (Beuermann et al. (1997)):

$$k_p^{MMA}\,(L{\cdot}mol^{-1}{\cdot}s^{-1}) = 2.67 \times 10^6\, e^{\frac{-22.4\,(kJ{\cdot}mol^{-1})}{RT}} \tag{4.1}$$

and k_p for methyl acrylate between -19 °C and 32 °C as reported in Equation 4.2 (Buback et al. (1998)):

$$k_p^{MA}\,(L{\cdot}mol^{-1}{\cdot}s^{-1}) = 1.66 \times 10^7\, e^{\frac{-17.7\,(kJ{\cdot}mol^{-1})}{RT}} \tag{4.2}$$

The goal of this work was to develop a computational methodology to study acrylate polymerization reactions that is quantitatively accurate yet computationally affordable. Given the validation of the present results against experimental data, the methodology can then be extended with confidence to other reactions in acrylate systems, including copolymerization and side reactions such as transfer and scission.

4.2 Method and Computational Details

Propagation of methyl methacrylate and methyl acrylate was studied using the addition of monomeric, dimeric and trimeric radicals to monomer as shown in Figure 4.2. *Gaussian 03* was used for all of the calculations (Frisch et al. (2004)). All the reactants and products were first optimized using unrestricted B3LYP/6-31G(d) via conventional gradient-based optimization (Foresman (2002); Schlegel (1982)). However, the optimized geometry is dependent on the initial structure provided as input, particularly for large species with many degrees of freedom. Although a Boltzmann distribution of low energy conformers will exist during reaction, we sought to find the lowest energy conformations for the reactants and the products. In order to overcome the barriers between "*local*" minimum conformations and locate "*global*" minimum conformations, potential energy scans were performed for each single bond in the optimal structure identified by conventional optimization. Unrestricted B3LYP/6-31G(d) was also used for all potential scans. If lower energy conformers

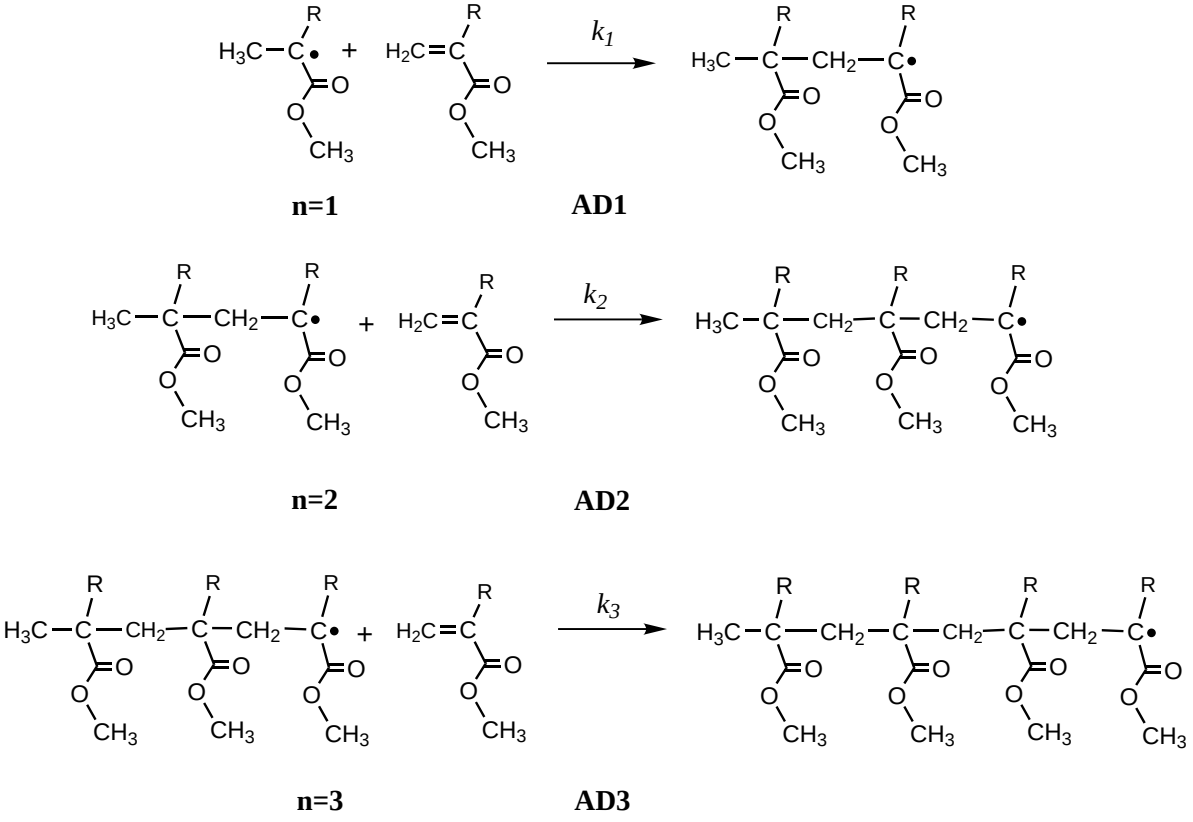

Figure 4.2: Methyl methacrylate and methyl acrylate addition reactions were studied as a function of chain length. ADn is used to denote the different calculations performed, where n is the number of monomeric units in the radical reactant. For methyl methacrylate, R is a CH_3 group, and for methyl acrylate, R is a hydrogen atom.

were identified, a new set of potential energy scans was carried out until no conformations of lower energy were obtained. Although one-dimensional torsional scans do not guarantee that the global minimum will be located, much of the variation in conformations is derived from torsional motions around single bonds, and our approach did indeed often identify conformations that were lower in energy than the one obtained by conventional optimization.

To locate transition state structures, the QST3 method was used, which requires the optimized reactants, product and an estimate of the transition state (Peng et al. (1996)). Because all the addition reactions follow the same basic reaction path, i.e., addition of the radical center to the unsaturated C=C bond of the monomer, the estimated transition state was constructed by elongating the carbon-carbon single bond in the $\beta-$position to the radical center of the addition product to a bond length of 2.3 Å. Transition states were identified as saddle points on the potential energy surface, possessing one imaginary frequency. Once possible transition state structures were identified, they were verified using intrinsic reaction coordinate (IRC) following with a step size of 0.1 amu$^{0.5}$-Bohr. Unrestricted B3LYP/6-31G(d) was used for both the QST3 and the IRC calculations. Frequencies were also calculated using unrestricted B3LYP/6-31G(d), and the zero-point vibrational energy (ZPVE) was calculated using a scale factor of 0.9806 (Scott and Radom (1996)). A scale factor of 1.0002 was used in the calculation of partition functions based on the recommended scale factors for ΔH_{vib} and ΔS_{vib} reported by Scott and Radom (1996).

With the optimized structures in hand, the electronic energy, E_e, was obtained from single point calculations using unrestricted B3LYP with three different basis sets (6-31G(d), 6-31G(d,p) and 6-311G(d,p)), MPWB1K/6-31G(d,p), which was optimized against barrier heights based on nine elementary reactions by Zhao and Truhlar (2004) and B1B95/6-31G(d,p) (Becke (1996)) for both methyl methacrylate and methyl acrylate. In addition to the gas phase values calculated, their application to condensed phase chemistry was evaluated using a polarizable continuum model (PCM), in which the solvent was treated as a polarizable continuum, and the solute was placed in a cavity within the solvent (Cances et al. (1997)). Dielectric constants of methyl methacrylate (ε) equal to 6.32 and methyl acrylate (ε) equal to 7.03 were used to simulate the bulk reaction environment (Speight (2004)). Reaction rate constants for propagation were then calculated using Equation 4.3 at a series of temperatures from 298.15 to 800 K based on transition state theory

(Pfaendtner and Broadbelt (2007a)):

$$k(T) = \kappa(T)\frac{k_B T}{h}(c^o)^{1-m}\frac{Q^{\ddagger}}{Q_{mon}Q_{rad}}e^{-\Delta E_0/RT} \tag{4.3}$$

where $\kappa(T)$ is the tunneling factor, k_B is Boltzmann's constant (1.3806×10^{-23} J·mol^{-1}·K^{-1}), h is Planck's constant (6.6261×10^{-34} J·s), m is the number of reactants, which is two for propagation, c° is the standard state concentration (mol·L^{-1}) to which the quantum chemical calculations are referenced, $\frac{P}{RT}$, where P is 1 atm, and ΔE_0 is the difference between $E_{\circ}$ of the transition state and the reactants, which is defined as the summation of the electronic energy (E_e) and the zero-point vibrational energy (ZPVE):

$$E_{\circ} = E_e + ZPVE \tag{4.4}$$

ZPVE is the contribution to the energy from vibration at 0 K as defined in Equation 4.5 (McQuarrie and Simon (1999)):

$$ZPVE = \frac{1}{2}\sum_{i}^{3N-6} h\nu_i \tag{4.5}$$

in which N is the number of atoms, and ν_i represents the frequencies. For transition states, $3N-7$ frequencies are included in the ZPVE. The tunneling factor ($\kappa(T)$) was assumed to be one for the radical addition reactions studied here. Tunneling effects would be important in related radical reactions, such as atom transfer reactions (Coote (2005); Pfaendtner et al. (2006)), and would need to be calculated explicitly such as we have done in other work studying intramolecular and intermolecular hydrogen transfer of peroxy radicals (Pfaendtner and Broadbelt (2007b); Pfaendtner et al. (2006)).

A critical part of obtaining accurate values of $k(T)$ is specifying the values of $Q^{\ddagger}$, Q_{mon} and Q_{rad} in Equation 4.3, which are the partition functions for the transition state, the monomer and the radical. The partition function is conventionally considered to include contributions from four different modes: electronic (Q_e), translation (Q_{tr}), rotation (Q_r) and vibration (Q_{vib}) as shown in

Equation 4.6:

$$Q = Q_e Q_{tr} Q_r Q_{vib} \tag{4.6}$$

For species in their ground state, $Q_e = 1$, and Q_{tr} and Q_r are defined in standard textbooks (McQuarrie and Simon (1999)). Q_{vib} is the vibrational partition function based on the contributions from the individual frequencies, which are often calculated using the harmonic oscillator (HO) approximation. However, this is known to be inaccurate for some motions characterized by low frequencies, which are often better treated as hindered rotations. If there are many torsional motions with low frequencies, their contributions can be quite large, and the difference between the partition function values can be significant. To account for these hindered rotations, Q_{vib} is treated using an internal rotor model as shown in Equation 4.7:

$$Q = Q_e Q_{tr} Q_r Q_{vib} Q_{int,rot} \tag{4.7}$$

where $Q_{int,rot}$ is the contribution to the partition function of the low vibrational modes that are better treated as internal rotations. There is no well accepted cutoff value to define "*low*" frequencies. In the literature, 200 cm^{-1} was used as the upper limit to define low frequencies by some researchers (Heuts and Gilbert (1995)), while 300 cm^{-1} was used in other examples (Izgorodina and Coote (2006)). The frequencies lower than the cutoff value were taken out of Q_{vib} and replaced by $Q_{int,rot}$, which was calculated as the product of the partition functions of each rotor. For simple rotors whose potential can be expressed in the form of Equation 4.8 (where W is the rotation barrier height, n is the symmetry number of rotation, and θ is the torsional angle), McClurg et al. provided an asymptotic factor for specifying the partition function value $Q_{int,rot}$ which converges to that for a free rotor at high temperature and to a harmonic oscillator at low temperature (McClurg et al. (1997)).

$$V(\theta) = \frac{W}{2}(1 - cosn\theta) \tag{4.8}$$

However, this method is restricted to symmetric rotors and could not be used in methyl methacrylate or methyl acrylate propagation reactions.

In the present approach, we did not apply an arbitrary upper bound to define what was classified as a low frequency, and we used a method for calculating $Q_{int,rot}$ that was general for rotations of any symmetry. The number of low frequencies that were removed was set as the number of rotors, which included rotations about σ bonds and the bond defining the transition state. Although the bond defining the transition state is not a real bond, it is treated as a hindered rotor since the lowest positive frequency in the transition state mainly consists of torsional motion about this bond. Rather than simply removing the contribution of the N lowest frequencies from Q_{vib}, where N is the number of rotors, the low frequencies were examined to make sure they consisted of rotational components. Interestingly, all vibrational motions that were removed for all species had frequencies less than 200 cm^{-1}. For the reactants (monomer and radical) and the radical product, the lowest N frequencies all had rotational components. However, the transition states were different since some low frequencies are essentially a bending motion involving the monomer and radical. For example, as shown in Figure 4.3, frequency ν-2 (45.3 cm^{-1}) in the methyl methacrylate AD1 transition state involves the bending motion of the monomer and the radical. Frequencies that did not consist of torsional motions were not treated as hindered rotations and thus remained as part of the harmonic oscillator portion of Q_{vib}. For those frequencies removed from Q_{vib}, their contributions to ZPVE were also removed. The partition function of the m-th internal rotor was calculated using Equation 4.9:

$$Q_{int,rot,m} = \frac{1}{\sigma_m} \sum_i exp(-\frac{\epsilon_i}{k_B T}) \tag{4.9}$$

where σ_m is the symmetry number of the internal rotation and ϵ_i are the energy levels of the internal rotation, which were calculated by solving a one-dimensional Schrödinger equation:

$$-\frac{\hbar^2}{2I_{red}} \frac{d^2}{d\theta^2} \Psi + V(\theta)\Psi = \epsilon \Psi \tag{4.10}$$

where $\hbar$ is Planck's constant divided by 2π, Ψ is the wave function, θ is the torsional angle, and I_{red} is the reduced moment of inertia, which was defined as $I^{2,3}$ in accord with the systematic classification of moments of inertia by East et al. (East and Radom (1997)). $V(\theta)$ was determined from relaxed potential energy scans calculated using unrestricted B3LYP/6-31G(d) in intervals of 30 °; thus, a total 12 optimized conformations from 0° to 360° were obtained for each rotor. $V(\theta)$ was expanded using a full Fourier series as in Equation 4.11:

$$V(\theta) = \sum_{i=1}^{n} [a_i(1 - cosi\theta) + b_i sini\theta] \tag{4.11}$$

where a_i and b_i are the coefficients of the expansion. Equation 4.11 can be written in its matrix product form, and the coefficients a_i and b_i were determined by solving an overdetermined matrix. In order to ensure this matrix was overdetermined, the number of coefficients was less than the number of energy points during the rotation. For a scan interval of 30 °, n was set equal to three. This was demonstrated to be a sufficient number of coefficients to ensure acceptable fits for all potential energy scans. For example, potential energy scans for the four rotors in methyl methacrylate monomer outlined in Figure 4.4 are shown in Figure 4.5. The potential energy scans are shown as points, and the fitted curves using Equation 4.11 are shown as the lines. The four rotors shown in Figure 4.4 include both symmetric rotors (e.g., methyl group) and asymmetric rotors (e.g., methoxy group).

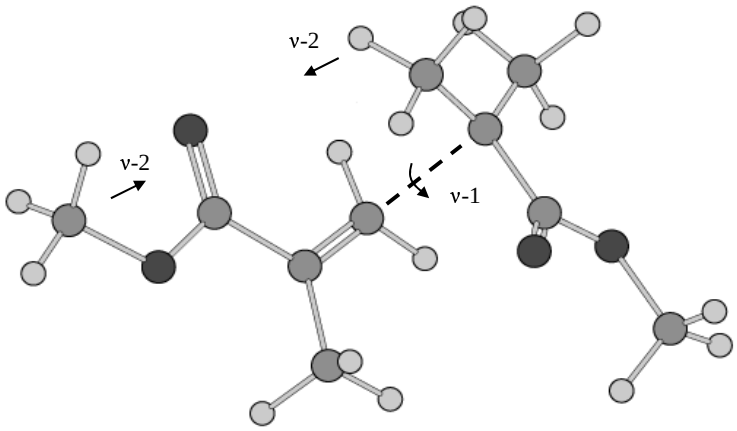

Figure 4.3: The transition state for the AD1 reaction of methyl methacrylate shown in Figure 4.2 and characteristic motions of two of its frequencies. ν-1 (20.3 cm^{-1}) is the lowest positive frequency, and it corresponds to the torsional motion about the bond defining the transition state. ν-2 (45.3 cm^{-1}) is the second lowest frequency, and it has no torsional component.

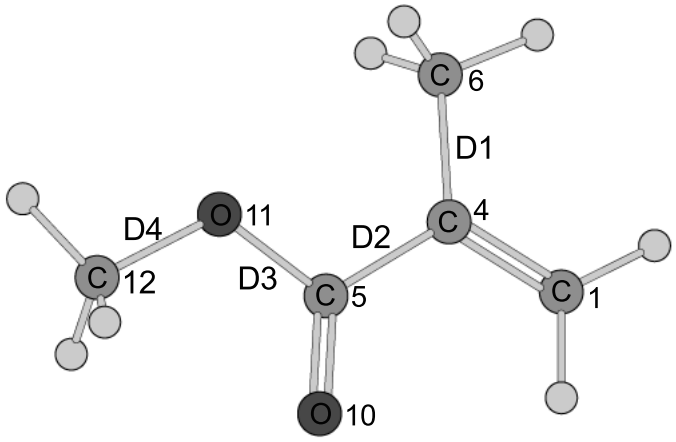

Figure 4.4: Potential energy scans were carried out for the four dihedral axes of methyl methacrylate monomer: D1 (C4,C6), D2 (C4,C5), D3 (C5,O11) and D4 (O11,C12).

The one-dimensional Schrödinger equation (Equation 4.10) was solved using the Fourier Grid Hamiltonian (FGH) method, in which the Hamiltonian operator was discretized over the torsional angle range, and the energy levels, ϵ_i (eigenvalues), were calculated by diagonalizing the Hamiltonian matrix (Balint-Kurti et al. (1992)). In this research, the Hamiltonian operator was discretized using 1000 points. Comparison of partition functions calculated for methyl methacrylate monomer showed that 1000 points gave results that were consistent with finer grids containing 5000 points; the maximum deviation was less than 1.2%, and the deviation decreased with increasing temperature, as shown in Table 4.2. The calculation of the reduced moment of inertia, solution of the Fourier coefficients and Schrödinger equation, and calculation of the partition functions was carried out with "*calck*" developed in our group (Pfaendtner et al. (2007)).

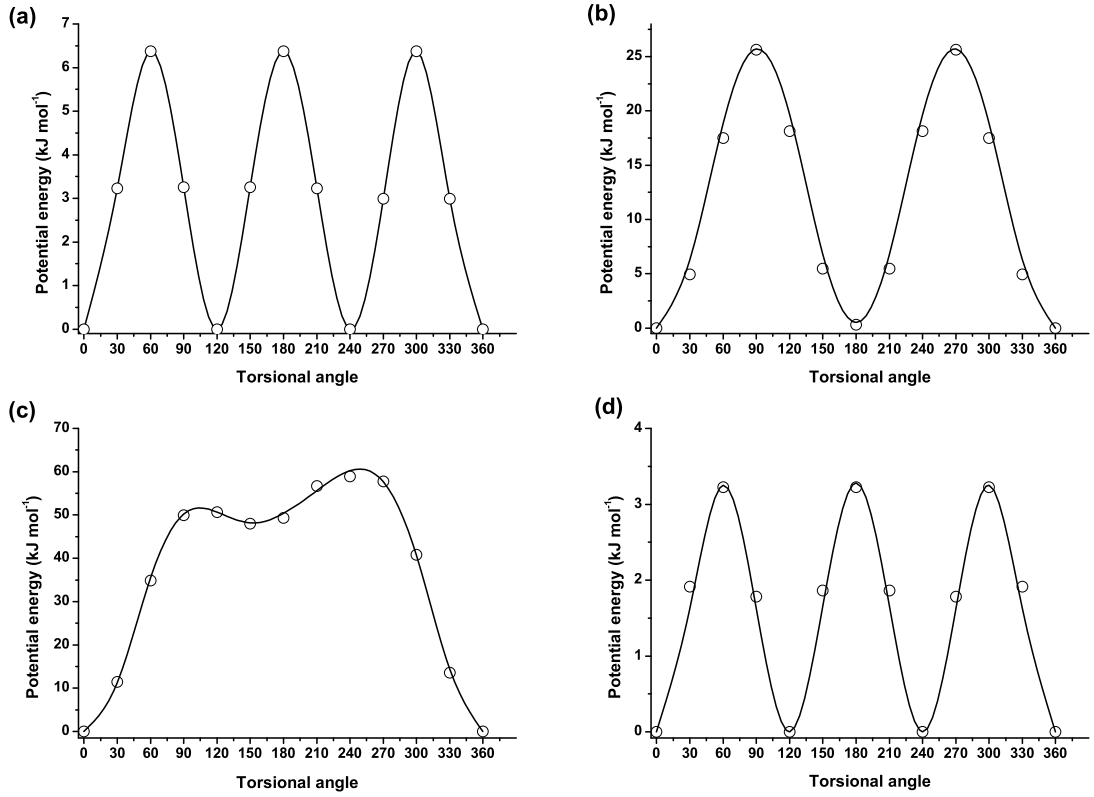

Figure 4.5: Potential energy scans for all the dihedrals defined for methyl methacrylate monomer in Figure 4.4: (a) D1, (b) D2, (c) D3 and (d) D4. The potential energy scans carried out in 30° increments using unrestricted B3LYP/6-31G(d) are shown as points, and the Fourier fits are shown as lines.

Table 4.1: $Q_{int,rot}$ of the four rotors of methyl methacrylate monomer defined in Figure 4.4 based on a one-dimensional internal rotor model as a function of the number of grid points used to solve the one-dimensional Schrödinger equation and temperature

	$Q_{int,rot,D1}$			$Q_{int,rot,D2}$			$Q_{int,rot,D3}$			$Q_{int,rot,D4}$		
T(K)	**1000**	**5000**	**%Dev.**	**1000**	**5000**	**%Dev.**	**1000**	**5000**	**%Dev.**	**1000**	**5000**	**%Dev.**
298.15	1.402	1.400	0.12	3.116	3.105	0.33	1.084	1.071	1.16	1.980	1.979	0.06
300	1.412	1.410	0.12	3.136	3.126	0.33	1.091	1.078	1.16	1.993	1.991	0.06
350	1.676	1.674	0.10	3.701	3.690	0.29	1.284	1.270	1.06	2.314	2.313	0.05
400	1.936	1.934	0.09	4.269	4.258	0.27	1.476	1.462	0.98	2.619	2.618	0.05
450	2.190	2.188	0.08	4.841	4.829	0.24	1.669	1.653	0.92	2.907	2.906	0.04
500	2.437	2.435	0.07	5.418	5.406	0.23	1.861	1.845	0.86	3.182	3.180	0.04
550	2.678	2.676	0.06	5.999	5.987	0.21	2.054	2.037	0.82	3.443	3.442	0.03
600	2.912	2.910	0.06	6.586	6.573	0.20	2.248	2.230	0.77	3.692	3.691	0.03
700	3.360	3.358	0.05	7.772	7.759	0.17	2.638	2.619	0.71	4.161	4.160	0.03
800	3.783	3.781	0.04	8.974	8.960	0.15	3.035	3.015	0.65	4.595	4.594	0.02

4.3 Results and Discussion

4.3.1 Geometry Optimization

All the reactants and products in the reactions shown in Figure 4.2 were optimized conventionally using *Gaussian 03* and the "*opt*" keyword. Relaxed potential energy scans were carried out for each single bond and the bond defining the transition state for TS structures using the "*opt(modredundant)*" keyword. These one-dimensional scans were used to calculate $V(\theta)$ in Equation 4.10 but also to identify lower energy conformations that conventional geometry optimization did not locate. As an example of this, Figure 4.6 shows the energy profile for the scan of a CH_3 group of methyl methacrylate monomer (D4 in Figure 4.4), in which the initial point A (torsional angle equals 0) corresponds to the conformation obtained using conventional optimization (conformation A in Figure 4.6). From this plot, we can see that even for one of the simplest structures in this research, methyl methacrylate monomer, a lower energy structure (conformation B in Figure 4.6) was identified from the one-dimensional potential energy scan, which was about 1.8 kJ·mol^{-1} lower in electronic energy. Thus, the conformation with the lowest energy from the scan (conformation B in Figure 4.6) was used as input for further optimization. For all structures, this process was repeated until no conformations of lower energy were identified.

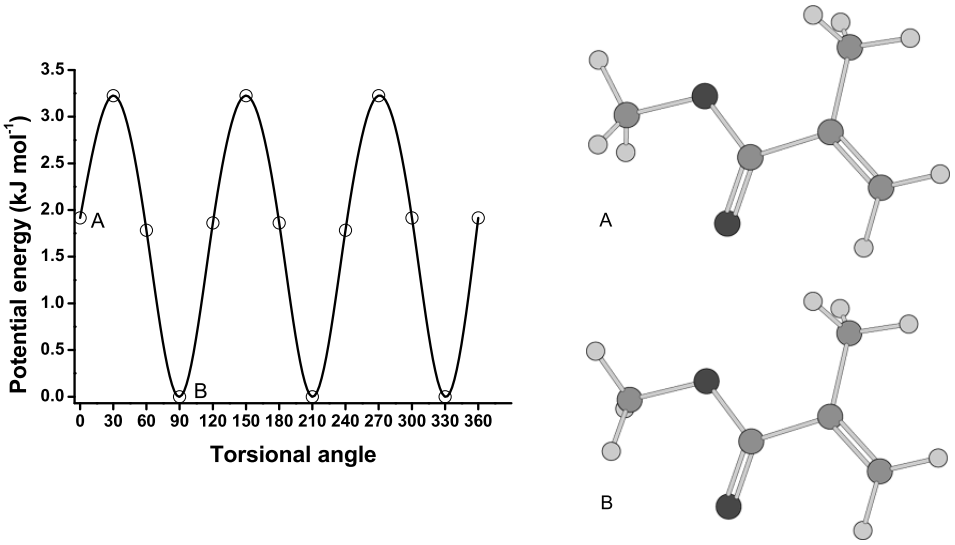

Figure 4.6: Energy profile for the rotation of a methyl group of methyl methacrylate monomer (D4 in Figure 4.4) based on a conformation optimized using unrestricted B3LYP/6-31G(d) and conventional optimization. Note that the structure identified via the combination of the potential energy scan and conventional optimization (conformation B) is lower than that identified via conventional optimization (conformation A).

The bond length of the bond defining the transition state indicates the relative progress along the reaction coordinate. The transition states of the AD1 to AD3 reactions for methyl methacrylate obtained from unrestricted B3LYP/6-31G(d) are shown in Figure 4.7. The bond lengths of the bond defining the methyl methacrylate transition states of AD1, AD2 and AD3 are 2.268 Å, 2.242 Å and 2.235 Å, respectively, which are different by less than 0.04 Å. The bond lengths of the bond defining the methyl acrylate transition states of AD1, AD2 and AD3 are 2.302 Å, 2.299 Å and 2.296 Å, respectively, which are different by less than 0.01 Å. The dihedral angles formed by the methyl methacrylate transition state bond C_1=$C_2 \cdots C_3$-C_4 as shown in Figure 4.7 are 168.5°, 174.9° and 177.0° for AD1, AD2 and AD3, respectively, and the corresponding dihedral angles for methyl acrylate are 172.3°, 179.3° and 174.0° for AD1, AD2 and AD3, respectively. These four carbon atoms are nearly in the same plane, which corresponds to the stable conformation of the product.

4.3.2 Calculation Method and Basis Set Comparison

One of the most challenging aspects of using quantum chemistry to study large molecules is to find a suitable method and basis set. This is especially important when activation energies are of interest since the reaction energy barrier is sensitive to the calculation method. Although high level methods such as QCISD(T)/6-311G(d,p) and CBS-RAD have been used in previous research related to radical addition reactions (Fischer and Radom (2001)), they have been applied to relatively small reactions and are too expensive for reaction systems that involve a large number of atoms like methyl methacrylate and methyl acrylate propagation. Since the geometry is not highly sensitive to the method/basis set, unrestricted B3LYP/6-31G(d) was used for geometry optimization, location of transition states and potential energy scans. However, the activation energy based on E_e calculated with unrestricted B3LYP/6-31G(d) was too high compared to experimental results as summarized in Table 4.2 and Table 4.3. For AD3 of methyl methacrylate, the unrestricted

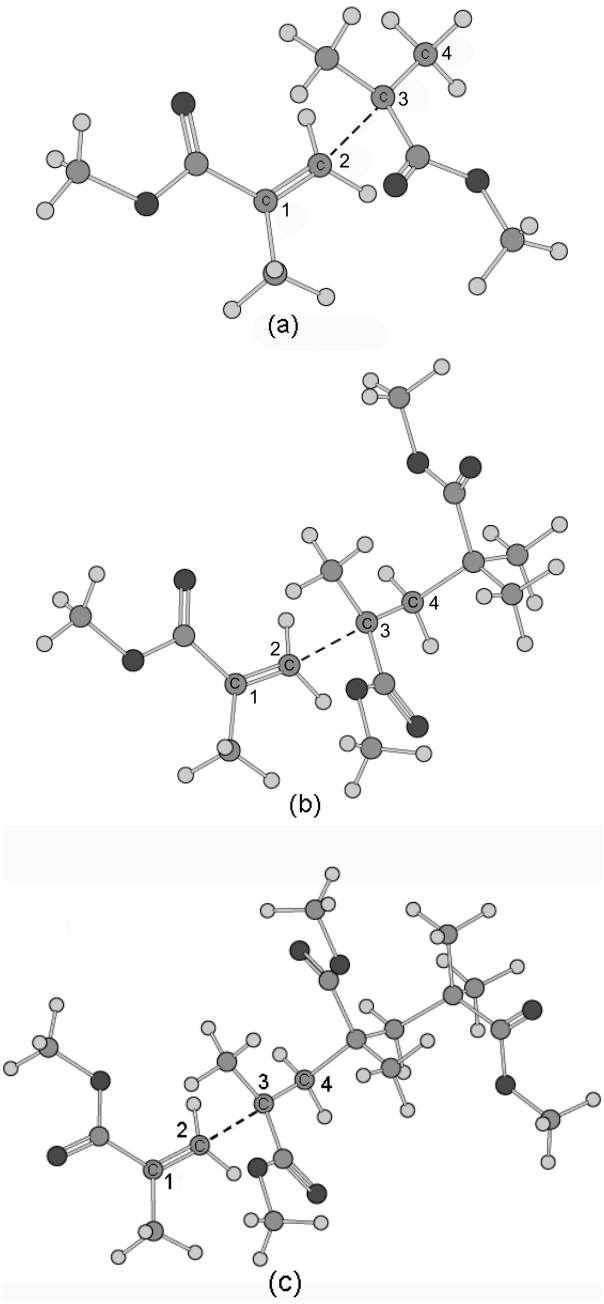

Figure 4.7: Transition state structures for the (a) AD1, (b) AD2 and (c) AD3 reactions of methyl methacrylate located using unrestricted B3LYP/6-31G(d).

Table 4.2: Electronic energy (E_e), zero point-corrected energy ($E_\circ$) of reaction and activation energy (E_a) for both the harmonic oscillator (HO) and hindered rotor (HR) models as a function of chain length (AD1, AD2 and AD3 in Figure 4.2) for methyl methacrylate propagation.

AD1	**UB3LYP 6-31G(d)**	**UB3LYP 6-31G(d,p)**	**UB3LYP 6-311G(d,p)**	**MPWB1K 6-31G(d,p)**	**B1B95 6-31G(d,p)**
ΔE_e	23.5	23.4	27.7	12.2	23.4
$\Delta E_\circ$	28.4	28.3	32.6	17.1	28.3
E_a^{HR}	38.9	38.8	43.1	27.7	38.8
E_a^{HO}	35.2	35.1	39.4	24.0	35.1
AD2	**UB3LYP 6-31G(d)**	**UB3LYP 6-31G(d,p)**	**UB3LYP 6-311G(d,p)**	**MPWB1K 6-31G(d,p)**	**B1B95 6-31G(d,p)**
ΔE_e	28.5	28.6	34.0	12.2	26.4
$\Delta E_\circ$	33.0	33.1	38.5	16.7	30.9
E_a^{HR}	44.3	44.5	49.9	28.0	42.3
E_a^{HO}	40.3	40.4	45.8	23.9	38.2
AD3	**UB3LYP 6-31G(d)**	**UB3LYP 6-31G(d,p)**	**UB3LYP 6-311G(d,p)**	**MPWB1K 6-31G(d,p)**	**B1B95 6-31G(d,p)**
ΔE_e	32.1	32.1	37.8	15.2	28.4
$\Delta E_\circ$	36.2	36.2	41.9	19.3	32.5
E_a^{HR}	39.6	39.6	45.3	22.7	35.9
E_a^{HO}	43.6	43.6	49.3	26.8	40.0

[1] Units: kJ·mol^{-1}

[2] Methyl methacrylate propagation E_a obtained from PLP-SEC: 22.4 kJ·mol^{-1}

[3] ZPVE values were calculated using UB3LYP/6-31G(d) with a scale factor of 0.9806. ZPVE(AD1)=4.9 kJ·mol^{-1}, ZPVE(AD2)=4.5 kJ·mol^{-1}, ZPVE(AD3)=4.1 kJ·mol^{-1}.

B3LYP/6-31G(d) activation energy is about 17 kJ·mol^{-1} higher than that from PLP-SEC. For AD3 of methyl acrylate, the unrestricted B3LYP/6-31G(d) activation energy is about 10 kJ·mol^{-1} higher than the experimental value. For unrestricted B3LYP, larger basis sets did not improve the agreement with the experimental results: for methyl methacrylate AD3, the activation energies calculated with unrestricted B3LYP/6-31G(d,p) and B3LYP/6-311G(d,p) are about 17 kJ·mol^{-1} and 23 kJ·mol^{-1} higher, respectively, than the experimental result; for methyl acrylate AD3, the activation energies calculated with unrestricted B3LYP/6-31G(d,p) and B3LYP/6-311G(d,p) are about 10 kJ·mol^{-1} and 14 kJ·mol^{-1} higher, respectively, than the experimental result.

Table 4.3: Electronic energy (E_e), zero point-corrected energy ($E_\circ$) of reaction and activation energy (E_a) for both the harmonic oscillator (HO) and hindered rotor (HR) models as a function of chain length (AD1, AD2 and AD3 in Figure 4.2) for methyl acrylate propagation.

AD1	**UB3LYP 6-31G(d)**	**UB3LYP 6-31G(d,p)**	**UB3LYP 6-311G(d,p)**	**MPWB1K 6-31G(d,p)**	**B1B95 6-31G(d,p)**
ΔE_e	18.3	18.6	22.3	13.9	16.0
$\Delta E_\circ$	22.7	23.0	26.7	18.3	20.4
E_a^{HR}	31.1	31.4	35.1	26.4	28.8
E_a^{HO}	30.2	30.5	34.2	25.5	27.9
AD2	**UB3LYP 6-31G(d)**	**UB3LYP 6-31G(d,p)**	**UB3LYP 6-311G(d,p)**	**MPWB1K 6-31G(d,p)**	**B1B95 6-31G(d,p)**
ΔE_e	16.8	17.1	21.2	10.9	14.6
$\Delta E_\circ$	20.3	20.6	24.7	14.4	18.1
E_a^{HR}	28.9	29.2	33.3	22.8	26.7
E_a^{HO}	28.5	28.8	32.9	22.4	26.3
AD3	**UB3LYP 6-31G(d)**	**UB3LYP 6-31G(d,p)**	**UB3LYP 6-311G(d,p)**	**MPWB1K 6-31G(d,p)**	**B1B95 6-31G(d,p)**
ΔE_e	21.2	21.6	25.3	15.3	19.2
$\Delta E_\circ$	24.4	24.8	28.5	18.5	22.4
E_a^{HR}	27.5	27.9	31.6	21.5	25.5
E_a^{HO}	32.9	33.3	37.0	26.9	30.9

[1] Units: kJ·mol^{-1}

[2] Methyl acrylate propagation E_a obtained from PLP-SEC: 17.7 kJ·mol^{-1}

[3] ZPVE values were calculated using UB3LYP/6-31G(d) with a scale factor of 0.9806. ZPVE(AD1)=4.4 kJ·mol^{-1}, ZPVE(AD2)=3.5 kJ·mol^{-1}, ZPVE(AD3)=3.2 kJ·mol^{-1}.

The use of two other DFT methods, MPWB1K/6-31G(d,p) and B1B95/6-31G(d,p), to perform single point E_e calculations for methyl methacrylate was also explored as shown in Table 4.2. MPWB1K was specified in the keyword line in *Gaussian 03* by using "MPWB95" with the user-defined statement "*Iop*(3/76=0560004400)". As shown in Table 4.2, the change in the electronic energy of reaction with level of theory is very striking, which in turn translates into dramatic differences in the activation energies. The $\Delta E_\circ$ values calculated using MPWB1K/6-31G(d,p) were the lowest, which were on average 15 kJ·mol^{-1} lower than those calculated using B3LYP/6-31G(d) for methyl methacrylate. The activation energy obtained using MPWB1K/6-31G(d,p) of 22.7 kJ mol^{-1} for methyl methacrylate AD3 is the closest to the experimental E_a for methyl methacrylate propagation, which is 22.4 kJ mol^{-1}.

MPWB1K/6-31G(d,P) and B1B95/6-31G(d,p) were also used to calculate kinetic parameters for methyl acrylate addition reactions. The results are shown in Table 4.3. The results in Table 4.3 have very similar tendencies as those reported for methyl methacrylate in Table 4.2. For a given ADn reaction, the activation energies based on E_e calculated with unrestricted B3LYP/6-31G(d) are higher than those based on MPWB1K/6-31G(d,p) and B1B95/6-31G(d,p). However, the differences are smaller compared with the corresponding reactions for methyl methacrylate. For example, for the methyl acrylate AD3 reaction, the difference between unrestricted B3LYP/6-31G(d) and MPWB1K/6-31G(d,p) is about 6 kJ·mol^{-1}, while for the methyl methacrylate AD3 reaction, the difference is about 17 kJ·mol^{-1}. The activation energy based on MPWB1K/6-31G(d,p) for the methyl acrylate AD3 reaction with low frequencies treated using the internal rotation model (21.5 kJ·mol^{-1}) is the closest to the E_a value measured using PLP-SEC, which is 17.7 kJ·mol^{-1}, as was the case for methyl methacrylate.

Although calculations involving additional acrylate radicals are warranted before generalization is possible, we conclude that MPWB1K/6-31G(d,p) is an attractive method for obtaining results for acrylate polymerization with quantitative accuracy.

4.3.3 Low Frequency Treatment

In order to carry out the one-dimensional hindered rotation treatment, the sensitivity of the potential energy profiles to the step size and the level of theory was explored. Step sizes of 10° and 30° were both used for the methyl methacrylate AD1 reaction. Comparison of the data and their Fourier fits is provided in Figure 4.8. It is clear that the Fourier fits are nearly identical, and thus the properties calculated based on these scans would be the same. The agreement between the fits based on step sizes of 10° and 30° was similar for both the monomeric radical and the transition state. Therefore, the more coarse step size of 30° was used for all subsequent calculations.

Three *ab initio* methods (unrestricted B3LYP/6-31G(d), HF/6-31G(d) and HF/3-21G) and two semi-empirical methods (AM1 and PM3) were used to carry out potential energy scans, and the results were compared. Potential energy scans of methyl methacrylate monomer based on these five methods are shown in Figure 4.9. For symmetric tops, these methods afford similar potential energy shapes, but the barrier heights are different by as much as 30 kJ mol^{-1}. For asymmetric tops as shown in Figure 4.9 (c), B3LYP/6-31G(d) and HF/6-31G(d) have similar shapes and barrier heights, but the other three methods are different in both shape and barrier height. These results show that smaller basis sets and semi-empirical methods are not a viable option for investigating methyl methacrylate polymerization. Therefore, all of the internal rotor partition functions in this research were calculated based on potential energy scans with unrestricted B3LYP/6-31G(d). It is also interesting to note that the barrier height is not only determined by the type of rotating group, but it also depends on the environment where the group is located. For example, the barrier height of the CH_3 group defined as D4 in Figure 4.4 is about 3 kJ·mol^{-1} lower than that defined as D1. It is attractive to have a "general" barrier height for a type of group because of the prevalence of repeating groups in polymerization chemistry, so that the treatment of internal rotations can be greatly simplified. However, analysis of each of the rotating tops in the monomer, radicals and transition states showed that it is not quantitatively accurate for methyl methacrylate and methyl

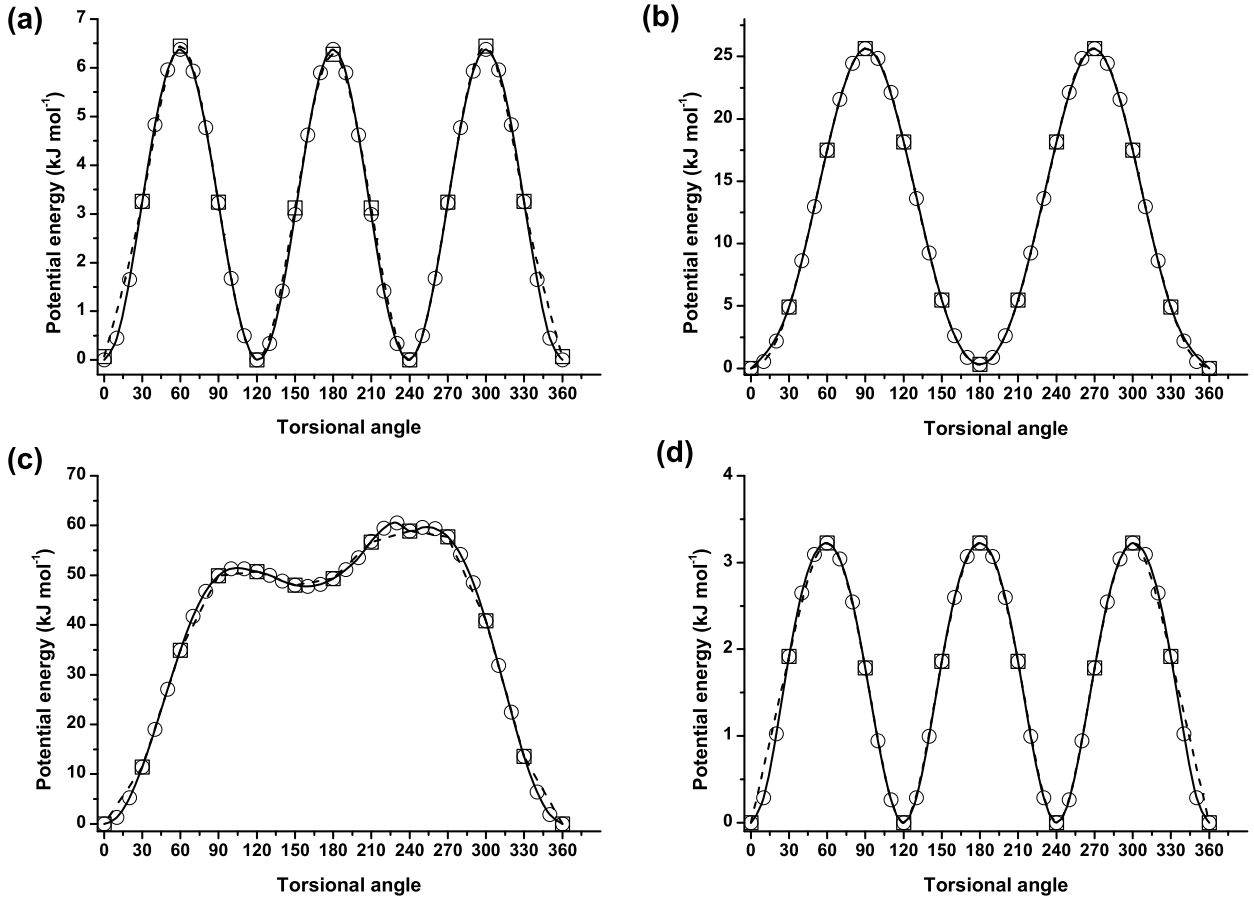

Figure 4.8: Potential energy scans for all the dihedrals defined for methyl methacrylate monomer in Figure 4.4: (a) D1, (b) D2, (c) D3 and (d) D4 at intervals of 10° (circles, solid line) and 30° (squares, dashed line) using unrestricted B3LYP/6-31G(d).

acrylate polymerization to assign a single barrier height for a type of rotating top since the rotation is inevitably influenced by its surrounding groups.

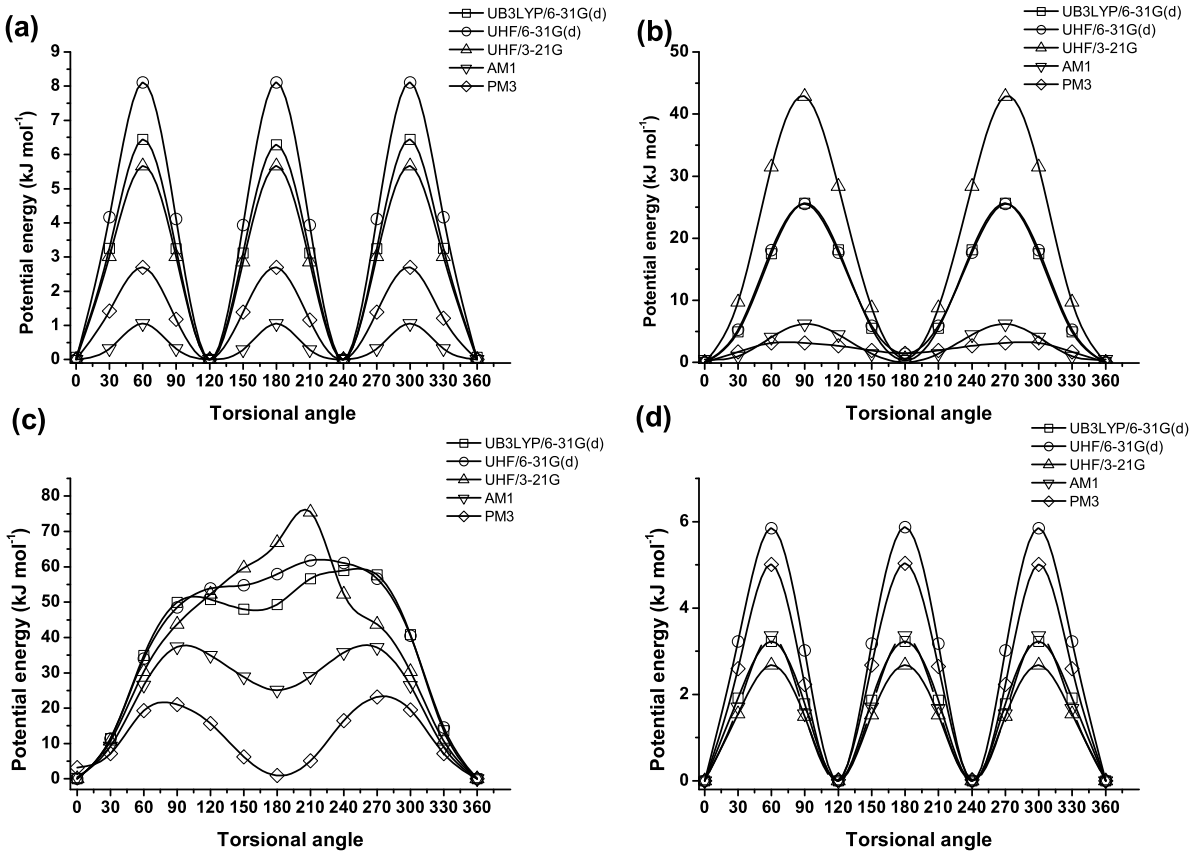

Figure 4.9: Comparison of potential energy scans for the dihedral angles of methyl methacrylate monomer using various methods. The dihedrals are defined as in Figure 4.4: (a) D1, (b) D2, (c) D3 and (d) D4.

4.3.4 Kinetics

Based on geometries optimized using unrestricted B3LYP/6-31G(d), frequencies calculated using B3LYP/6-31G(d) and electronic energies calculated using MPWB1K/6-31G(d,p), rate coefficients were calculated based on Equation 4.3 from 298.15 K to 800 K for both methyl methacrylate and methyl acrylate from AD1 to AD3. Kinetic parameters, A and E_a, were then regressed from a plot of ln$k$ versus 1/T as shown in Figures 4.10 and 4.11 for methyl methacrylate and methyl acrylate, respectively. The impact of the one-dimensional hindered rotor treatment was explored by comparing the A and E_a values for both the harmonic oscillator and hindered rotation models. The rate coefficients were based on the lowest energy conformers for the reactants, although a range of rate coefficients would actually be expected based on conversion of reactants of many possible low energy conformations. The frequency factors and activation energies for methyl methacrylate propagation are summarized in Table 4.4, and those for methyl acrylate propagation are compiled in Table 4.5. It is clear from these results that treating low frequencies using the one-dimensional internal rotation model has an effect on both the activation energy and the frequency factor values. For methyl methacrylate, the difference of E_a between the harmonic oscillator model and the internal rotation model for each reaction is about 4 kJ·mol^{-1}, which translates into a factor of four in k_p at 50 °C. The frequency factors based on the one-dimensional internal rotation model are higher than those based on the harmonic oscillator model for both methyl methacrylate and methyl acrylate: the ratio of A^{HR}/A^{HO} varies from 2.8 to 10.5 for methyl methacrylate, and for methyl acrylate, the ratio varies from 1.9 to 7.4. The activation energies calculated based on the one-dimensional internal rotation model are not uniformly higher or lower than those based on the harmonic oscillator model: for methyl methacrylate, the difference varies from -4.1 kJ·mol^{-1} to 4.1 kJ·mol^{-1}, while for methyl acrylate, the difference varies from -5.4 kJ·mol^{-1} to 0.9 kJ·mol^{-1}. The best agreement between the calculated results and the experimental values for both monomers is for AD3 using the one-dimensional internal rotation model: for methyl methacrylate, E_a differs

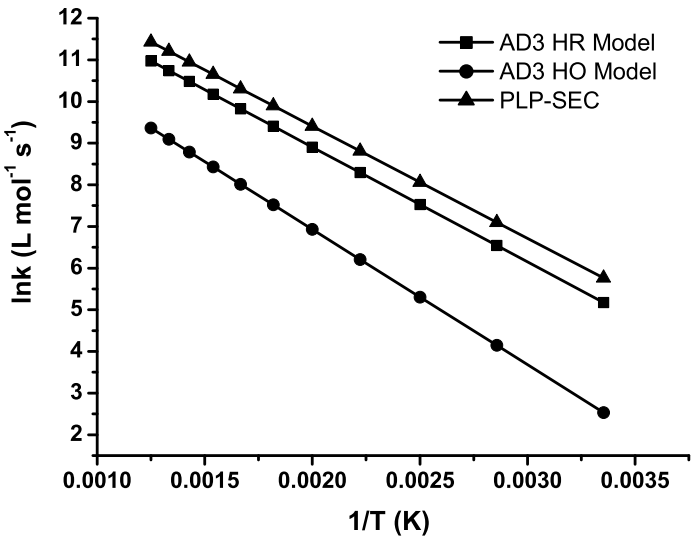

Figure 4.10: Plot of ln$k$ versus 1/T for methyl methacrylate propagation over a temperature range of 298.15 K to 800 K. The A and E_a values regressed from this plot are listed in Table 4.4.

by only 0.3 kJ·mol^{-1} and the frequency factor ratio ($A^{HR,AD3}/A^{PLP}$) is 0.6; for methyl acrylate, E_a differs by 3.8 kJ·mol^{-1} and the frequency factor ratio is 3.6. Overall, the k_p results from the hindered rotor model are in better agreement with the experimental data than the results from the harmonic oscillator model, as shown in Figures 4.10 and 4.11.

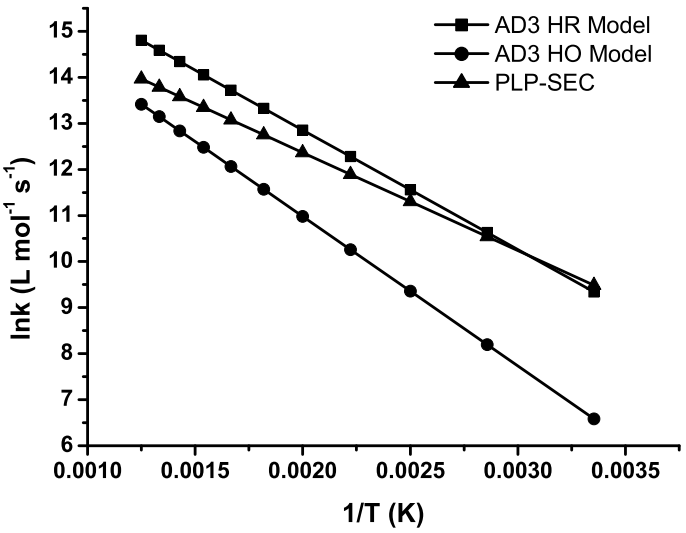

Figure 4.11: Plot of ln$k$ versus 1/T for methyl acrylate propagation over a temperature range of 298.15 K to 800 K. The A and E_a values regressed from this plot are listed in Table 4.5.

Table 4.4: Frequency factors (A: L·mol^{-1}·s^{-1}), activation energies (E_a: kJ·mol^{-1}) and rate constants (k_p: L·mol^{-1}·s^{-1}) at 50 °C for methyl methacrylate propagation calculated as a function of chain length (AD1-AD3 in Figure 4.2) using geometries optimized with unrestricted B3LYP/6-31G(d) and single point E_e calculations using MPWB1K/6-31G(d,p). A and E_a were regressed based on k_p values from 298.15 K to 800 K. Plots of ln$k$ versus 1/T are shown in Figure 4.10.

	HR Model			HO Model				
	A	E_a	k_p	A	E_a	k_p	A^{HR}/A^{HO}	$E_a^{HR} - E_a^{HO}$
AD1	3.72×10^6	27.7	1.24×10^2	4.68×10^5	24.0	6.17×10^1	7.9	3.7
AD2	7.41×10^6	28.0	2.21×10^2	7.08×10^5	23.9	9.70×10^1	10.5	4.1
AD3	1.55×10^6	22.7	3.32×10^2	5.50×10^5	26.8	2.56×10^1	2.8	-4.1
	A	E_a	k_p	$A^{HR,AD3}/A^{PLP}$			$E_a^{HR,AD3} - E_a^{PLP}$	
PLP-SEC	2.67×10^6	22.4	6.39×10^2	0.6			0.3	

Table 4.5: Frequency factors (A: L·mol^{-1}·s^{-1}), activation energies (E_a: kJ·mol^{-1}) and rate constants (k_p: L·mol^{-1}·s^{-1}) at 50 °C for methyl acrylate propagation calculated as a function of chain length (AD1-AD3 in Figure 4.2) using geometries optimized with unrestricted B3LYP/6-31G(d) and single point E_e calculations using MPWB1K/6-31G(d,p). A and E_a were regressed based on k_p values from 298.15 K to 800 K. Plots of ln$k$ versus 1/T are shown in Figure 4.11.

	HR Model			HO Model				
	A	E_a	k_p	A	E_a	k_p	A^{HR}/A^{HO}	$E_a^{HR} - E_a^{HO}$
AD1	7.24×10^7	26.4	3.91×10^3	9.77×10^6	25.5	7.38×10^2	7.4	0.9
AD2	6.31×10^7	22.8	1.30×10^4	1.70×10^7	22.4	4.07×10^3	3.7	0.4
AD3	6.03×10^7	21.5	2.02×10^4	3.16×10^7	26.9	1.42×10^3	1.9	-5.4
	A	E_a	k_p	$A^{HR,AD3}/A^{PLP}$			$E_a^{HR,AD3} - E_a^{PLP}$	
PLP-SEC	1.66×10^7	17.7	2.29×10^4	3.6			3.8	

Because computational time and resources prohibited going to chain lengths longer than four in the radical product, it is not possible to assess whether the predicted A, E_a and k_p values have reached an asymptotic value. However, the excellent agreement with the experimental data and the diminishing impact of units far from the reactive center suggest that it is reasonable to use addition of a trimeric radical to monomer to predict rate coefficients for propagation of methyl methacrylate and methyl acrylate.

4.3.5 Solvation Model Results

The experimental data were determined from bulk polymerization, while the predicted results were based on calculations in vacuum. It has been shown in previous research that kinetic parameters for free radical polymerization are not sensitive to the presence of solvent (Heuts and Gilbert (1995)), so it is reasonable that our calculated results were in excellent agreement with experiment. However, to probe this further, a polarizable continuum model (PCM) was used to study the influence of solvent on the conformation of the transition state and the kinetic parameters. "*SCRF(PCM,Read)*" with "*EPS*=6.32" were used as keywords in Gaussian 03 to conduct this analysis for methyl methacrylate, and "*EPS*=7.03" was used as a keyword for methyl acrylate. Comparison of the results with those from vacuum calculations reveals that the conformations of the reactants and the transition state are not affected strongly. For methyl methacrylate AD3 TS, the bond lengths (including the bond defining the transition state) differed by less than 0.001 Å and the angles differed by less than 0.5°. The difference in the E_a value for methyl methacrylate AD3 was 1.9 kJ·mol^{-1}. For methyl acrylate AD3 TS, the bond lengths (including the bond defining the transition state) differed by less than 0.001 Å, and the angles differed by less than 0.3°. The difference in the AD3 E_a value was 1.0 kJ·mol^{-1}.

4.4 Conclusion

A computational methodology based on quantum chemistry and transition state theory has been used to calculate kinetics parameters for methyl methacrylate and methyl acrylate propagation reactions. A combination of conventional geometry optimization and relaxed potential scans for each single bond and the bond defining the transition state was used in order to locate “global” minimum conformations. Three density functional theory methods with different basis sets were evaluated for calculating activation energies of methyl methacrylate addition reactions, and the results showed that MPWB1K/6-31G(d,p) provided values that were the closest to and in very good agreement with experimental data. This choice of method and basis set was also verified for methyl acrylate. The addition reactions of monomeric, dimeric and trimeric radicals to monomer were analyzed for both methyl methacrylate and methyl acrylate, and the results showed that addition of a trimeric radical to monomer offered results that were the most consistent with experimental data. Calculations employing a solvation model revealed that the solvent effect was not marked for either methyl methacrylate or methyl acrylate propagation reactions. Two different treatments were used in the calculation of the contribution of low frequencies to the kinetic parameters. The results based on the one-dimensional internal rotation model are closer to experimental data than those based on the harmonic oscillator model.

Chapter 5

Copolymerization of Methyl Methacrylate and Methyl Acrylate

5.1 Introduction

Copolymerization is one of the most commonly used approaches to produce polymers which combine or synergize properties of two or more different parent polymers. For example, the adhesive and cohesive properties of acrylate coating resins can be balanced by controlling the proportions of monomers in the recipe (Meyer and Keurentjes (2005)). The kinetics of copolymerization can be quite complicated. There are four different possible combinations of monomers and radical ends, and often the reactivity is influenced by penultimate or further removed units on the propagating radical, further diversifying the number of kinetic parameters that are necessary to capture the composition of the copolymer product. There are no experimental methods capable of directly measuring individual k_p values for different combinations of monomers and radicals. The advent of pulsed laser polymerization in combination with size exclusion chromatography (PLP-SEC) has enabled the determination of the overall propagation rate coefficient ($k_{p,copo}$) for copolymerization systems as well as k_p values for homopolymerization (Beuermann and Buback (2002); Buback

et al. (2001); Coote and Davis (1999); Coote et al. (1997a,b); Hutchinson et al. (1997); Kululj and Davis (1998)). Reactivity ratios relating individual k_p values for homopolymerization and cross propagation can then be determined based on fitting in the context of a copolymerization model. One such model, the terminal model (TM), classifies the propagating radicals based only on the terminal unit. As depicted in Figure 5.1, four reaction rate constants ($k_{11}, k_{12}, k_{21}, k_{22}$) are required to represent all the addition reactions for a binary copolymerization system described according to the terminal model. Two reactivity ratios, r_1 and r_2, are defined as $r_1 = k_{11}/k_{12}$ and $r_2 = k_{22}/k_{21}$, and thus quantify the relative rate of propagation of a radical with its own monomer compared to propagation with the other monomer. Fukuda et al. derived the expression in Equation 5.1 for the overall propagation rate constant ($k_{p,copo}$) as a function of the homopolymerization rate constants of monomer 1 and monomer 2 (k_{11}, k_{22}), reactivity ratios (r_1 and r_2) and monomer fractions (f_1 and f_2) based on the terminal model (Fukuda et al. (1985)). Thus, if $k_{p,copo}$ values are measured at various monomer fractions, the reactivity ratios can be regressed from Equation 5.1:

$$k_{p,copo} = \frac{r_1 f_1^2 + 2 f_1 f_2 + r_2 f_2^2}{(r_1 f_1/k_{11}) + (r_2 f_2/k_{22})} \tag{5.1}$$

The reactivity ratios can also be regressed from the composition in the copolymer product as a function of monomer fractions as shown in Equation 5.2:

$$F_1 = \frac{r_1 f_1^2 + f_1 f_2}{r_1 f_1^2 + 2 f_1 f_2 + r_2 f_2^2} \tag{5.2}$$

where F_1 is the fraction of monomer 1 in the copolymer product. Typically, F_i values are measured using spectroscopic methods that are sensitive to the quantity of a specific functional group or structure, such as NMR and near infrared. However, the reactivity ratios determined using these two methods do not match in some cases. This mismatch has been attributed by Fukuda et al. to the neglect of the influence of penultimate units inherent in the assumptions of the TM (Fukuda et al. (1985)).

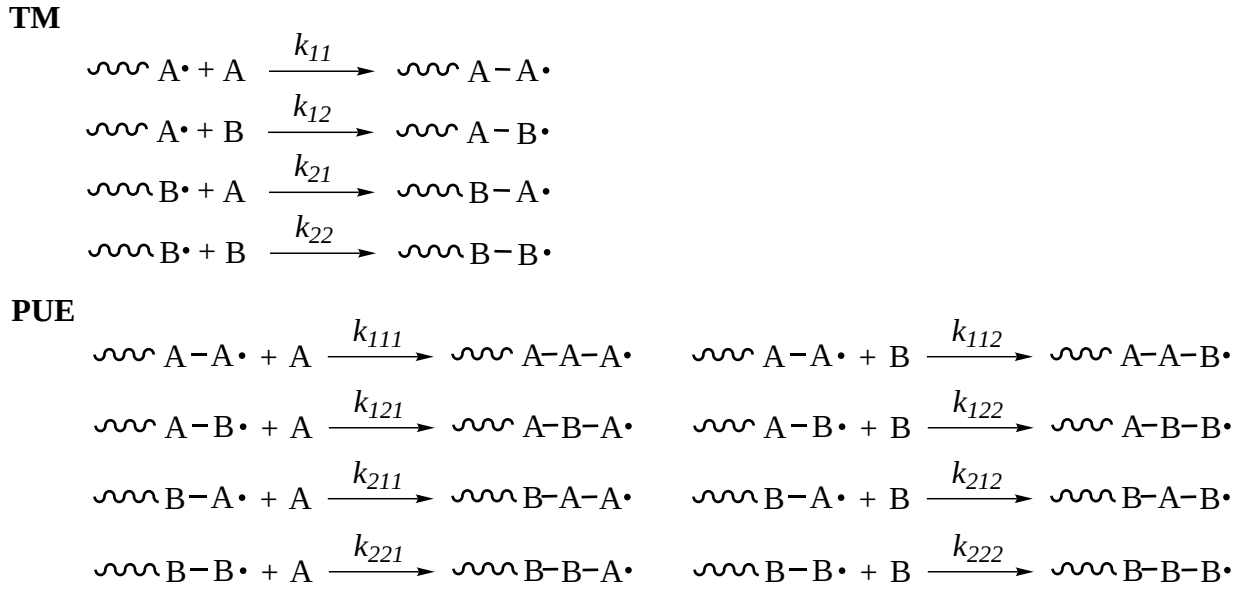

Figure 5.1: Terminal model (TM) and penultimate effect (PUE) model of binary copolymerization.

To solve this inconsistency, the penultimate effect (PUE) model was developed (Fukuda et al. (1985)). In the PUE model, the reactivity of a radical is dependent on both the terminal and penultimate units. As illustrated in Figure 5.1, eight reaction rate constants (k_{hij}, $h, i, j = 1, 2$) are required to cover all the addition reactions for a binary copolymerization system. Four reactivity ratios (r_{ij}) and two radical reactivity ratios (s_i) are introduced as follows:

$$r_{11} = \frac{k_{111}}{k_{112}}, \quad r_{12} = \frac{k_{122}}{k_{121}}, \quad r_{22} = \frac{k_{222}}{k_{221}}, \quad r_{21} = \frac{k_{211}}{k_{212}}, \quad s_1 = \frac{k_{211}}{k_{111}}, \quad s_2 = \frac{k_{122}}{k_{222}}$$

The overall propagation rate coefficient ($k_{p,copo}$) is then expressed based on the homopolymerization rate constants and reactivity ratios as in Equation 5.3.

$$k_{p,copo} = \frac{\bar{r}_1 f_1^2 + 2 f_1 f_2 + \bar{r}_2 f_2^2}{(\bar{r}_1 f_1 / \bar{k}_{11}) + (\bar{r}_2 f_2 / \bar{k}_{22})} \tag{5.3}$$

where the average reactivity ratios ($\bar{r}_1$ and $\bar{r}_2$) and rate coefficients ($\bar{k}_{ii}$) are defined as in Equation 5.4.

$$\bar{r}_i = r_{ji} \frac{r_{ii} f_i + f_j}{r_{ji} f_i + f_j} \quad \bar{k}_{ii} = k_{iii} \frac{r_{ii} f_i + f_j}{r_{ii} f_i + f_j / s_i} \tag{5.4}$$

The composition of each monomer in the copolymer (F_i) is then written based on the average reactivity ratios defined in Equation 5.4 as in Equation 5.5.

$$F_1 = \frac{\bar{r}_1 f_1^2 + f_1 f_2}{\bar{r}_1 f_1^2 + 2 f_1 f_2 + \bar{r}_2 f_2^2} \tag{5.5}$$

The PUE model including six ratios ($r_{11}, r_{12}, r_{21}, r_{22}, s_1$ and s_2) is called the explicit penultimate effect (EPUE) model. If it is assumed that the reactivity ratios of different penultimate units are close, i.e., $r_{11} \approx r_{21} = r_1$ and $r_{22} \approx r_{12} = r_2$, the implicit penultimate effect (IPUE) model is obtained, which uses four ratios (r_1, r_2, s_1 and s_2) to describe the overall propagation rate coefficient and copolymer composition.

While both the TM and PUE models have been widely used to study copolymerization and quantify the governing parameters, neither of these two methods can be used to determine the kinetic parameters (E_a and A) for the individual reactions directly. In addition, determination of the

kinetic parameters indirectly by assuming a model can be confounded by other reactions taking place at the reaction conditions necessary to extract meaningful E_a and A values. For example, in PLP-SEC, secondary reactions like transfer reactions need to be suppressed, so the PLP-SEC experiments are carried out at low temperatures (Beuermann et al. (1996); Buback et al. (1998)). Thus, it may not be possible to measure the parameters of interest over a wide temperature range. Therefore, it is attractive to have a methodology to determine all of the kinetic parameters governing copolymerization directly in the absence of any competing reactions. The ability to predict kinetic parameters would enable modeling of copolymerization processes and offer guidance for the development of novel monomers.

In previous research, we developed a methodology based on quantum chemistry and transition state theory to calculate kinetic parameters for the homopolymerization of methyl methacrylate and methyl acrylate (Yu et al. (2008)). We demonstrated that k_p values in excellent agreement with experiment could be calculated based on *ab initio* calculations. In the present work, the same methodology was used to calculate the kinetic parameters for the copolymerization of methyl methacrylate and methyl acrylate. Terminal model and penultimate model kinetic parameters were obtained by varying the radical reactants, and the results were compared to experimental data.

In addition, the ability to calculate individual rate parameters for self- and cross-propagation reactions explicitly allowed the applicability of different descriptions of radical reactivity to be tested for acrylates. A number of researchers have investigated the ability of simple structure-reactivity relationships to capture reactivity trends in radical reactions (Fischer and Radom (2001); Pfaendtner et al. (2006); Wong et al. (1994)). In particular, the Evans-Polanyi relationship, in which the activation energy (E_a) and heat of reaction (ΔH_r) are linearly correlated as shown in Equation 5.6, has been tested.

$$E_a = E_0 + \alpha \Delta H_r \tag{5.6}$$

The coefficients E_0 and α are constant for reactions in the same family. The Evans-Polanyi relationship is an empirical description which only includes the influence of enthalpic factors on the activation energy. It has been shown that there are additional factors influencing the activation energy such as polar and steric effects (Fischer and Radom (2001)). In order to investigate the factors that influence the activation energy fully, a more detailed analysis, such as that provided by a state correlation diagram (SCD) (Pross (1995); Shaik and Canadell (1990)), is warranted. Nevertheless, the Evans-Polanyi relationship is still widely used to estimate activation energies because of its simplicity and its ability to capture a large portion of the variation of E_a values with structure. The detailed calculations performed here offer the opportunity to test the Evans-Polanyi relationship and its utility in estimating reactivity ratios based on enthalpic differences alone.

Additional analysis of the various rate parameters governing the copolymerization of methyl acrylate and methyl methacrylate was carried out based on frontier orbital theory. Addition reactions involve an interaction between the singly occupied molecular orbital (SOMO) of the radical with the highest occupied molecular orbital (HOMO) or the lowest unoccupied molecular orbital (LUMO) of the monomer as shown in Figure 5.2 (Lozano et al. (1999)). The decisive factor in determining which interaction occurs is the energy gap of the SOMO-HOMO compared to that for the SOMO-LUMO: if the radical has a lower energy SOMO, the energy gap of the SOMO-HOMO is smaller than the SOMO-LUMO gap, the interaction of the SOMO with the HOMO determines the reactivity, and the reaction is electrophilic for the radical; on the other hand, if the energy gap of the SOMO-LUMO is smaller, the reactivity is determined by the SOMO-LUMO interaction and the reaction is nucleophilic for the radical.

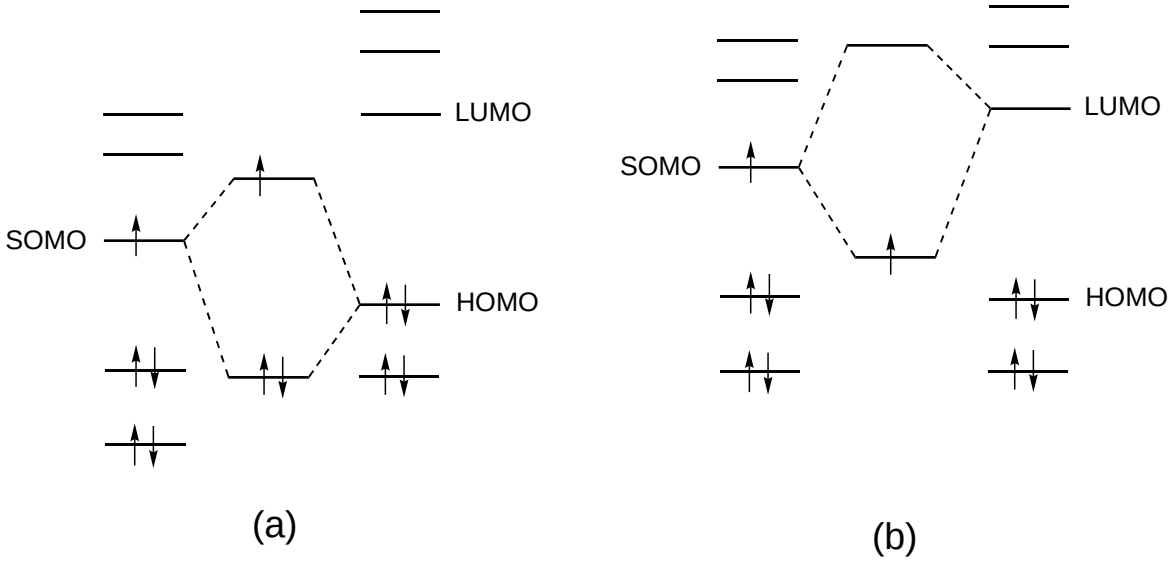

Figure 5.2: Interaction of frontier orbitals in radical addition reactions involving the singly occupied molecular orbital (SOMO) of the radical and the highest occupied and lowest unoccupied molecular orbitals (HOMO and LUMO, respectively) of the monomer. (a) the interaction of SOMO with HOMO (b) the interaction of SOMO with LUMO.

5.2 Computational Methodology

Twenty eight addition reactions of monomeric, dimeric and trimeric radicals to monomers in all possible different combinations were studied for methyl methacrylate-methyl acrylate copolymerization as shown in Figure 5.3, in which "A" stands for methyl methacrylate and "B" denotes methyl acrylate. Based on the number of units in the radical, the reactions are divided into three groups: AD1, AD2 and AD3, where ADn denotes an addition reaction involving a radical reactant of length n.

The AD1 set includes four reactions, which are used to simulate the terminal model only. The AD2 set includes eight reactions, which are used to simulate both the penultimate model and the terminal model, if the reactivity ratios are calculated as the average values of those for radicals with the same end unit, but different penultimate units. To explore the influence of the penpenultimate unit, an additional methyl methacrylate or methyl acrylate unit was added to the eight AD2 radicals to construct sixteen AD3 reactions, from which the TM and PUE parameters were calculated based on average ratios. For all reactions, the kinetic parameters (k_p, A and E_a) were calculated individually. The heats of reactions (ΔH_r) for these reactions were also calculated. The Evans-Polanyi equation (Fischer and Radom (2001)), which empirically correlates the activation energy and heat of reaction, was also investigated.

AD1:

$$A\bullet + A \xrightarrow{k_{11}} A\text{–}A\bullet \qquad A\bullet + B \xrightarrow{k_{12}} A\text{–}B\bullet$$

$$B\bullet + A \xrightarrow{k_{21}} B\text{–}A\bullet \qquad B\bullet + B \xrightarrow{k_{22}} B\text{–}B\bullet$$

AD2:

$$A\text{–}A\bullet + A \xrightarrow{k_{111}} A\text{–}A\text{–}A\bullet \qquad A\text{–}A\bullet + B \xrightarrow{k_{112}} A\text{–}A\text{–}B\bullet$$

$$A\text{–}B\bullet + A \xrightarrow{k_{121}} A\text{–}B\text{–}A\bullet \qquad A\text{–}B\bullet + B \xrightarrow{k_{122}} A\text{–}B\text{–}B\bullet$$

$$B\text{–}A\bullet + A \xrightarrow{k_{211}} B\text{–}A\text{–}A\bullet \qquad B\text{–}A\bullet + B \xrightarrow{k_{212}} B\text{–}A\text{–}B\bullet$$

$$B\text{–}B\bullet + A \xrightarrow{k_{221}} B\text{–}B\text{–}A\bullet \qquad B\text{–}B\bullet + B \xrightarrow{k_{222}} B\text{–}B\text{–}B\bullet$$

AD3:

$$A\text{–}A\text{–}A\bullet + A \xrightarrow{k_{A,111}} A\text{–}A\text{–}A\text{–}A\bullet \qquad A\text{–}A\text{–}A\bullet + B \xrightarrow{k_{A,112}} A\text{–}A\text{–}A\text{–}B\bullet$$

$$A\text{–}A\text{–}B\bullet + A \xrightarrow{k_{A,121}} A\text{–}A\text{–}B\text{–}A\bullet \qquad A\text{–}A\text{–}B\bullet + B \xrightarrow{k_{A,122}} A\text{–}A\text{–}B\text{–}B\bullet$$

$$A\text{–}B\text{–}A\bullet + A \xrightarrow{k_{A,211}} A\text{–}B\text{–}A\text{–}A\bullet \qquad A\text{–}B\text{–}A\bullet + B \xrightarrow{k_{A,212}} A\text{–}B\text{–}A\text{–}B\bullet$$

$$A\text{–}B\text{–}B\bullet + A \xrightarrow{k_{A,221}} A\text{–}B\text{–}B\text{–}A\bullet \qquad A\text{–}B\text{–}B\bullet + B \xrightarrow{k_{A,222}} A\text{–}B\text{–}B\text{–}B\bullet$$

$$B\text{–}A\text{–}A\bullet + A \xrightarrow{k_{B,111}} A\text{–}A\text{–}A\text{–}A\bullet \qquad B\text{–}A\text{–}A\bullet + B \xrightarrow{k_{B,112}} A\text{–}A\text{–}A\text{–}B\bullet$$

$$B\text{–}A\text{–}B\bullet + A \xrightarrow{k_{B,121}} A\text{–}A\text{–}B\text{–}A\bullet \qquad B\text{–}A\text{–}B\bullet + B \xrightarrow{k_{B,122}} A\text{–}A\text{–}B\text{–}B\bullet$$

$$B\text{–}B\text{–}A\bullet + A \xrightarrow{k_{B,211}} A\text{–}B\text{–}A\text{–}A\bullet \qquad B\text{–}B\text{–}A\bullet + B \xrightarrow{k_{B,212}} A\text{–}B\text{–}A\text{–}B\bullet$$

$$B\text{–}B\text{–}B\bullet + A \xrightarrow{k_{B,221}} A\text{–}B\text{–}B\text{–}A\bullet \qquad B\text{–}B\text{–}B\bullet + B \xrightarrow{k_{B,222}} A\text{–}B\text{–}B\text{–}B\bullet$$

Figure 5.3: Addition reactions of monomeric, dimeric and trimeric radicals to monomers in methyl methacrylate-methyl acrylate copolymerization; “A” stands for methyl methacrylate and “B” stands for methyl acrylate; ADn is used to denote an addition reaction involving a radical reactant of length n.

All electronic energy calculations and vibrational frequencies were calculated using *Gaussian 03* (Frisch et al. (2004)). All the reactant and product conformations were optimized using unrestricted B3LYP/6-31G(d) first via conventional optimization. However, the conventional optimization method employed is based on the gradient in energy and can only locate local minima (Foresman (2002)), and thus the optimized geometry is sensitive to the input structure. Therefore, a combination of conventional optimization and relaxed potential energy scans for all the single bond dihedrals was used. This method is based on the fact that different conformations are mainly due to variations in the rotation about single bonds. Specifically, one-dimensional relaxed potential energy scans were carried out with the keyword "*modredundant*" with 30° as the scan interval. If a lower energy structure was detected, it was optimized conventionally, and the process was repeated until no conformations of lower energy were obtained. The detailed method and comparison of different levels of theory and scan intervals for performing the one-dimensional scans have been discussed previously (Pfaendtner et al. (2007); Yu et al. (2008)).

Transition state structures were identified using the QST3 method, which requires the reactants, product and an estimated transition state (TS) conformation as input (Gaussian Inc. (1990)). Based on our experience with homopolymerization, the estimated TS conformations were constructed by elongating the product carbon-carbon bond to 2.3 Å. Transition states were confirmed to have one imaginary frequency, which corresponded to the motion along the reaction coordinate, and intrinsic reaction coordinate (IRC) following with a step size of 0.1 amu$^{0.5}$-Bohr was used to verify that the correct reactants and product were obtained.

Because of the size of the species studied here, it is critical to have a quantum chemical calculation method/basis set which is accurate yet computationally affordable. Various hybrid density functional theory (DFT) methods and basis sets were compared in our previous research for the homopolymerization of methyl methacrylate and methyl acrylate (Yu et al. (2008)). It was found that the modified Perdew-Wang and Becke functional (MPWB1K) with the basis set of 6-31G(d,p) provided activation energies and k_p values which are in very good agreement with experimen-

tal data. Therefore, MPWB1K/6-31G(d,p) was also used to calculate the electronic energy for the copolymerization reactions. The zero-point vibrational energy (ZPVE) was calculated using UB3LYP/6-31G(d) with a scale factor of 0.9806 (Scott and Radom (1996)). A scale factor of 1.0002 was used in the calculation of partition functions based on the recommended scale factors for ΔH_{vib} and ΔS_{vib} reported by Scott and Radom (1996).

The reaction rate constant at a specific temperature was calculated using Equation 5.7 (Pfaendtner et al. (2006)):

$$k(T) = \kappa(T)\frac{k_B T}{h}(c^o)^{1-m}\frac{Q^{\ddagger}}{Q_{mon}Q_{rad}}e^{-\Delta E_0/RT} \tag{5.7}$$

in which $\kappa(T)$ is the tunneling factor, which deviates from a value of one for reactions involving motion of light atoms such as hydrogen transfer, but can be set equal to one for propagation reactions of acrylates. k_B is Boltzmann's constant (1.3806×10^{-23} J·mol^{-1}· K^{-1}), h is Planck's constant (6.6261×10^{-34} J·s), m is the number of reactants, which is two for propagation, c° is the standard state concentration (mol·L^{-1}) to which the quantum chemical calculations are referenced, $\frac{P}{RT}$, where P is 1 atm, and ΔE_0 is the difference between E_0 of the transition state and the reactants, which is defined as the summation of the electronic energy (E_e) and the zero-point vibrational energy (ZPVE):

$$E_0 = E_e + ZPVE \tag{5.8}$$

The ZPVE is the contribution to the energy from vibration at 0 K as defined in Equation 5.9 (McQuarrie and Simon (1999)):

$$ZPVE = \frac{1}{2}\sum_{i}^{3N-6} h\nu_i \tag{5.9}$$

in which N is the number of atoms, and ν_i represents the frequencies. For transition states, $3N-7$ frequencies are included in the ZPVE. The final quantity in Equation 5.7 is the partition function (Q), which is conventionally written as the product of different modes as shown in Equation 5.10

(McQuarrie and Simon (1999)).

$$Q = Q_e Q_{tr} Q_r Q_{vib} \tag{5.10}$$

where Q_e is the electronic partition function, which is one for the ground state, Q_{tr} accounts for the translational motion and Q_r is for the species' rotational motion as a whole. The remaining motions are vibrational and captured by Q_{vib}, which is typically calculated using a harmonic oscillator model. However, the harmonic oscillator model is not an accurate description of all of these motions, especially those associated with low frequencies, which are mainly composed of rotational motions. The importance of treating low frequencies using a more suitable model has been realized and applied in recent research (Heuts and Gilbert (1995); Huang et al. (1998); Izgorodina and Coote (2006); Pfaendtner et al. (2006); Speybroeck et al. (2001); Sumathi et al. (2001); Van Cauter et al. (2006)). In our methodology, we separated these low frequencies from the harmonic oscillator partition function and treated them using a one-dimensional internal rotor model. Thus, the partition function written in Equation 5.10 is revised as Equation 5.11.

$$Q = Q_e Q_{tr} Q_r Q_{vib} Q_{int,rot} \tag{5.11}$$

where $Q_{int,rot}$ is the contribution from those vibrations better treated as internal rotations. To obtain $Q_{int,rot}$, all the single bonds were treated as rotation axes. For transition states, the bond defining the transition state was also treated as a rotation axis since it was found that the lowest positive frequency mainly consists of the torsional motion about the bond defining the transition state. As an example, the nine internal rotors in the transition state for addition of methyl methacrylate monomeric radical to monomer is shown in Figure 5.4.

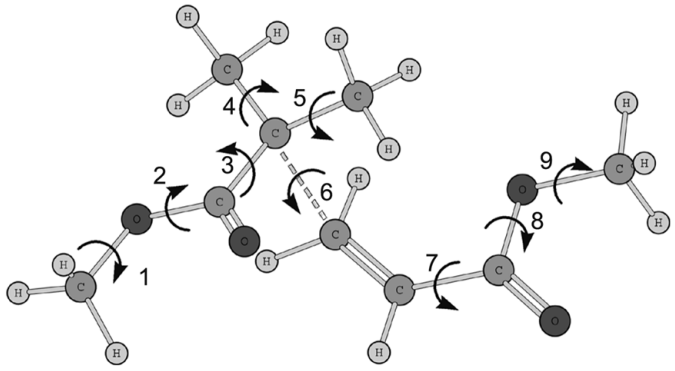

Figure 5.4: Internal rotations about all eight single bonds and the bond defining the transition state for the transition state of the methyl methacrylate AD1 (Figure 5.3) reaction were considered.

The partition function for the *m*-th rotation was calculated based on the definition of the partition function as shown in Equation 5.12:

$$Q_{int,rot,m} = \frac{1}{\sigma_m} \sum_i exp(-\frac{\epsilon_i}{k_B T}) \tag{5.12}$$

in which σ_m is the symmetry number of the *m*-th internal rotor and ϵ_i are the energy levels calculated by solving the one-dimensional Schrödinger equation shown in Equation 5.13:

$$-\frac{\hbar^2}{2I_{red}} \frac{d^2}{d\theta^2} \Psi + V(\theta)\Psi = \epsilon \Psi \tag{5.13}$$

where $\hbar$ is Planck's constant divided by 2π, Ψ is the wave function and θ is the rotation angle. I_{red} is the reduced moment of inertia ($I_{red}^{2,3}$ defined by East et al. (East and Radom (1997))). $V(\theta)$ is the potential energy expressed as a function of torsional angle, which is in the form of a full Fourier expansion as shown in Equation 5.14.

$$V(\theta) = \sum_{i=1}^{n} [a_i(1 - cosi\theta) + b_i sini\theta] \tag{5.14}$$

Equation 5.14 can be expressed in the form of a matrix product, and the coefficients a_i and b_i are then determined by solving an overdetermined function. It has been verified that energy scans with 12 sampling points and $n = 3$ in Equation 5.14 are sufficient to capture both symmetric and asymmetric energy profiles (Yu et al. (2008)). The one-dimensional Schrödinger equation was solved with the Fourier Grid Hamiltonian (FGH) method, in which the Hamiltonian operator was expressed in the form of a matrix and the energy levels were determined by diagonalizing the matrix (Balint-Kurti et al. (1992)). In the construction of the Hamiltonian operator matrix, the rotation range from 0 to 360 degrees was discretized using 1000 grid points, which was verified to have partition functions in agreement with those from finer grid sizes (Pfaendtner et al. (2007); Yu et al. (2008)).

The activation energy (E_a) and frequency factor (A) were determined from the regression of $\ln k_p(T)$ versus 1/T over the temperature range of 296.15 to 800 K in 50 K intervals, according to

Equation 5.15.

$$lnk_p(T) = lnA - \frac{E_a}{RT} \tag{5.15}$$

Monomer reactivity and radical reactivity ratios were calculated based on k_p values, and the $k_{p,copo}$ and F_i values were calculated using the expressions presented above for the TM and PUE models. The calculated ratios, $k_{p,copo}$ and F_i values were compared to experimental data regressed or measured at 23 °C and 1000 bar by Buback and Müller (2007). In order to be able to compare the calculated values to those of Buback and coworkers at 1000 bar, the results from the quantum chemistry calculations, which are at ambient pressure, were adjusted using the activation volume ($\Delta V^{\ddagger}$) as shown in Equation 5.16 (Odian (2004)).

$$\frac{dlnk_p}{dp} = -\frac{\Delta V^{\ddagger}}{RT} \tag{5.16}$$

The activation volume ($\Delta V^{\ddagger}$) for methyl methacrylate is -16.7 cm^3·mol^{-1} and for methyl acrylate is -11.7 cm^3·mol^{-1} (Beuermann et al. (1994); Buback et al. (1998)). No activation volume value for a methyl methacrylate and methyl acrylate copolymerization system is reported, so the average value of the two monomers of -14.2 cm^3·mol^{-1} was used. The ratios of the rate coefficients between ambient pressure and 1000 bar at various temperatures based on these activation volumes are listed in Table 5.1. At 23 °C, the ratios are 2.0 for methyl methacrylate, 1.6 for methyl acrylate and 1.8 for the mixture of methyl methacrylate and methyl acrylate. Note that our assumption of an average value for the copolymer system based on the two monomeric components and the relatively close values of $\Delta V^{\ddagger}$ for methyl methacrylate and methyl acrylate will lead to reactivity ratios that are nearly independent of pressure.

Table 5.1: Ratios of propagation rate coefficients at 1000 bar to those at ambient pressure calculated using Equation 5.16 over the temperature range of 296.15−476.15 K. Activation volume for methyl methacrylate: -16.7 $cm^3 \cdot mol^{-1}$; activation volume for methyl acrylate: -11.7 $cm^3 \cdot mol^{-1}$; activation volume for a methyl methacrylate and methyl acrylate copolymer system is calculated as the average of the two monomers: -14.2 $cm^3 \cdot mol^{-1}$.

Temperature (K)	$\frac{k_{p,1000\ bar}}{k_{p,1\ atm}}$(MMA)	$\frac{k_{p,1000\ bar}}{k_{p,1\ atm}}$(MMA/MA)	$\frac{k_{p,1000\ bar}}{k_{p,1\ atm}}$(MA)
296.15	2.0	1.8	1.6
326.15	1.9	1.7	1.5
356.15	1.8	1.6	1.5
386.15	1.7	1.6	1.4
416.15	1.6	1.5	1.4
446.15	1.6	1.5	1.4
476.15	1.5	1.4	1.3

The following reactivity ratios and rate coefficients for methyl methacrylate-methyl acrylate copolymerization at 23 °C and 1000 bar provided by Buback et al. were used for comparison (Buback and Müller (2007)).

- Reactivity ratios based on TM fitted from composition plot

  $r_1 = 3.03, r_2 = 0.20$

- Reactivity ratios based on TM fitted from $k_{p,copo}$ measured using PLP-SEC

  $r_1 = 1.95, r_2 = 0.21$

- Monomer reactivity and radical reactivity ratios based on IPUE model fitted from $k_{p,copo}$ measured using PLP-SEC

  $r_1 = 2.40, r_2 = 0.18, s_1 = 1.46, s_2 = 0.38$

- Homopolymerization propagation rate coefficients of methyl methacrylate and methyl acrylate at 23 °C and 1000 bar

  $k_{p,MMA} = 702$ L·mol^{-1}·s^{-1}, $k_{p,MA} = 18,088$ L·mol^{-1}·s^{-1}

5.3 Results and Discussion

5.3.1 Geometries and Transition States

Interesting features related to the reactivity of the different radical and monomer combinations were apparent from the geometries of the transition states. For example, the conformations of the transition states for the four AD1 reactions are shown in Figure 5.5. Comparison of all of the transition states shows that for the same radical, the bond length defining the transition state formed by the radical and methyl acrylate is about 0.01 Å shorter than that in the transition state structure formed with methyl methacrylate, which reveals that the transition states involving methyl

methacrylate monomer are located earlier along the reaction coordinate. The bond lengths defining the transition state of addition of radicals to methyl methacrylate vary from 2.239 Å to 2.313 Å, while those for addition to methyl acrylate vary from 2.222 Å to 2.302 Å. An earlier transition state translates into a lower activation energy and higher reaction exothermicity, which is consistent with the calculated activation energies and heats of reaction reported below.

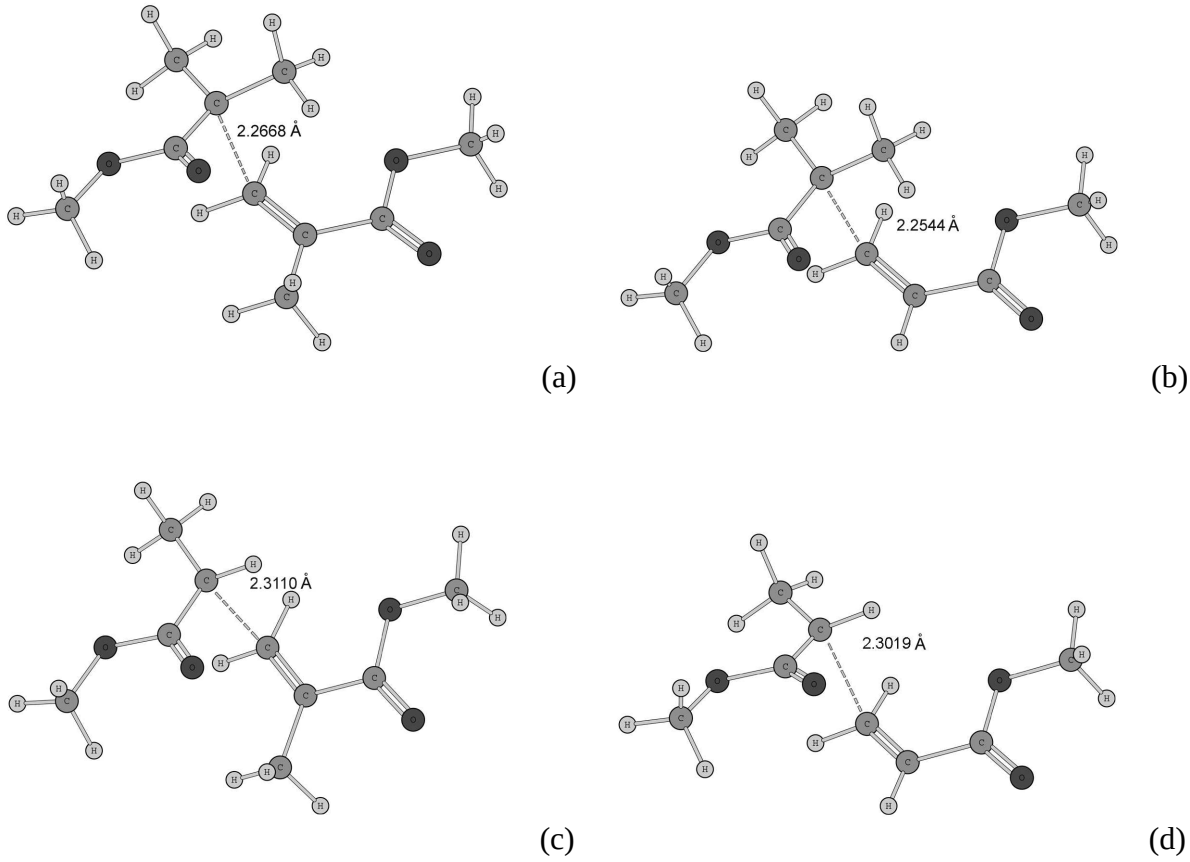

Figure 5.5: Structures and bond lengths of transition states for the four methyl methacrylate-methyl acrylate AD1 copolymerization reactions summarized in Figure 5.3. (a) Methyl methacrylate radical - methyl methacrylate monomer (b) Methyl methacrylate radical - methyl acrylate monomer (c) Methyl acrylate radical - methyl methacrylate monomer (d) Methyl acrylate radical - methyl acrylate monomer.

5.3.2 Kinetics

The activation energies and frequency factors of the four reactions involving the addition of a monomeric radical to monomer (AD1) are listed in Table 5.2. It can be seen that for both methyl methacrylate and methyl acrylate monomeric radicals, the activation energies for the addition to methyl methacrylate monomer are lower than the corresponding ones for the addition to methyl acrylate monomer. The difference for methyl methacrylate radical is about 7 kJ·mol^{-1}, while that for methyl acrylate radical is about 4 kJ·mol^{-1}. This is consistent with simple radical stability arguments and indicates that the activation energy differences are dominated by enthaplic effects. Addition to methyl methacrylate monomer involves the formation of a more stable tertiary radical, compared to the formation of a secondary radical in the case of methyl acrylate monomer. Thus, addition to methyl methacrylate monomer is enthalpically preferred. This preference also manifests itself in the reaction exothermicity: methyl methacrylate radical reacting with methyl methacrylate monomer is 1.3 kJ·mol^{-1} more exothermic than addition to methyl acrylate monomer, while for methyl acrylate radical, reaction with methyl methacrylate is 6.3 kJ·mol^{-1} more exothermic than addition to methyl acrylate. However, addition to the less bulky methyl acrylate is entropically preferred. For the same radical, reaction with methyl acrylate monomer has a higher frequency factor such that $A_{11}/A_{12} = 0.28$ and $A_{21}/A_{22} = 0.24$. The calculated homopolymerization rate constants ($k_{11} = 9.53 \times 10^1$ L·mol^{-1}·s^{-1}, $k_{22} = 2.57 \times 10^3$ L·mol^{-1}·s^{-1}) are 13% and 14% of the measured homopolymerization rate constants of methyl methacrylate and methyl acrylate ($k_{p,MMA} = 7.02 \times 10^2$ L·mol^{-1}·s^{-1}, $k_{p,MA} = 1.81 \times 10^4$ L·mol^{-1}·s^{-1}), respectively. These results at higher pressure are consistent with our previous results at atmospheric pressure, where we recommended using trimeric radicals at a minimum to achieve results that were in excellent quantitative agreement with experiment (Yu et al. (2008)). Nonetheless, the AD1 results still capture the reactivity trends observed in the experimental values.

Table 5.2: Activation energies (E_a), frequency factors (A), heats of reaction (ΔH_r) and rate constants (k_p at 23 °C, 1000 bar) for the methyl methacrylate-methyl acrylate AD1 (TM) reactions; geometry optimization and frequency calculations were performed using UB3LYP/6-31G(d), electronic energies were calculated using MPWB1K/6-31G(d,p), and low frequencies were treated using a one-dimensional internal rotor model; A: methyl methacrylate, B: methyl acrylate; rate coefficients were first calculated at ambient pressure and adjusted to 1000 bar using the factors listed in Table 5.1. (k_p: L·mol^{-1}·s^{-1}, E_a: kJ·mol^{-1}, A: L·mol^{-1}·s^{-1}, ΔH_r: kJ·mol^{-1})

Reactions		E_a	A	ΔH_r(23 °C)	k_p(23 °C, 1000 bar)
A$\cdot + A \longrightarrow AA\cdot$	k_{11}	27.7	3.72×10^{6}	-50.1	9.53×10^{1}
A$\cdot + B \longrightarrow AB\cdot$	k_{12}	34.6	1.32×10^{7}	-48.8	1.85×10^{1}
B$\cdot + A \longrightarrow BA\cdot$	k_{21}	22.5	1.74×10^{7}	-76.5	3.33×10^{3}
B$\cdot + B \longrightarrow BB\cdot$	k_{22}	26.4	7.24×10^{7}	-70.2	2.57×10^{3}

Table 5.3: Calculated TM reactivity ratios (r_1, r_2) for methyl methacrylate-methyl acrylate copolymerization based on the four AD1 reactions in Figure 5.3 over the temperature range of 296.15−476.15 K and at 1000 bar; kinetic parameters are listed in Table 5.2, and the pressure adjustment ratios are listed in Table 5.1.

T(K)	r_1	r_2
296.15	5.14	0.77
326.15	3.94	0.90
356.15	3.15	1.02
386.15	2.61	1.14
416.15	2.23	1.25
446.15	1.94	1.36
476.15	1.72	1.46

It is next interesting to evaluate the reactivity ratios predicted from the AD1 reactions, i.e., the terminal model. These are tabulated in Table 5.3 as a function of temperature. Buback et al. determined reactivity ratios based on the terminal model at 23 °C and 1000 bar from two different types of experimental data: (1) polymer composition (Mayo-Lewis plot): r_1=3.03, r_2=0.20 (2) the overall propagation rate constant $k_{p,copo}$ measured using PLP-SEC: $r_1 = 1.95$, $r_2 = 0.21$. The ratios determined based on the calculated kinetic parameters at the same conditions are $r_1 = 5.14$ and $r_2 = 0.77$. While these quantities have the same trend, i.e., k_{11} is higher than k_{12} and k_{22} is lower than k_{21}, they are not in perfect quantitative agreement. This is consistent with our previous assertion that monomeric radials are simply too small to capture polymeric reactions quantitatively.

Table 5.4: Activation energies (E_a), frequency factors (A), heats of reaction (ΔH_r) and rate constants (k_p at 23 °C, 1000 bar) for the methyl methacrylate-methyl acrylate AD2 (PUE) reactions; geometry optimization and frequency calculations were performed using UB3LYP/6-31G(d), electronic energies were calculated using MPWB1K/6-31G(d,p), and low frequencies were treated using a one-dimensional internal rotor model; A: methyl methacrylate, B: methyl acrylate; rate coefficients were first calculated at ambient pressure and adjusted to 1000 bar using the factors listed in Table 5.1. (k_p: L·mol^{-1}·s^{-1}, E_a: kJ·mol^{-1}, A: L·mol^{-1}·s^{-1}, ΔH_r: kJ·mol^{-1})

Reactions		E_a	A	ΔH_r(23 °C)	k_p(23 °C, 1000 bar)
AA· + $A \longrightarrow AAA\cdot$	k_{111}	28.0	7.41×10^6	-41.2	1.68×10^2
AA· + $B \longrightarrow AAB\cdot$	k_{112}	31.1	4.68×10^6	-37.1	2.72×10^1
AB· + $A \longrightarrow ABA\cdot$	k_{121}	19.0	8.91×10^6	-75.2	7.00×10^3
AB· + $B \longrightarrow ABB\cdot$	k_{122}	22.0	1.35×10^7	-68.0	3.19×10^3
BA· + $A \longrightarrow BAA\cdot$	k_{211}	26.8	4.47×10^6	-47.5	1.52×10^2
BA· + $B \longrightarrow BAB\cdot$	k_{212}	29.8	7.76×10^6	-42.8	7.65×10^1
BB· + $A \longrightarrow BBA\cdot$	k_{221}	21.7	2.19×10^7	-78.4	5.80×10^3
BB· + $B \longrightarrow BBB\cdot$	k_{222}	22.8	6.31×10^7	-70.8	9.65×10^3

The results for the dimeric radical addition reactions (AD2) are tabulated in Table 5.4. The activation energies (E_a) and frequency factors (A) of the eight AD2 reactions in Figure 5.3 are listed. The reactivities of methyl methacrylate and methyl acrylate have the same tendencies as were observed for the AD1 results, i.e., reaction of radicals with methyl methacrylate monomer is enthalpically favored as reflected by lower activation energies ($0.9 - 3.1$ kJ·mol^{-1} lower) and more exothermic heats of reaction ($4.1 - 7.6$ kJ·mol^{-1} more exothermic). The ratios of the frequency factors are $A_{111}/A_{112} = 1.58$, $A_{121}/A_{122} = 0.66$, $A_{211}/A_{212} = 0.58$ and $A_{221}/A_{222} = 0.35$. In general, addition to methyl acrylate is slightly favored entropically. The calculated propagation rate constants of methyl methacrylate (1.68×10^2 L·mol·s^{-1}) and methyl acrylate (9.65×10^3 L·mol·s^{-1}) at 23 °C and 1000 bar are closer to the measured data ($k_{p,MMA} = 7.02\times10^2$ L·mol^{-1}·s^{-1}, $k_{p,MA} = 1.81\times10^4$ L·mol^{-1}·s^{-1}) than those obtained using the AD1 model. However, they are not as close as those obtained in our earlier work for the addition of trimeric radicals.

Reactivity ratios characterizing the terminal model were calculated based on the AD2 reactions as listed in Table 5.5. Two different r_1 and two different r_2 values were calculated from the eight reactions, where a given r_i value had the same penultimate unit for the radicals. It is clear that the calculated r_i values based on different penultimate units are not consistent. For example, the two r_2 values calculated based on the $AB\cdot$ and $BB\cdot$ radicals are opposite at 23 °C: $k_{122}/k_{121} < 1$ while $k_{222}/k_{221} > 1$. The two r_1 values are both greater than one, but the values are not close ($k_{111}/k_{112} = 6.17$, $k_{211}/k_{212} = 1.99$). Thus, there are two possibilities: terminal model kinetics are not a good description of this copolymerization system or dimeric radicals are not sufficient to capture the correct penultimate unit effects. To explore the latter possibility, monomer and radical reactivity ratios for the EPUE model were also calculated based on these AD2 reactions as listed in Table 5.6 over a range of temperatures and at 1000 bar. At the experimental conditions (23 °C, 1000 bar), the calculated monomer reactivity ratios ($r_{11} = 6.17$, $r_{21} = 1.99$, $r_{22} = 1.67$, $r_{12} = 0.46$) and radical reactivity ratios ($s_1 = 0.91$, $s_2 = 0.33$) have noticeable deviation from those determined from PLP-SEC measurements using the IPUE model: $r_1 = 2.40$, $r_2 = 0.18$, s_1=1.46, s_1=0.38. This reinforces our earlier contention based on homopolymerization studies that using addition of dimeric radicals is not sufficient to predict reactivity measurements in polymeric systems.

Table 5.5: Calculated TM reactivity ratios (r_1, r_2) for methyl methacrylate-methyl acrylate copolymerization based on the eight AD2 reactions in Figure 5.3 over the temperature range of 296.15−476.15 K and at 1000 bar; kinetic parameters are listed in Table 5.4, and the pressure adjustment ratios are listed in Table 5.1.

	r_1		r_2	
T(K)	k_{111}/k_{112}	k_{211}/k_{212}	k_{122}/k_{121}	k_{222}/k_{221}
296.15	6.17	1.99	0.46	1.67
326.15	5.80	1.77	0.51	1.75
356.15	5.50	1.61	0.56	1.83
386.15	5.26	1.49	0.60	1.89
416.15	5.07	1.39	0.64	1.95
446.15	4.91	1.31	0.68	2.00
476.15	4.77	1.24	0.72	2.05

Table 5.6: Calculated EPUE monomer reactivity ratios (r_{11}, r_{21}, r_{22}, r_{12}) and radical reactivity ratios (s_1, s_2) for methyl methacrylate-methyl acrylate copolymerization based on the eight AD2 reactions in Figure 5.3 over the temperature range of 296.15−476.15 K and at 1000 bar; kinetic parameters are listed in Table 5.4, and the pressure adjustment ratios are listed in Table 5.1.

T(K)	r_{11} k_{111}/k_{112}	r_{21} k_{211}/k_{212}	r_{22} k_{222}/k_{221}	r_{12} k_{122}/k_{121}	s_1 k_{211}/k_{111}	s_2 k_{122}/k_{222}
296.15	6.17	1.99	1.67	0.46	0.91	0.33
326.15	5.80	1.77	1.75	0.51	0.82	0.32
356.15	5.50	1.61	1.83	0.56	0.75	0.31
386.15	5.26	1.49	1.89	0.60	0.70	0.30
416.15	5.07	1.39	1.95	0.64	0.66	0.29
446.15	4.91	1.31	2.00	0.68	0.63	0.29
476.15	4.77	1.24	2.05	0.72	0.60	0.28

Therefore, we further extended the chain length of the radicals studied and investigated the reaction of trimeric radicals (AD3 in Figure 5.3). Two different groups of radicals were studied: radicals with methyl methacrylate (A) as the penpenultimate unit (A-AD3) and radicals with methyl acrylate (B) as the penpenultimate unit (B-AD3). This provided both a more realistic mimic of polymeric reactions while also allowing the investigation of penpenultimate unit effects. The activation energies and frequency factors of the eight A-AD3 reactions and the eight B-AD3 reactions are listed in Table 5.7. The methyl methacrylate monomer is still enthalpically preferred as reflected in the lower activation energies ($2.6 - 3.4$ kJ·mol^{-1} lower) and more exothermic heats of reaction ($5.7 - 9.4$ kJ·mol^{-1} more exothermic). The ratios of the frequency factors when A is the penpenultimate unit are $\frac{A_{A,111}}{A_{A,112}} = 0.72$, $\frac{A_{A,121}}{A_{A,122}} = 0.64$, $\frac{A_{A,211}}{A_{A,212}} = 0.77$ and $\frac{A_{A,221}}{A_{A,222}} = 0.76$, which indicates that the addition to methyl acrylate is entropically favored. The calculated propagation rate coefficient for methyl methacrylate is 3.02×10^2 L·mol^{-1}·s^{-1} and 1.69×10^3 L·mol^{-1}·s^{-1} for methyl acrylate. The A-AD3 rate coefficient for methyl methacrylate is close to the experimental value (7.02×10^2 L·mol^{-1}·s^{-1}) while the A-AD3 rate coefficient for methyl acrylate is about one order of magnitude lower than the experimental methyl acrylate homopolymerization rate coefficient (1.84×10^4 L·mol^{-1}·s^{-1}). Note that the A-AD3 reaction for methyl acrylate is not truly homopolymerization, since the penpenultimate unit is methyl methacrylate. The disagreement of the calculated value and the experimental value indicate that penpenultimate unit effects are important here. For the eight AD3 reactions with methyl acrylate as the penpenultimate unit (B-AD3) in Figure 5.3, it can be seen that methyl methacrylate is still enthalpically preferred as reflected in the lower activation energies ($2.9 - 6.1$ kJ·mol^{-1} lower) and more exothermic heats of reaction ($4.2 - 14.8$ kJ·mol^{-1} more exothermic). Methyl acrylate is still entropically preferred as reflected in the higher frequency factors. The ratios of the frequency factors are: $\frac{A_{B,111}}{A_{B,112}} = 0.87$, $\frac{A_{B,121}}{A_{B,122}} = 0.81$, $\frac{A_{B,211}}{A_{B,212}} = 0.72$ and $\frac{A_{B,221}}{A_{B,222}} = 0.21$. The calculated propagation rate coefficient for methyl acrylate (1.56×10^4 L·mol^{-1}·s^{-1}) at 23 °C and 1000 bar is in very good agreement with the experimental data ($k_{p,MA} = 1.81 \times 10^4$ L·mol^{-1}·s^{-1}). The better agreement of the rate coefficient for methyl

Table 5.7: Activation energies (E_a), frequency factors (A), heats of reaction (ΔH_r) and rate constants (k_p at 23 °C, 1000 bar) for the methyl methacrylate-methyl acrylate AD3 reactions where either methyl methacrylate (A) or methyl acrylate (B) is the penpenultimate unit; geometry optimization and frequency calculations were performed using UB3LYP/6-31G(d), electronic energies were calculated using MPWB1K/6-31G(d,p), and low frequencies were treated using a one-dimensional internal rotor model; rate coefficients were first calculated at ambient pressure and adjusted to 1000 bar using the ratios listed in Table 5.1. (k_p: L·mol^{-1}·s^{-1}, E_a: kJ·mol^{-1}, A : L·mol^{-1}·s^{-1}, ΔH_r: kJ·mol^{-1})

Reactions		E_a	A	ΔH_r(23 °C)	k_p(23 °C, 1000 bar)
AAA· + A⟶$AAAA$·	$k_{A,111}$	22.7	1.55×10^6	-52.3	3.02×10^2
BAA· + A⟶$BAAA$·	$k_{B,111}$	22.5	1.82×10^6	-48.5	3.85×10^2
AAA· + B⟶$AAAB$·	$k_{A,112}$	25.5	2.14×10^6	-45.7	1.21×10^2
BAA· + B⟶$BAAB$·	$k_{B,112}$	25.4	2.10×10^6	-44.3	1.24×10^2
AAB· + A⟶$AABA$·	$k_{A,121}$	20.1	5.75×10^6	-65.1	2.90×10^3
BAB· + A⟶$BABA$·	$k_{B,121}$	17.4	3.47×10^6	-64.2	5.27×10^3
AAB· + B⟶$AABB$·	$k_{A,122}$	23.5	8.91×10^6	-57.5	1.10×10^3
BAB· + B⟶$BABB$·	$k_{B,122}$	20.3	4.27×10^6	-54.0	2.00×10^3
ABA· + A⟶$ABAA$·	$k_{A,211}$	21.9	2.82×10^6	-50.7	6.88×10^2
BBA· + A⟶$BBAA$·	$k_{B,211}$	22.7	2.51×10^6	-53.6	4.43×10^2
ABA· + B⟶$ABAB$·	$k_{A,212}$	25.3	3.63×10^6	-45.0	2.24×10^2
BBA· + B⟶$BBAB$·	$k_{B,212}$	26.4	3.47×10^6	-50.3	1.36×10^2
ABB· + A⟶$ABBA$·	$k_{A,221}$	18.5	4.68×10^6	-80.3	4.51×10^3
BBB· + A⟶$BBBA$·	$k_{B,221}$	15.4	1.26×10^7	-87.4	4.31×10^4
ABB· + B⟶$ABBB$·	$k_{A,222}$	21.3	6.17×10^6	-70.9	1.69×10^3
BBB· + B⟶$BBBB$·	$k_{B,222}$	21.5	6.03×10^7	-72.6	1.56×10^4

acrylate homopolymerization for the B-AD3 reaction supports the assertion above that the penpenultimate unit still has an influence on the absolute rate coefficient values for methyl acrylate, while the influence of the penpenultimate unit for methyl methacrylate is less pronounced (i.e., $k_{A,111}$ and $k_{B,111}$ are similar and in good agreement with the experimental value).

The calculated TM ratios based on the AD3 reactions are listed in Table 5.8. The r_i values were calculated for reactions that had the same penpenultimate and penultimate units; thus four r_1 values and four r_2 values were calculated based on the sixteen reactions. The calculated ratios for different penpenultimate and penultimate units are extremely consistent: at 23 °C, the four r_1 values are: 2.50, 3.08, 3.11 and 3.25; the four r_2 values are: 0.38, 0.38, 0.38 and 0.36. The AD3 reactions also allow monomer and radical reactivity ratios for the explicit PUE model to be calculated as listed in Table 5.9 over a range of temperatures and at 1000 bar. Note that the r_{ij} values in Table 5.9 are the same as the r_i values reported in Table 5.8 but are repeated in Table 5.9 with their more specific r_{ij} designation that characterizes the EPUE model. The results from the trimeric radical addition reactions capture the experimental PUE reactivity ratios very well. For the A-AD3 reactions, at 23 °C and 1000 bar, the calculated monomer reactivity ratios ($r_{11} = 2.50$, $r_{21} = 3.08$, $r_{22} = 0.38$, $r_{12} = 0.38$) and radical reactivity ratios (s_1=2.27, s_2=0.65) are in quite good agreement with those fitted based on experiment at 23 °C and 1000 bar: $r_1 = 2.40$, $r_2 = 0.18$, s_1=1.46, s_2=0.38. The ratios calculated using the B-AD3 reactions also have values that are consistent with experiment: $r_{11} = 3.11$, $r_{21} = 3.25$, $r_{22} = 0.36$, $r_{12} = 0.38$, s_1=1.46 and s_2=0.38.

Table 5.8: Calculated TM reactivity ratios (r_1, r_2) for methyl methacrylate-methyl acrylate copolymerization based on the sixteen AD3 reactions in Figure 5.3 over the temperature range of 296.15−476.15 K and at 1000 bar; kinetic parameters are listed in Table 5.7, and the pressure adjustment ratios are listed in Table 5.1.

	r_1 (A-AD3)		r_1 (B-AD3)	
T(K)	$k_{A,111}/k_{A,112}$	$k_{A,211}/k_{A,212}$	$k_{B,111}/k_{B,112}$	$k_{B,211}/k_{B,212}$
296.15	2.50	3.08	3.11	3.25
326.15	2.37	2.71	2.77	2.83
356.15	2.27	2.44	2.51	2.52
386.15	2.19	2.23	2.31	2.29
416.15	2.13	2.07	2.15	2.11
446.15	2.07	1.94	2.03	1.96
476.15	2.02	1.83	1.92	1.84
	r_2 (A-AD3)		r_2 (B-AD3)	
T(K)	$k_{A,122}/k_{A,121}$	$k_{A,222}/k_{A,221}$	$k_{B,122}/k_{B,121}$	$k_{B,222}/k_{B,221}$
296.15	0.38	0.38	0.38	0.36
326.15	0.43	0.42	0.42	0.46
356.15	0.48	0.46	0.46	0.56
386.15	0.53	0.50	0.50	0.66
416.15	0.57	0.54	0.53	0.76
446.15	0.61	0.57	0.56	0.86
476.15	0.64	0.60	0.59	0.96

Table 5.9: Calculated EPUE monomer reactivity ratios (r_{11}, r_{21}, r_{22}, r_{12}) and radical reactivity ratios (s_1, s_2) for methyl methacrylate-methyl acrylate copolymerization based on the sixteen AD3 reactions in Figure 5.3 over the temperature range of 296.15−476.15 K and at 1000 bar; kinetic parameters are listed in Table 5.7, and the pressure adjustment ratios are listed in Table 5.1.

	r_{11}	r_{21}	r_{22}	r_{12}	s_1	s_2
T(K)	$k_{A,111}/k_{A,112}$	$k_{A,211}/k_{A,212}$	$k_{A,222}/k_{A,221}$	$k_{A,122}/k_{A,121}$	$k_{A,211}/k_{A,111}$	$k_{A,122}/k_{A,222}$
296.15	2.50	3.08	0.38	0.38	2.27	0.65
326.15	2.37	2.71	0.42	0.43	2.09	0.70
356.15	2.27	2.44	0.46	0.48	1.95	0.74
386.15	2.19	2.23	0.50	0.53	1.84	0.78
416.15	2.13	2.07	0.54	0.57	1.75	0.82
446.15	2.07	1.94	0.57	0.61	1.68	0.85
476.15	2.02	1.83	0.60	0.64	1.62	0.88
	r_{11}	r_{21}	r_{22}	r_{12}	s_1	s_2
T(K)	$k_{B,111}/k_{B,112}$	$k_{B,211}/k_{B,212}$	$k_{B,222}/k_{B,221}$	$k_{B,122}/k_{B,121}$	$k_{B,211}/k_{B,111}$	$k_{B,122}/k_{B,222}$
296.15	3.11	3.25	0.36	0.38	1.15	0.13
326.15	2.77	2.83	0.46	0.42	1.17	0.12
356.15	2.51	2.52	0.56	0.46	1.18	0.12
386.15	2.31	2.29	0.66	0.50	1.20	0.11
416.15	2.15	2.11	0.76	0.53	1.21	0.11
446.15	2.03	1.96	0.86	0.56	1.22	0.10
476.15	1.92	1.84	0.96	0.59	1.23	0.10

Overall analysis of the calculated rate coefficients and reactivity ratios based on AD1, AD2, A-AD3 and B-AD3 reactions is consistent with the recommendation put forth previously in our homopolymerization study (Yu et al. (2008)). AD1 and AD2 capture the general features of the copolymerization reactions, i.e., methyl methacrylate monomer is always favored enthalpically as reflected by the lower activation energies and more exothermic heats of reaction, and methyl acrylate is entropically favored as evidenced by the higher frequency factors. However, the monomeric and dimeric radicals are not sufficient to capture the absolute values of the rate coefficients and the reactivity ratios. Our results promote the use of at least three units for the propagating radical since effects of the long chain need to be captured and the penpenultimate unit may also have an influence on the rate coefficients. For methyl methacrylate and methyl acrylate, we have shown that the influence of the penpenultimate unit on the activation energy is small, and the EPUE reactivity ratios are affected negligibly. It is also verified that the implicit penultimate model is an accurate description of methyl methacrylate-methyl acrylate copolymerization based on the absolute values of the individual kinetic parameters, as shown by the ratios in Table 5.9: $k_{A,111}/k_{A,112} \approx k_{A,211}/k_{A,212} \approx k_{B,111}/k_{B,112} \approx k_{B,211}/k_{B,212}$ and $k_{A,222}/k_{A,221} \approx k_{A,122}/k_{A,121} \approx k_{B,222}/k_{B,221} \approx k_{B,122}/k_{B,121}$.

5.3.3 Prediction of Composition and Overall Rate Coefficient

The next step was to use the calculated values of all the individual rate coefficients to predict additional quantities for the different models that are experimentally measured: the composition in the copolymer as a function of the composition of the monomer in the feed and the overall rate coefficient for copolymerization, $k_{p,copo}$. Using the results from the trimeric radicals in which penpenultimate effects were incorporated and averaging the different values listed in Table 5.8, the two TM reactivity ratios at 23 °C and 1000 bar were obtained:

$$r_1 = 2.99 \quad r_2 = 0.38$$

Based on averaging the monomer reactivity and radical reactivity ratios for the two different pen-penultimate units reported in Table 5.9, the six EPUE reactivity ratios at 23 °C and 1000 bar were obtained.

$$r_{11} = 2.81 \quad r_{21} = 3.17 \quad r_{22} = 0.37 \quad r_{12} = 0.38$$
$$s_1 = 1.71 \quad s_2 = 0.39$$

Furthermore, the implicit penultimate unit effect model reactivity ratios (r_1 and r_2) were calculated based on further averaging as $r_1 = (r_{11} + r_{21})/2$ and $r_1 = (r_{12} + r_{22})/2$:

$$r_1 = 2.99 \quad r_2 = 0.38 \quad s_1 = 1.71 \quad s_2 = 0.39$$

Thus, there are three different sets of reactivity ratios that can be used to predict the composition and the overall rate coefficient. In the prediction of $k_{p,copo}$, propagation rate coefficients calculated based on $AAA\cdot + A$ ($k_{A,111} = 3.02 \times 10^2$ L·mol^{-1}·s^{-1}) and $BBB\cdot + B$ ($k_{B,222} = 1.56 \times 10^4$ L·mol^{-1}·s^{-1}) were used for methyl methacrylate and methyl acrylate homopolymerization, respectively.

Using these values, Mayo-Lewis plots of F_{MMA} versus f_{MMA} for methyl methacrylate-methyl acrylate copolymerization at 23 °C and 1000 bar based on the EPUE model (Equations 5.4 and 5.5), IPUE model (Equation 5.5) and TM (Equation 5.2) were constructed and are shown in Figure 5.6. The predicted composition curves are in very good agreement with the experimental data. These three curves for the TM, IPUE and EPUE models almost overlap, indicating that in the prediction of copolymer composition, the simplified TM and IPUE models are good surrogates for the more detailed EPUE model. Note that the TM and IPUE models give the exact same values because $\bar{r}_i$ of the IPUE model equals r_i of the TM based on the averaging done here and Equation 5.2 and Equation 5.5 thus afford equivalent results. The compositions based on the EPUE model are within 1% of those based on the IPUE model or the TM.

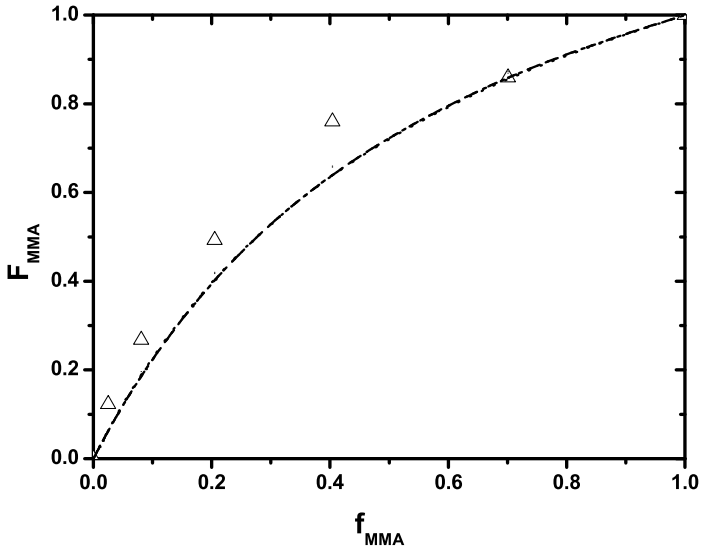

Figure 5.6: Mayo-Lewis plot for methyl methacrylate (MMA)-methyl acrylate copolymerization at 23 °C and 1000 bar: experimental data (triangles) (Buback and Müller (2007)), terminal model (dashed line, r_1 and r_2 are the average values of the data listed in Table 5.8: $r_1 = 2.99$, $r_2 = 0.38$), explicit penultimate effect model (dotted line, r_{ij} are average values of the data listed in Table 5.9: $r_{11} = 2.81$, r_{21}=3.17, r_{12}=0.38, $r_{22} = 0.37$), implicit penultimate effect model (dashed-dotted line, r_j values are the average of the EPUE r_{ij} values: $r_1 = 2.99$, $r_2 = 0.38$).

With the activation energies and frequency factors for all of the individual reactions in hand, it is interesting to calculate the temperature dependence of the monomer reactivity and radical reactivity ratios of the EPUE model over the range of 296.15 to 596.15 K at 1000 bar. These values are calculated based on the activation energies and frequency factors from the A-AD3 reactions and are plotted in Figure 5.7. As expected, the values are all approaching a value of 1.0 at high temperature, but this plot nicely illustrates the rate at which this high temperature asymptote is reached. It is more interesting to see what impact these changes have on the copolymer composition as a function of temperature. The predicted compositions at temperatures of 296.15 K, 373.15 K and 423.15 K are shown in Figure 5.8. With increasing temperature, the curves are approaching the line of parity, which means the preference of the radicals to react with methyl methacrylate is becoming less significant. This example illustrates how *ab initio* calculations can be used to predict the topology of copolymers.

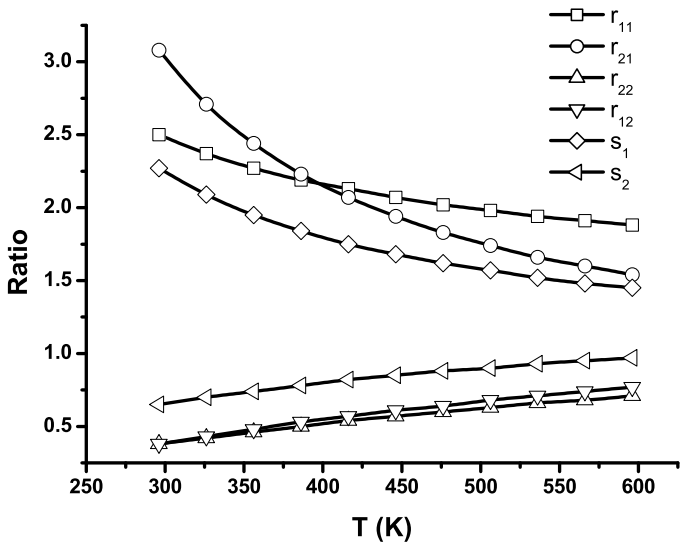

Figure 5.7: Change in the monomer reactivity and radical reactivity ratios characterizing the EPUE model with temperature over the range of 296.15 K to 596.15 K at 1000 bar. The activation energies and frequency factors are from the A-AD3 reactions as listed in Table 5.7.

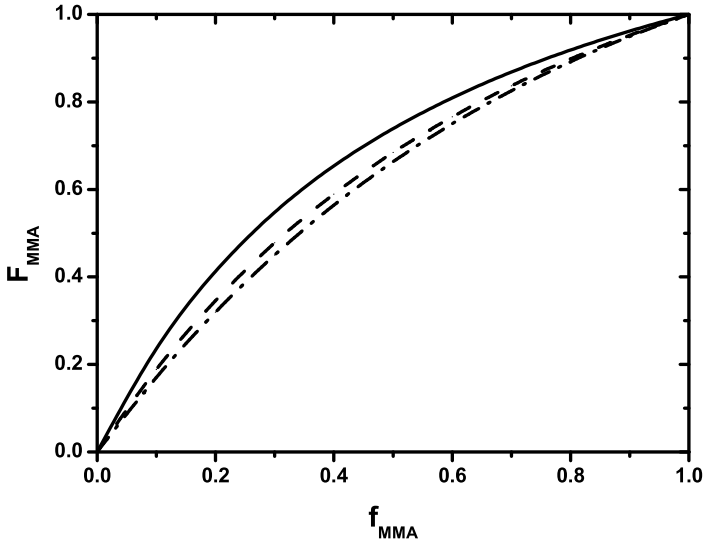

Figure 5.8: Mayo-Lewis plots for methyl methacrylate (MMA)-methyl acrylate copolymerization at three temperatures, 296.15 K (solid line), 373.15 K (dashed line) and 423.15 K (dashed-dotted line)) and 1000 bar based on the EPUE model. The activation energies and frequency factors are from the A-AD3 reactions in Table 5.7.

The predicted values of the overall rate constants ($k_{p,copo}$) as a function of the monomer fraction calculated with the TM, IPUE and EPUE models are shown in Figure 5.9. The results are generally in agreement with the experimental values. The deviation is because the calculated value for k_p of methyl methacrylate homopolymerization is about a factor of two too low, which is most pronounced as the mixture becomes more rich in methyl methacrylate. The calculated value for k_p of methyl acrylate is in better quantitative agreement with the experimental value, which results in the predicted $k_{p,copo}$ matching very well at low methyl methacrylate fractions. The predicted rate coefficients using the EPUE are very close to those predicted using the IPUE model, as can be seen from the plot. However, these results are distinctly different from the values calculated using the TM in the intermediate f_{MMA} region, which are lower than the those based on the two penultimate models. Thus, while the penultimate models are not differentiated by the composition values, the effect of the penultimate unit does manifest itself to a small but measurable extent in $k_{p,copo}$.

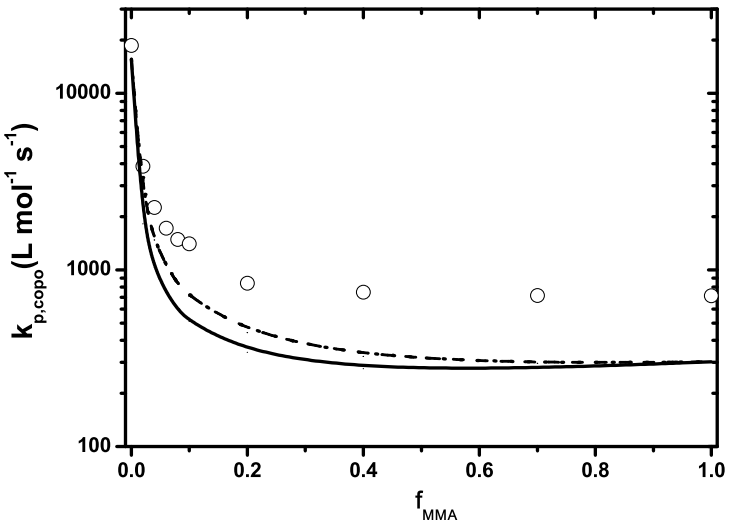

Figure 5.9: Propagation rate constant ($k_{p,copo}$) for methyl methacrylate (MMA)-methyl acrylate copolymerization at 23 °C and 1000 bar: PLP-SEC data (circles) (Buback and Müller (2007)), explicit penultimate effect model prediction (dashed line), implicit penultimate effect model prediction (dotted line) and terminal model prediction (solid line); $k_{p,MMA}$ and $k_{p,MA}$ were calculated using $AAA \cdot +A$ (3.02×10^2 L·mol^{-1}·s^{-1}) and $BBB \cdot +B$ (1.56×10^4 L·mol^{-1}·s^{-1}), respectively; the reactivity ratios for TM : $r_1 = 2.99$, $r_2 = 0.38$; the monomer reactivity and radical reactivity ratios for EPUE : $r_{11} = 2.81$, $r_{21} = 3.17$, $r_{22} = 0.37$, $r_{12} = 0.38$, $s_1 = 1.71$ and $s_2 = 0.39$; the monomer reactivity and radical reactivity ratios for IPUE : $r_1 = 2.99$, $r_2 = 0.38$, $s_1 = 1.71$ and $s_2 = 0.39$.

5.3.4 Reactivity Analysis using Frontier Orbital Theory

Analysis of the energy gaps between the SOMO of the radical and the HOMO or the LUMO of the monomer for all twenty eight reactions studied revealed that the gap between the SOMO and the HOMO is always lower than that between the SOMO and the LUMO, which indicates that all these reactions are electrophilic. The SOMO-HOMO energy gaps are tabulated in Table 5.10. It is clear that the methyl group on the α carbon in methyl methacrylate monomer increases the electron density on the double bond so that the energy gap between the SOMO for a given radical and the HOMO is lower than that for methyl acrylate monomer.

There are also interesting groupings that emerge when the SOMO-HOMO energy values are analyzed. As shown in Figure 5.10, the twenty eight points gather into three groups labelled as G1, G2 and G3. For points in the same group, the reactions all have the same terminal unit and monomer: G1 includes all the reactions of the radicals with methyl acrylate as the terminal unit and methyl methacrylate as the monomer (X-B·+A); G2 includes all the "*homopolymerization*" reactions in which the radical terminal unit is the same as the monomer (X-A·+A, X-B·+B); G3 encompasses all of the reactions of the type X-A·+B. It is clear that all the reactions with the same terminal unit and monomer have very similar SOMO-HOMO gaps, revealing that the penultimate or penpenultimate unit has little impact on this energy value. It is also interesting that there is a rough correlation between E(SOMO-HOMO) and activation energy; as E(SOMO-HOMO) increases, the activation energy increases. Clearly, the fine structure of the points within one group would not be captured by a single linear correlation between E_a and E(SOMO-HOMO). For example, although methyl methacrylate and methyl acrylate homopolymerization both have similar E(SOMO-HOMO) values and comprise G2, their E_a values are clearly different. However, the general trend is still a useful diagnostic aid. This suggests that by simply performing quantum chemistry calculations on stable structures, a general estimate of E_a could be obtained without having to perform more challenging transition state searches.

Table 5.10: The energy gaps between the SOMO energies of the radical and the HOMO energies of the monomer and activation energies (E_a) for all twenty eight addition reactions studied. The group number corresponds to the circled clusters in Figure 5.10, A: methyl methacrylate, B: methyl acrylate. (energy: kJ·mol^{-1})

Radical	**Monomer**	E(SOMO-HOMO)	E_a	Group
A·	A	138.68	27.70	G2
A·	B	187.96	34.60	G3
B·	A	87.40	22.50	G1
B·	B	136.68	26.41	G2
AA·	A	136.26	28.00	G2
AA·	B	185.55	31.10	G3
BA·	A	138.70	26.75	G2
BA·	B	187.99	29.80	G3
AB·	A	82.49	19.02	G1
AB·	B	131.78	21.98	G2
BB·	A	78.48	21.70	G1
BB·	B	127.77	22.80	G2
AAA·	A	133.14	22.70	G2
AAA·	B	182.43	25.50	G3
BAA·	A	132.12	22.49	G2
BAA·	B	181.41	25.44	G3
AAB·	A	86.14	20.11	G1
AAB·	B	135.42	23.54	G2
BAB·	A	83.10	17.43	G1
BAB·	B	132.38	20.27	G2
ABA·	A	127.56	21.90	G2
ABA·	B	176.84	25.29	G3
BBA·	A	135.48	22.66	G2
BBA·	B	184.76	26.38	G3
ABB·	A	95.03	18.52	G1
ABB·	B	144.32	21.34	G2
BBB·	A	81.10	15.42	G1
BBB·	B	130.39	21.50	G2

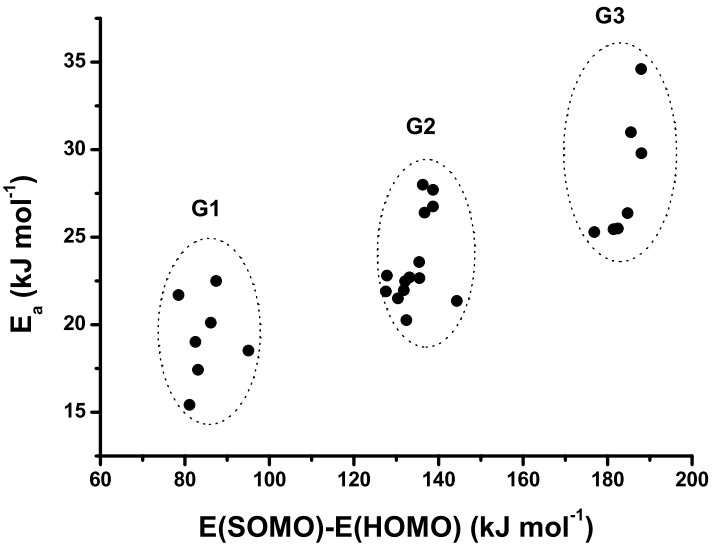

Figure 5.10: Activation energy as a function of the energy gap between the SOMO energy level of the radical and the HOMO energy level of the monomer (Table 5.10). Orbital energy levels were calculated using MPWB1K/6-31G(d,p).

5.3.5 Correlation Between E_a and ΔH_r

Finally, the relationship between the activation energy (E_a) and the heat of reaction (ΔH_r) as defined by the Evans-Polanyi relationship was also investigated based on the sixteen AD3 reactions as shown in the plot in Figure 5.11. A linear relationship is apparent:

$$E_a = 33.0 + 0.185\Delta H_r \tag{5.17}$$

with a relatively high regression coefficient (R^2 equals 0.77). It is interesting to compare this correlation to others reported in the literature for radical addition to alkenes. A limiting correlation between E_a and ΔH_r for radical addition to alkene was proposed by Fischer and Radom as an upper bound and is shown as Equation 5.18 (Fischer and Radom (2001)):

$$E_a = 50.0 + 0.220\Delta H_r \tag{5.18}$$

The correlation is also plotted as the dashed line in Figure 5.11. The limiting correlation represents the activation energy that would be observed for a given heat of reaction if only enthalpic effects were at play, i.e., polar and steric effects can be neglected. The relationship regressed based on the sixteen AD3 reactions clearly falls below this upper bound; the E_0 value is about 17 kJ·mol^{-1} lower than the upper limit, and the slope is less pronounced. This is consistent with the ideas put forth by Fischer and Radom, in which polar effects result in only negative deviations from the upper bound, and the electrophilic polar effects specifically lead to a slope that is smaller than that given by the enthalpy effect alone.

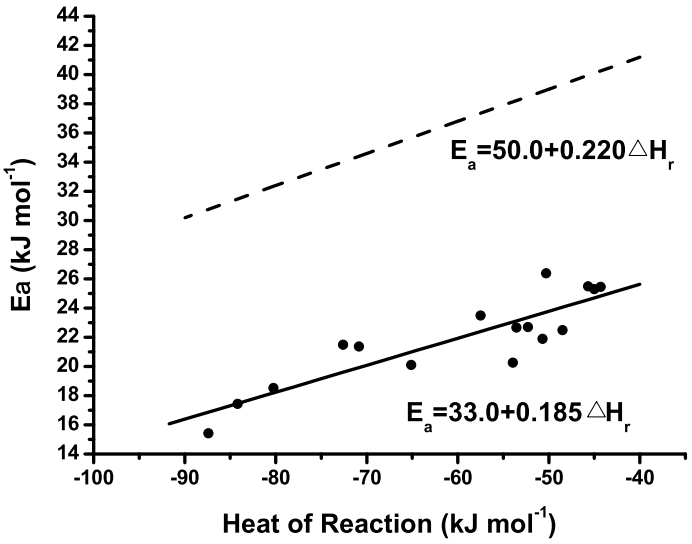

Figure 5.11: Activation energy (E_a) as a function of heat of reaction (ΔH_r) for the sixteen AD3 reactions summarized in Table 5.7; the linear relationship (solid line) regressed is: $E_a = 33.0 + 0.185\Delta H_r$, $R^2 = 0.77$; the dashed line is the upper limiting correlation between E_a and ΔH_r for radical addition to alkenes presented by Fischer and Radom (2001).

5.4 Conclusion

Methyl methacrylate and methyl acrylate copolymerization reactions were studied using addition of monomeric, dimeric and trimeric radicals to monomers using quantum chemistry and transition state theory. The use of radicals of different lengths allowed penultimate and penpenultimate effects to be explored and different models of copolymerization (TM, EPUE and IPUE) to be tested. Unrestricted B3LYP/6-31G(d) was used for geometry optimization and potential energy scans, and the electronic energies were calculated using MPWB1K/6-31G(d,p). Low frequencies were treated using a one-dimensional internal rotor model in the calculation of partition functions for rate constants and thermodynamic properties. It was found that addition reactions involving monomeric or dimeric radicals offered results that were qualitatively consistent with experimental data, but quantitatively accurate monomer and radical reactivity ratios and rate coefficients were not obtained. However, rate coefficients and monomer and radical reactivity ratios for the TM and PUE models which were in good agreement with those fitted from experimental data were obtained when the radical chain length was three. Although the penpenultimate unit had a negligible influence on the activation energy values, its entropic influence was reflected in the frequency factor and thus the rate coefficient. The predicted copolymer composition using the TM, IPUE and EPUE models are very close while the predicted overall rate coefficients ($k_{p,copo}$) based on the EPUE and IPUE models had measurable differences from that based on the TM. The reactivity was analyzed based on frontier orbital theory. All reactions studied involved the interaction between the SOMO of the radical and the HOMO of the monomer, indicating electrophilic addition, and a general correlation between the activation energy and the SOMO/HOMO energy gap was observed. Finally, the relationship between the activation energy and the reaction enthalpy based on the sixteen AD3 reactions was examined, and the Evans-Polanyi relationship was shown to be obeyed.

Chapter 6

Depropagation, 1,5-Hydrogen Transfer, β-scission and Mid-chain Radical Propagation in Methyl Acrylate Polymerization

6.1 Introduction

Conventional acrylate resins in the automobile coating industry are undergoing a revolution in their formulation and the mechanism by which they are created. These changes are driven by environmental regulations that demand lower amounts of volatile organic compounds (VOCs) (Adamsons et al. (1998); Grady et al. (2002)). Traditional resins are composed of high molecular weight polymers which are produced at low temperature ($< 80\ ^{\circ}$C). In order to decrease the viscosity during the coating process, a high content of organic solvent (70%) needs to be used; the polymeric coating layer is formed upon evaporation of the organic solvent. New generation acrylate resins require low solvent content since they are mainly composed of low molecular weight polymers

with crosslinkable functional groups such as hydroxyl and epoxy. With an added curing agent, the coated resins can undergo crosslinking reactions to form a polymeric coating on metal surfaces (Adamsons et al. (1998)). High-temperature polymerization is an economical way to produce such low molecular weight polymers. High polymerization temperatures ($> 120°$C and often $< 180°$C) prompt secondary reactions, such as depropagation and intramolecular transfer reactions of polymeric radicals (Hakim et al. (2000)). The mid-chain radicals formed via transfer reactions can react with monomers to form branched chains or react via β-scission to form smaller radical chains and unsaturated polymers.

The ability to predict the topology and molecular weight of polymers synthesized at elevated temperatures as a function of reaction conditions would thus be valuable to guide the design of acrylate resins. However, modeling a polymerization system at high temperature requires that accurate kinetic parameters are available for all of the associated secondary reactions. Because all the reactions are coupled, it is difficult to measure the rate coefficients for individual reactions experimentally. The advent of PLP-SEC makes it possible to measure accurate propagation rate coefficients for monomers which satisfy the requirement that secondary reactions are negligible on the time scale of the laser interval (Beuermann et al. (1997, 2000, 1996); Buback et al. (2001, 1998); Coote et al. (1997a); Hutchinson et al. (1997)). Direct evidence of secondary reactions can be obtained from measurements such as electron spin resonance (ESR), nuclear magnetic resonance (NMR) and electron spray ionization-Fourier transform mass spectrometry (ESI-FTMS) (Ahmad et al. (1998); McCord et al. (1997); Plessis et al. (2001, 2000); Willemse et al. (2005)). However, accurate determination of the rate coefficients for secondary reactions is still infeasible, and any quantitative assessment of their contribution requires regression in the context of a model.

An alternative to experimental measurements is to predict rate coefficients using theoretical approaches. While radical reactions have been studied extensively using quantum chemistry in different research fields (Coote (2005); Fischer and Radom (2001); Pfaendtner et al. (2006)), the successful application of quantum chemistry and transition state theory for polymeric reactions has

emerged more recently and has focused primarily on propagation reactions (Bebe et al. (2006); Fischer and Radom (2001); Heuts and Gilbert (1995); Huang et al. (1998); Van Cauter et al. (2006)). In previous research, we developed and applied a computational methodology to determine propagation kinetic parameters for methyl methacrylate and methyl acrylate homopolymerization, and the methodology was verified by comparing the calculated data to values measured with PLP-SEC (Yu et al. (2008)). The methodology was then applied to copolymerization of methyl methacrylate and methyl acrylate to predict absolute values of rate coefficients for all self- and cross-reactions, calculate reactivity ratios, and explore penultimate and penpenultimate effects.

In the present study, we used the computational approach to determine rate coefficients for four different secondary reactions in methyl acrylate polymerization: depropagation, 1,5-hydrogen transfer, β-scission and mid-chain propagation. Various short-chain mimics were used to capture the nature of the polymeric chain for the different reactions. A balance was sought between capturing the environment around the reactive site(s) realistically and reasonable computational times. Depropagation was studied using a tetrameric methyl acrylate radical as the reactant. This is precisely the reverse of the propagation reaction that we studied previously, in which addition of trimeric radicals to monomer was shown to give rate coefficients that were in very good agreement with experimental measurements. In order to study the influence of the backbone units which are not involved in the formation of the six-membered ring in the transition state structure for 1,5-hydrogen transfer, both a trimeric radical and a pentameric radical were studied. A trimeric mid-chain radical was used in the calculation of rate coefficients for mid-chain propagation. Finally, a hexameric radical was used to investigate the kinetic parameters for the two different possible β-scission routes of mid-chain radicals. A summary of the different reactions studied is provided in Figure 6.1.

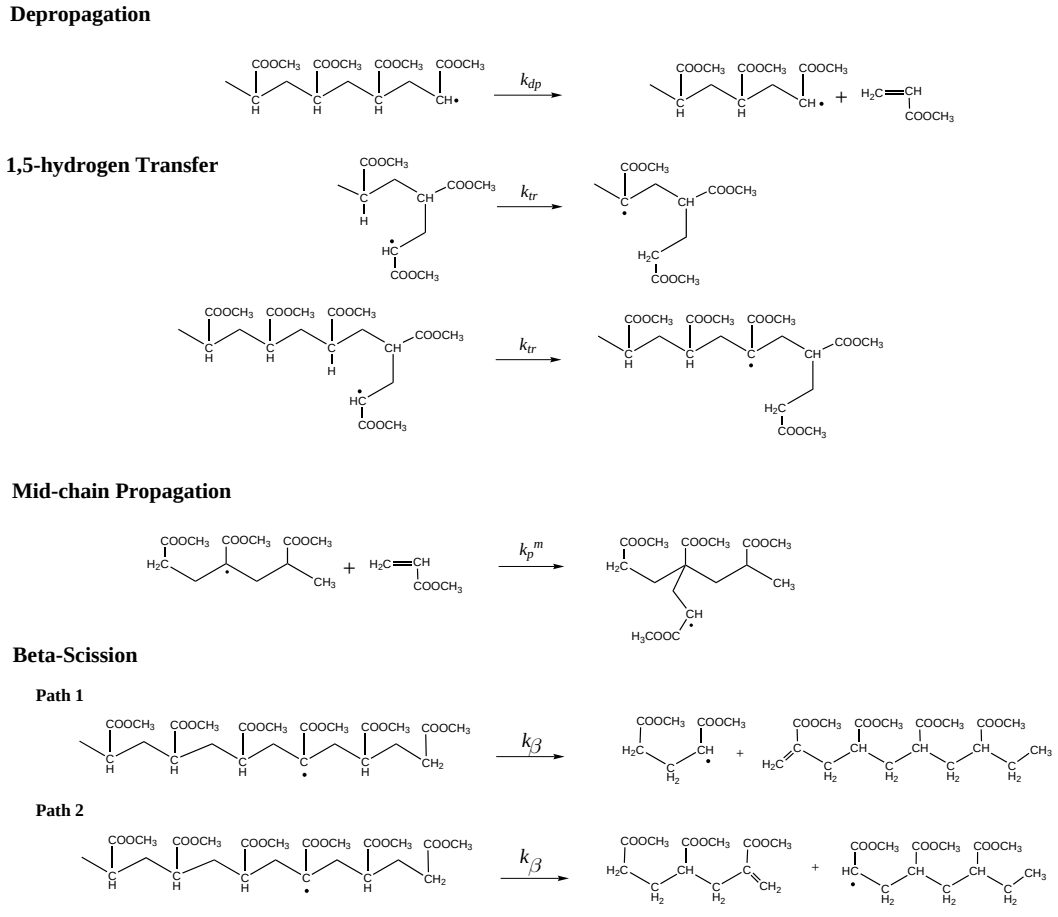

Figure 6.1: Depropagation, 1,5-hydrogen transfer, mid-chain propagation and β-scission in methyl acrylate polymerization. For depropagation, a tetrameric radical was used as the reactant. For 1,5-hydrogen transfer, both a trimeric and a pentameric radical were studied. Mid-chain propagation was explored using a trimeric radical. Two β-scission pathways for decomposition of a hexameric radical were examined.

6.2 Computational Methodology

Gaussian 03 was used for all of the calculations including geometry optimization, potential energy scans, energy evaluations and thermodynamic calculations (Frisch et al. (2004)). All the reactants and products were first optimized using unrestricted B3LYP/6-31G(d) via conventional gradient-based optimization (Foresman (2002); Schlegel (1982)). However, the optimized geometry is dependent on the initial structure provided as input, particularly for large species with many degrees of freedom. Although a Boltzmann distribution of low energy conformers will exist during reaction, we sought to find the lowest energy conformations for the reactants and the products. In order to overcome the barriers between "*local*" minimum conformations and locate "*global*" minimum conformations, potential energy scans were performed for each single bond in the optimal structure identified by conventional optimization. Unrestricted B3LYP/6-31G(d) was also used for all potential energy scans. If lower energy conformers were identified, a new set of potential energy scans was carried out until no conformations of lower energy were obtained. Although one-dimensional torsional scans do not guarantee that the global minimum will be located, much of the variation in conformations is derived from torsional motions around single bonds, and our approach did indeed often identify conformations that were lower in energy than the one obtained by conventional optimization.

To locate transition state structures, the QST3 method was used, which requires the optimized reactant(s), product(s) and an estimate of the transition state (Peng et al. (1996)). An estimate for the transition state of depropagation, which has the same transition state as the propagation reaction, was constructed by elongating the carbon-carbon single bond in the $\beta-$position to the radical center of the addition product to a bond length of 2.3 Å. The same estimated bond length was also used to generate initial guesses for the transition states of mid-chain propagation and β-scission. The estimated transition state for the 1,5-hydrogen transfer reaction was constructed by scanning the energy as the length of the bond between the abstracted hydrogen atom and the

carbon atom in the fifth position was elongated. Transition states were identified as saddle points on the potential energy surface, possessing one imaginary frequency. Once possible transition state structures were identified, they were verified using intrinsic reaction coordinate (IRC) following. Unrestricted B3LYP/6-31G(d) was used for both the QST3 and the IRC calculations. Frequencies were also calculated using unrestricted B3LYP/6-31G(d), and the zero-point vibrational energy (ZPVE) was calculated using a scale factor of 0.9806 (Scott and Radom (1996)). A scale factor of 1.0002 was used in the calculation of partition functions based on the recommended scale factors for ΔH_{vib} and ΔS_{vib} reported by Scott and Radom (1996).

With the optimized structures in hand, the electronic energy, E_e, was obtained from single point calculations using MPWB1K/6-31G(d,p), which was optimized against barrier heights based on nine elementary reactions by Zhao and Truhlar (2004). Reaction rate constants were then calculated using Equation 6.1 at a series of temperatures from 298.15 to 800 K based on transition state theory (Pfaendtner and Broadbelt (2007a)):

$$k(T) = \kappa(T)\frac{k_B T}{h}(c^o)^{1-m}\frac{Q^{\ddagger}}{Q_{reactant(s)}}e^{-\Delta E_0/RT} \tag{6.1}$$

where $\kappa(T)$ is the tunneling factor, k_B is Boltzmann's constant (1.3806×10^{-23} J·mol^{-1}·K^{-1}), h is Planck's constant (6.6261×10^{-34} J·s), m is the number of reactants, which is two for mid-chain propagation and one for depropagation, β-scission and 1,5-hydrogen transfer, c° is the standard state concentration (mol·L^{-1}) to which the quantum chemical calculations are referenced, $\frac{P}{RT}$, where P is 1 atm, and ΔE_0 is the difference between $E_{\circ}$ of the transition state and the reactant(s), which is defined as the summation of the electronic energy (E_e) and the zero-point vibrational energy (ZPVE):

$$E_{\circ} = E_e + ZPVE \tag{6.2}$$

ZPVE is the contribution to the energy from vibration at 0 K as defined in Equation 6.3 (McQuarrie and Simon (1999)):

$$ZPVE = \frac{1}{2}\sum_{i}^{3N-6} h\nu_i \tag{6.3}$$

in which N is the number of atoms, and ν_i represents the frequencies. For transition states, $3N-7$ frequencies are included in the ZPVE. The tunneling coefficient ($\kappa(T)$) accounts for quantum effects in the motion along the reaction path (Coote (2005)), which is important for reactions with a narrow reaction barrier and involving light atoms, such as hydrogen transfer (Coote (2005); Pfaendtner and Broadbelt (2007b); Pfaendtner et al. (2006)). The most widely used classical approximation for tunneling is the Wigner approximation which is given as Equation 6.4 (Wigner (1932)):

$$\kappa(T) = 1 - \frac{1}{24}(\frac{ih\nu^{\ddagger}}{k_B T})^2 \tag{6.4}$$

in which $\nu^{\ddagger}$ is the imaginary frequency in the transition state which represents the motion along the reaction coordinate. The Wigner approximation is frequently used, but it is known to underestimate tunneling effects since it only accounts for the contributions near the top of the barrier (Truong et al. (1999)). Semi-classical approximations calculate the tunneling coefficient in terms of the probability for a wave function to go through the energy barrier, which is called the path integral formulation. Three semi-classical approximations were used and compared in this research including the small curvature tunneling (SCT), the zero curvature tunneling (ZCT) and the Eckart approximations. The $\kappa(T)$ values for these approximations were evaluated using the software CSEO (*www.cseo.net*).

A critical part of obtaining accurate values of $k(T)$ is specifying the values of $Q^{\ddagger}$ and $Q_{reactant(s)}$ in Equation 6.1, which are the partition functions for the transition state and the reactant(s). The partition function is conventionally considered to include contributions from four different modes: electronic (Q_e), translation (Q_{tr}), rotation (Q_r) and vibration (Q_{vib}) as shown in Equation 6.5:

$$Q = Q_e Q_{tr} Q_r Q_{vib} \tag{6.5}$$

For species in their ground state, $Q_e = 1$, and Q_{tr} and Q_r are defined in standard textbooks (McQuarrie and Simon (1999)). Q_{vib} is the vibrational partition function based on the contributions from the individual frequencies, which are often calculated using the harmonic oscillator (HO) approximation. However, this is known to be inaccurate for some motions characterized by low frequencies, which are often better treated as hindered rotations. If there are many torsional motions with low frequencies, their contributions can be quite large, and the difference between the partition function values can be significant. To account for these hindered rotations, Q_{vib} is treated using an internal rotor model as shown in Equation 6.6:

$$Q = Q_e Q_{tr} Q_r Q_{vib} Q_{int,rot} \tag{6.6}$$

where $Q_{int,rot}$ is the contribution to the partition function of the low vibrational modes that are better treated as internal rotations. In the present approach, we did not apply an arbitrary upper bound to define what was classified as a low frequency, and we used a method for calculating $Q_{int,rot}$ that was general for rotations of any symmetry. The number of low frequencies that were removed was set as the number of rotors, which included rotations about σ bonds and the bond defining the transition state. Although the bond defining the transition state is not a real bond, it is treated as a hindered rotor since the lowest positive frequency in the transition state mainly consists of torsional motion about this bond. Rather than simply removing the contribution of the N lowest frequencies from Q_{vib}, where N is the number of rotors, the low frequencies were examined to make sure they consisted of rotational components. Interestingly, all vibrational motions that were removed for all these reactions had frequencies less than 200 cm^{-1}. For those motions which do not have torsional components, they remain in the partition function and are treated conventionally using the harmonic oscillator model. For the 1,5-hydrogen transfer reactions, the transition states involve a six-membered ring composed of four single bonds which were not treated as rotations.

The partition function of the m-th internal rotor was calculated using Equation 6.7:

$$Q_{int,rot,m} = \frac{1}{\sigma_m} \sum_i exp(-\frac{\epsilon_i}{k_B T}) \tag{6.7}$$

where σ_m is the symmetry number of the internal rotation and ϵ_i are the energy levels of the internal rotation, which were calculated by solving a one-dimensional Schrödinger equation:

$$-\frac{\hbar^2}{2I_{red}} \frac{d^2}{d\theta^2} \Psi + V(\theta)\Psi = \epsilon\Psi \tag{6.8}$$

where $\hbar$ is Planck's constant divided by 2π, Ψ is the wave function, θ is the torsional angle, and I_{red} is the reduced moment of inertia, which was defined as $I^{2,3}$ in accord with the systematic classification of moments of inertia by East and Radom (1997). $V(\theta)$ was determined from relaxed potential energy scans calculated using unrestricted B3LYP/6-31G(d) in intervals of 30 °; thus, a total 12 optimized conformations from 0° to 360° were obtained for each rotor. $V(\theta)$ was expanded using a full Fourier series as in Equation 6.9:

$$V(\theta) = \sum_{i=1}^{n} [a_i(1 - cosi\theta) + b_i sini\theta] \tag{6.9}$$

where a_i and b_i are the coefficients of the expansion. Equation 6.9 can be written in its matrix product form, and the coefficients a_i and b_i were determined by solving an overdetermined matrix. It has been shown in previous research that for a scan interval of 30°, $n = 3$ in Equation 6.9 performs well in fitting the potential energy scans for both symmetric and asymmetric tops (Yu et al. (2008)).

The one-dimensional Schrödinger equation (Equation 6.8) was solved using the Fourier Grid Hamiltonian (FGH) method, in which the Hamiltonian operator was discretized over the torsional angle range, and the energy levels, ϵ_i (eigenvalues), were calculated by diagonalizing the Hamiltonian matrix (Balint-Kurti et al. (1992)). In this research, the Hamiltonian operator was discretized using 1000 points, which has been shown to be accurate compared with finer grids containing 5000 points (Yu et al. (2008)). The calculation of the reduced moment of inertia, solution of the Fourier

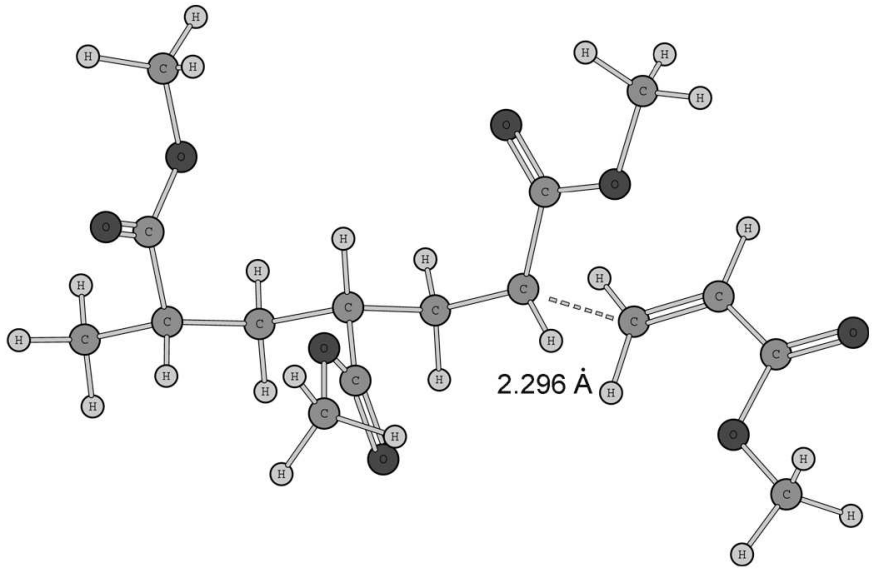

Figure 6.2: The transition state structure for the depropagation of methyl acrylate tetrameric radical located using B3LYP/6-31G(d). The bond defining the transition state is 2.296 Å.

coefficients and Schrödinger equation, and calculation of the partition functions were carried out with "*calck*" developed in our group (Pfaendtner et al. (2007)).

6.3 Results and Discussion

6.3.1 Depropagation

The structure of the transition state for depropagation of a tetrameric radical is shown in Figure 6.2. The bond defining the transition state is 2.296 Å, and the carbon-carbon double bond in the monomer has elongated to a value of 1.366 Å, compared to its equilibrium value of 1.335 Å.

Values reported experimentally for rate coefficients and kinetic parameters of depropagation are scarce and can vary widely. For example, the depropagation kinetic parameters for butyl methacrylate (BMA) determined by Hutchinson et al. were reported as: $E_a = 75.6$ kJ·mol^{-1} and $A = 1.31 \times 10^{13}$ s^{-1} (Hutchinson et al. (1998)); in contrast, the depropagation kinetic parameters for BMA provided by Buback et al. were: $E_a = 147.4$ kJ·mol^{-1} and $A = 6.78 \times 10^{15}$ s^{-1} (Buback et al. (1999)). It is thus difficult to perform an absolute comparison of the calculated values to experimental data, but these ranges do provide some basis for assessing our calculated results. When the depropagation rate coefficients over the temperature range of 298.15-800 K were calculated for methyl acrylate and the frequency factor and activation energy were fitted from lnk_d versus 1/T, the values obtained were:

$$E_a = 119.0 \text{ kJ·mol}^{-1} \quad A = 9.12 \times 10^{13} \text{ s}^{-1}$$

which sit squarely in the ranges defined by the experimental data for the analogous monomer BMA.

The ceiling temperature (T_c) is the temperature at which the depropagation rate equals the propagation rate, i.e., the reaction is at equilibrium and $\Delta G_r = 0$. The ceiling temperature is dependent on the monomer concentration ($[M]$) as expressed in Equation 6.10.

$$T_c = \frac{\Delta H_r}{\Delta S_r + Rln[M]} \tag{6.10}$$

The experimental heat of reaction for methyl acrylate propagation (ΔH_r) is approximately -80 kJ·mol^{-1}. The estimated ceiling temperature in the case when the monomer concentration is 11.1 mol·L^{-1} and ΔS_r is assumed to be a typical value of -120 J·mol^{-1}·K^{-1} (Meyer and Keurentjes (2005)) is 527 °C. The calculated thermodynamic properties (ΔH_r, ΔS_r and ΔG_r) over the temperature range of 298.15-800 K are listed in Table 6.1. The calculated heat of reaction at 120 °C for propagation is around -70 kJ·mol^{-1}, and the calculated value of ΔS_r is around -160 J·mol^{-1}·K^{-1}. Using these values, the calculated ceiling temperature is around 227 °C, which is much lower than the value estimated using a representative ΔS_r value. Given the good agreement we have obtained

Table 6.1: The heat of reaction (ΔH_r), entropy change (ΔS_r), Gibbs free energy change (ΔG_r) and ceiling temperature based on these values and a monomer concentration of 11.1 M. The depropagation of methyl acrylate tetrameric radical is shown in Figure 6.1. (units: temperature: °C, ΔH_r: kJ·mol^{-1}, ΔS_r: J·mol^{-1}·K^{-1}, ΔG_r: kJ·mol^{-1})

T	ΔH_r	ΔS_r	ΔG_r	T_c
298.15	-72.6	-165.9	-23.1	224.5
300	-72.6	-165.8	-22.8	224.5
350	-71.7	-163.2	-14.6	227.6
400	-70.8	-160.7	-6.5	230.1
450	-69.8	-158.4	1.5	231.2
500	-68.7	-156.2	9.4	231.3
550	-67.6	-154.1	17.1	231.0
600	-66.5	-152.0	24.8	230.7
700	-64.1	-148.4	39.8	226.1
800	-61.7	-145.2	54.5	219.7

between calculated and experimental values of frequency factors, which encapsulate entropic effects, for different reactions, it is reasonable to expect that our calculated value of ΔS_r is sound.

6.3.2 1,5-Hydrogen Transfer

The 1,5-hydrogen transfer reaction is one of the most significant intramolecular transfer reactions for acrylate radicals. The transfer to the fifth position is preferred over other positions because a six-membered ring without significant ring strain is formed in the transition state, as shown in Figure 6.1 (Pfaendtner et al. (2006)). The formation of cyclic transition states that are free of ring strain is also applicable to mid-chain radicals. For example, an apparent 1,3-hydrogen transfer from a chain end is thought to occur via two successive hydrogen transfer reactions involving 1,7-hydrogen transfer of an end-chain radical, followed by a 1,5-hydrogen transfer of a mid-chain radical (Levine and Broadbelt (2008); Moscatelli et al. (2006)). The two-step process proceeds at a significantly faster rate than the strained 1,3-hydrogen transfer of an end-chain radical.

The transition states of the 1,5-hydrogen transfer reaction of a methyl acrylate trimeric end-chain radical and a methyl acrylate pentameric end-chain radical are shown in Figure 6.3. The bond length of the carbon-hydrogen bond at the fifth carbon is 1.321 Å for the trimeric radical and 1.350 Å for the pentameric radical. Thus, the transition state is slightly earlier for the trimeric radical, and the IRC calculations shown in Figure 6.4 reveal that the peak for the pentameric radical is narrower, indicating that the tunneling effect for the pentameric radical is more pronounced. This effect is captured by the simple Wigner correlation for tunneling: $\nu = -1494.29$ cm^{-1} for the trimeric radical and $\nu = -1612.27$ cm^{-1} for the pentameric radical, and thus the value of $\kappa(T)$ will be higher for the pentameric radical (Equation 6.4).

Figure 6.3: Transition state structures for 1,5-hydrogen transfer of trimeric (top) and pentameric (bottom) radicals of methyl acrylate located using UB3LYP/6-31G(d). The lengths of the bonds defining the transition states are shown. Carbon atoms labeled with a “1” are the radical center in the reactants, and carbon atoms labeled with a “5” are the carbon atom in the reactants from which the hydrogen atom is being abstracted.

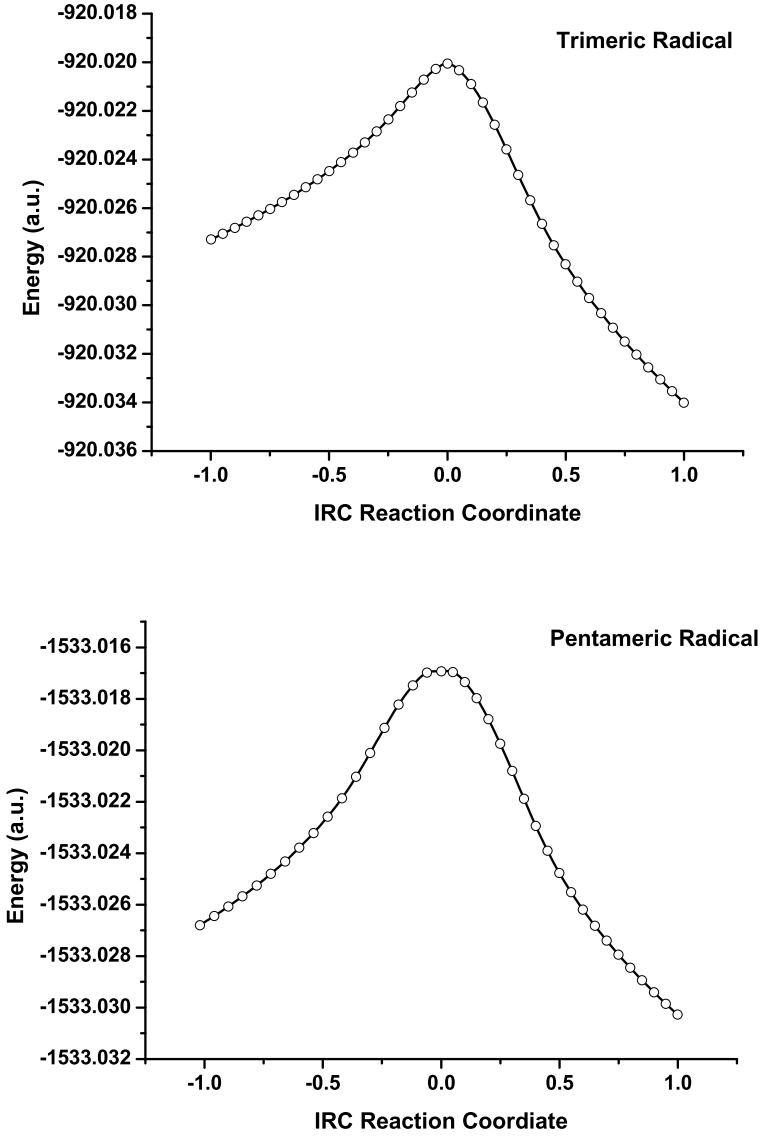

Figure 6.4: Intrinsic reaction coordinate (IRC) calculations for the 1,5-hydrogen transfer of trimeric and pentameric radicals of methyl acrylate using UB3LYP/6-31G(d). A step size of 0.05 amu$^{1/2}$·Bohr was used, and both the forward (positive direction) and reverse (negative direction) reactions proceed to 1.0 amu$^{1/2}$·Bohr.

Intrinsic reaction coordinate following of both of the transition state structures led to reactants that were local minima rather than the "global" minima identified by our optimization approach. The formation of the six-membered ring in the transition state structure required the transformation of the extended conformation of the global minimum (A in Figure 6.5) to the local minimum (B in Figure 6.5) via rotation. Based on the potential energy scans, it was revealed that the barrier to rotation is much smaller than the barrier for the reaction, so to calculate the overall transfer rate coefficient for the reaction from the global minimum energy structure, it was assumed that the global minimum (A) and the local minimum (B) are in equilibrium as quantified by Equation 6.11.

$$K_{eq}(T) = \frac{[B]}{[A]} = e^{-\frac{\Delta G(A \rightleftharpoons B)}{RT}} \tag{6.11}$$

$k_{TST}(T)$ was then calculated using Equation 6.1 based on the local minimum (B), and the overall rate coefficient, k_{tr}, is the product of the calculated rate coefficient and the equilibrium constant as shown in Equation 6.12.

$$k_{tr}(T) = K_{eq}(T) * k_{TST}(T) \tag{6.12}$$

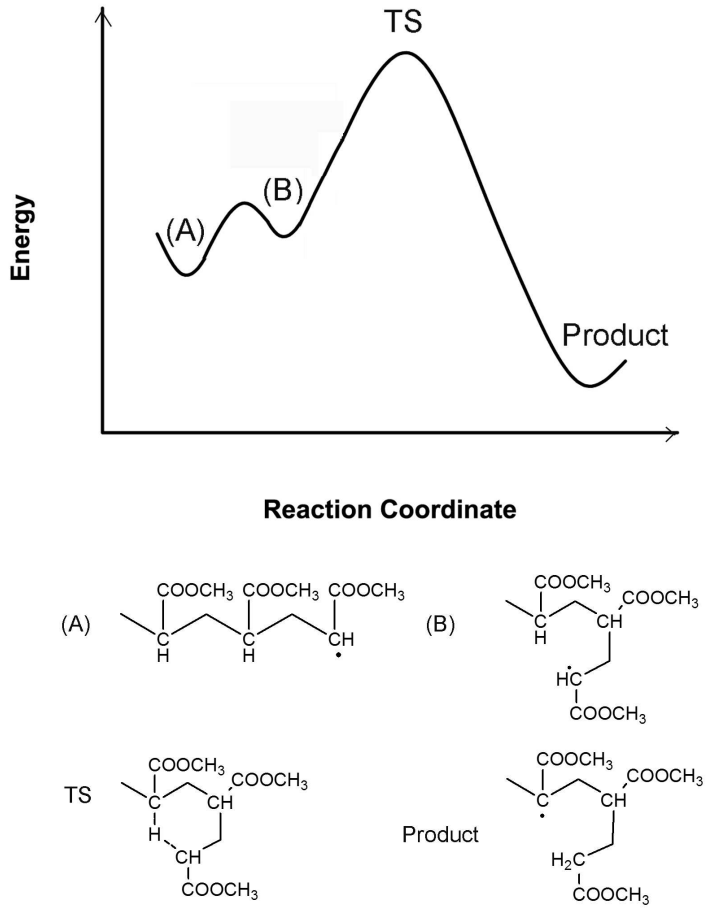

Figure 6.5: 1,5-hydrogen transfer reaction of methyl acrylate involves conversion of the global minimum (A) to a local minimum (B) through rotation which then leads to the transition state (TS).

To obtain $k_{TST}(T)$, it was necessary to calculate the tunneling coefficient, $\kappa(T)$. The tunneling coefficient was calculated using four approaches: the semi-classical Eckart, SCT and ZCT approximations and the empirical Wigner correction. The calculated coefficients for both the trimeric radical and the pentameric radical are summarized in Table 6.2. The tunneling coefficients for the pentameric radical are higher than those for the trimeric radical, which is consistent with the narrower potential peak shown in Figure 6.4. SCT is the most computationally rigorous method for calculating the tunneling coefficient and is thus used as a standard for comparison. For both trimeric and pentameric radicals, the Wigner and ZCT tunneling coefficients are lower than the SCT values for temperatures less than 500 K, while the Eckart tunneling coefficients are higher than those from the SCT approximation at all temperatures. The coefficients decrease quickly with increasing temperature, but the calculated kinetic parameters are clearly influenced by the tunneling coefficients since there is a broad range of $\kappa(T)$ values over the temperature range over which the kinetic parameters are regressed.

Table 6.2: Tunneling coefficients (κ) calculated using the Eckart, ZCT, SCT and Wigner approximations over the temperature range of 298-800 K for 1,5-hydrogen transfer of a trimeric or a pentameric radical.

	Trimeric Radical				**Pentameric Radical**			
T (K)	**Eckart**	**ZCT**	**SCT**	**Wigner**	**Eckart**	**ZCT**	**SCT**	**Wigner**
298	16.57	2.41	4.61	3.17	32.38	4.89	12.10	3.53
300	15.89	2.38	4.53	3.14	30.63	4.79	11.74	3.49
323	10.12	2.10	3.73	2.85	16.97	3.86	8.38	3.15
350	6.88	1.87	3.10	2.57	10.28	3.16	6.12	2.83
400	4.27	1.59	2.39	2.21	5.58	2.40	3.99	2.40
450	3.17	1.43	1.99	1.95	3.84	1.99	2.97	2.11
500	2.59	1.31	1.74	1.77	3.00	1.73	2.40	1.90
550	2.24	1.24	1.57	1.64	2.52	1.57	2.05	1.74
600	2.02	1.18	1.45	1.54	2.22	1.45	1.82	1.62
650	1.86	1.14	1.36	1.46	2.01	1.37	1.66	1.53
700	1.74	1.11	1.29	1.39	1.86	1.30	1.54	1.46
750	1.65	1.09	1.24	1.34	1.75	1.26	1.45	1.40
800	1.58	1.07	1.20	1.30	1.66	1.22	1.38	1.35

Two different DFT methods (UB3LYP/6-31G(d) and MPWB1K/6-31G(d,p)) were used to calculate the electronic energy difference between the reactant and the transition state. In previous research, it was found that the energy difference calculated using these two methods for addition reactions of methyl methacrylate and methyl acrylate was striking (Yu et al. (2008)); the difference in ΔE_e was as high as 17 kJ·mol^{-1}. However, it was found that intramolecular hydrogen transfer was less sensitive to the choice of the DFT method; the electronic energy difference (ΔE_e) calculated using MPWB1K/6-31G(d,p) was lower than that calculated using UB3LYP/6-31G(d), but the difference for the trimeric radical was only 0.5 kJ·mol^{-1} and for the pentameric radical was 2.6 kJ·mol^{-1}. For the results presented below, the electronic energies obtained using MPWB1K/6-31G(d,p) were employed.

The kinetic parameters regressed from ln$k$ versus 1/T over the temperature range of 298-800 K for the different approximations for the tunneling coefficients are shown in Table 6.3. It is obvious that the calculated rate constants for the trimeric radical using the Eckart coefficients are out of line with the other methods, which are in generally good agreement. For the pentameric radical, the SCT results are squarely in the middle of the results based on the other tunneling approximations. Comparison of the regressed kinetic parameters based on the two different sizes of the reactant radicals reveals that they are relatively close, indicating that the extra two units in the pentameric radical do not have a significant influence on the calculated kinetic parameters and that the trimeric radical is a sufficient model of intramolecular hydrogen transfer reactions of methyl acrylate polymeric radicals.

Table 6.3: Activation energies and frequency factors regressed with various tunneling coefficients over the temperature range of 298-800 K for 1,5-hydrogen transfer (k_{tr}) of a trimeric radical and a pentameric radical; k_p is calculated based on the kinetic parameters determined using PLP-SEC (Buback et al. (1998)): A=1.66$\times 10^7$ L·mol^{-1}·s^{-1}, $E_a = 17.7$ kJ·mol^{-1}.

Trimeric	Eckart	SCT	ZCT	Wigner
E_a (kJ·mol^{-1})	39.8	43.6	45.7	45.4
A (s^{-1})	7.98$\times 10^8$	1.20$\times 10^9$	1.49$\times 10^9$	1.79$\times 10^9$
k_{tr} (50 °C)	295.2	107.5	60.8	82.8
k_{tr}/k_p (50 °C)	0.013	0.005	0.003	0.004

Pentameric	Eckart	SCT	ZCT	Wigner
E_a (kJ·mol^{-1})	38.7	41.7	44.7	46.4
A (s^{-1})	6.58$\times 10^8$	9.53$\times 10^8$	1.38$\times 10^9$	2.11$\times 10^9$
k_{tr} (50 °C)	361.8	175.0	81.2	66.8
k_{tr}/k_p (50 °C)	0.016	0.008	0.004	0.003

Finally, it is valuable to compare the calculated values against experimental measurements. No accurate experimental measurements of the kinetic parameters of 1,5-hydrogen transfer of methyl acrylate are available. However, there is data for a similar monomer, butyl acrylate, for which the 1,5-hydrogen transfer rate coefficient of 682 s^{-1} was estimated by Nikitin and Hutchinson (2005). Using their value of the propagation rate coefficient, k_p, at 50 °C of 2.83×10^4 L·mol^{-1}·s^{-1}, the ratio of k_{tr}/k_p for butyl acrylate at 50 °C is 0.024. For methyl acrylate, our calculated results reveal that the transfer rate coefficient is 175.0 s^{-1} based on the pentameric radical for the most rigorous tunneling approximation, SCT, which is within a factor of four of the value for butyl acrylate. The calculated ratio (k_{tr}/k_p) of methyl acrylate (0.008) is within a factor of three of that of butyl acrylate (0.024) at 50 °C. A more recent report of PLP-ESR measurements of butyl acrylate by Willemse et al. shows that the difference of the activation energies between 1,5-hydrogen transfer and propagation is 18.8±3.7 kJ·mol^{-1} (Willemse et al. (2005)), which translates into E_a =36.5±3.9 kJ·mol^{-1} for the 1,5-hydrogen transfer reaction. The activation energy calculated in this research ($E_a = 41.7$ kJ·mol^{-1}) for the analogous monomer, methyl acrylate, is close to this range.

6.3.3 Mid-chain Radical Propagation

Mid-chain radical propagation involves the transition of a tertiary radical to a secondary radical as shown in Figure 6.1. The structure of the transition state calculated for this reaction is shown in Figure 6.6. The length of the bond defining the transition state is 2.31 Å, which is slightly longer than the length of the bond defining the transition state in the addition of an end-chain trimeric methyl acrylate radical to methyl acrylate monomer (2.29 Å).

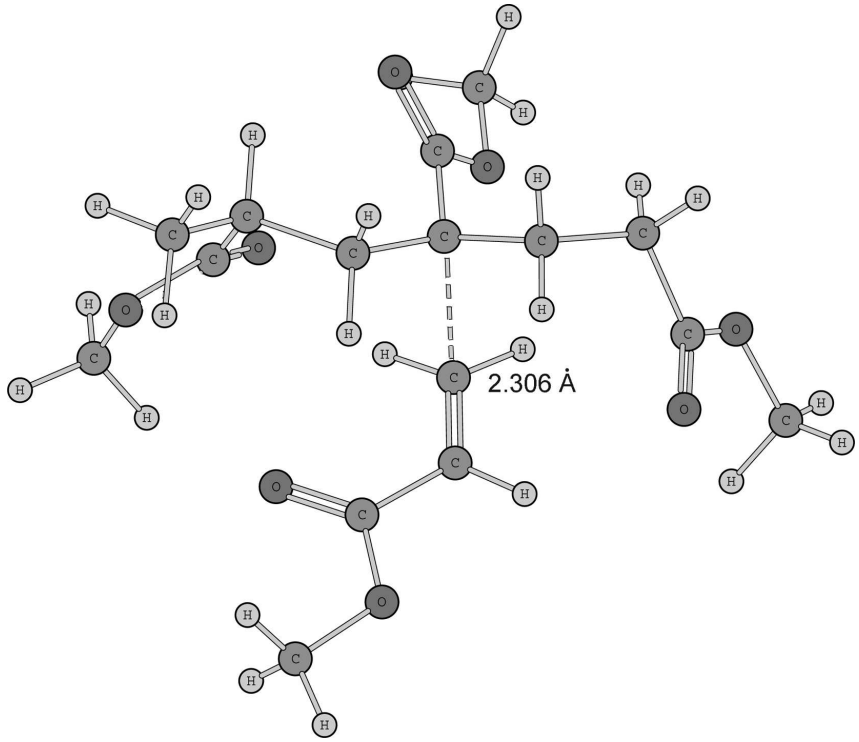

Figure 6.6: The structure of the transition state for the addition of methyl acrylate monomer to a trimeric methyl acrylate mid-chain radical located using UB3LYP/6-31G(d).

The kinetic parameters were regressed based on lnk_p^m versus 1/T over the temperature range of 298-800 K. The frequency factor and activation energy obtained are:

$$E_a = 29.8 \text{ kJ·mol}^{-1} \quad A = 1.10 \times 10^6 \text{ L·mol}^{-1}\text{·s}^{-1}$$

The activation energy is about 12 kJ·mol^{-1} higher than the value for methyl acrylate propagation (17.7 kJ·mol^{-1}) determined by PLP-SEC, while the frequency factor is about one order of magnitude lower than that for the propagation reaction (1.66$\times 10^7$ L·mol^{-1}). The values are reasonably similar to the average A and E_a values calculated for the addition of methyl acrylate monomer to a methyl methacrylate end-chain radical, which also involves the transition from a tertiary radical to a secondary radical ($E_a = 25.5$ kJ·mol^{-1}, $A = 2.14 \times 10^6$ L·mol^{-1}·s^{-1}), indicating that the enthalpic and entropic effects manifested in the kinetic parameters are related to the degree of substitution at the carbon atoms involved in the reaction.

The ratio of the rate coefficient for mid-chain radical propagation to that for end-chain radical propagation (k_p^m/k_p) is shown as a function of temperature in Figure 6.7. Because mid-chain radical propagation has a higher activation energy, it is more sensitive to increasing temperature, but propagation of an end-chain radical is still significantly faster over the temperature range shown. The ratio varies from 0.001 to 0.011 as the temperature increases from 300 K to 800 K.

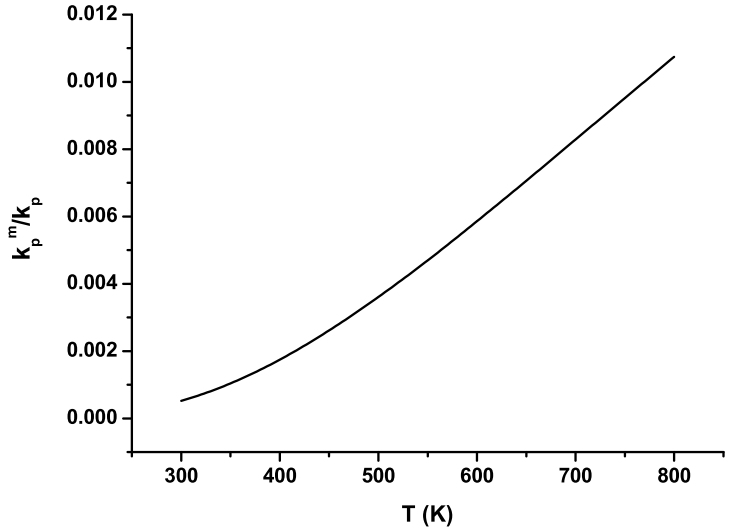

Figure 6.7: The ratio of k_p^m/k_p over the temperature range of 298-800 K. The kinetic parameters for k_p were measured with PLP-SEC: $A = 1.66 \times 10^7$ L·mol^{-1}·s^{-1}, $E_a = 17.7$ kJ·mol^{-1}; the kinetic parameters for mid-chain radical propagation, k_p^m, were calculated: $A = 1.10 \times 10^6$ L·mol^{-1}·s^{-1}, $E_a = 29.8$ kJ·mol^{-1}.

6.3.4 β-scission

The mid-chain radical formed by 1,5-hydrogen transfer can also undergo β-scission. A hexameric mid-chain radical with the radical at the fifth carbon was used to study β-scission as shown in Figure 6.1. Two paths for bond cleavage are possible: scission between the third and fourth carbon atoms to form a radical with three carbons on the backbone and a long chain unsaturated polymer, shown as path 1 in Figure 6.1; the bond between the sixth and the seventh carbon atoms can also break to form a trimeric unsaturated dead species and a long chain radical, shown as path 2 in Figure 6.1.

The transition states for these two paths are shown in Figure 6.8. The transition state of path 2 occurs slightly earlier as reflected in the shorter bond length characterizing the transition state. The frequency factors and activation energies for these two reactions are:

$$\text{Path 1:} \quad E_a = 125.5 \text{ kJ·mol}^{-1} \quad A = 9.55 \times 10^{13} \text{ s}^{-1}$$

$$\text{Path 2:} \quad E_a = 123.3 \text{ kJ·mol}^{-1} \quad A = 3.47 \times 10^{13} \text{ s}^{-1}$$

Path 1 is slightly favored at the temperatures of interest as quantified by the ratio of the rate coefficients of path 1 and path 2 summarized in Figure 6.9 over the temperature range of $298 - 800$ K. This indicates that the formation of low molecular weight products derived from the trimeric radical will be more abundant than the unsaturated pentamer and its progeny.

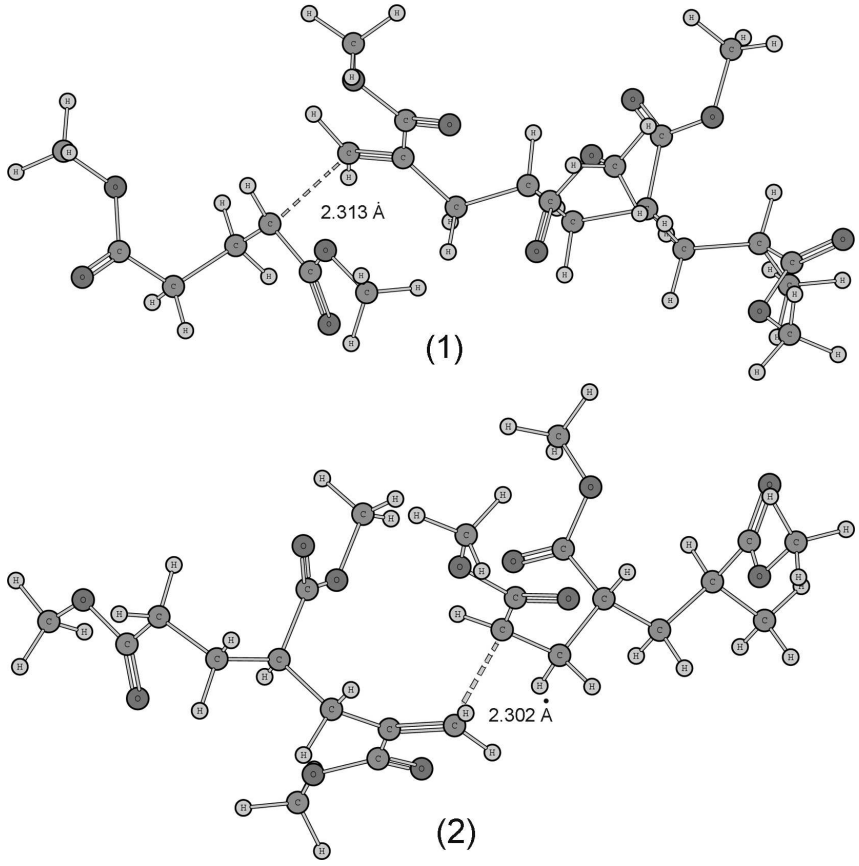

Figure 6.8: The structures of the transition states for β-scission of a hexameric mid-chain radical for the two different paths defined in Figure 6.1.

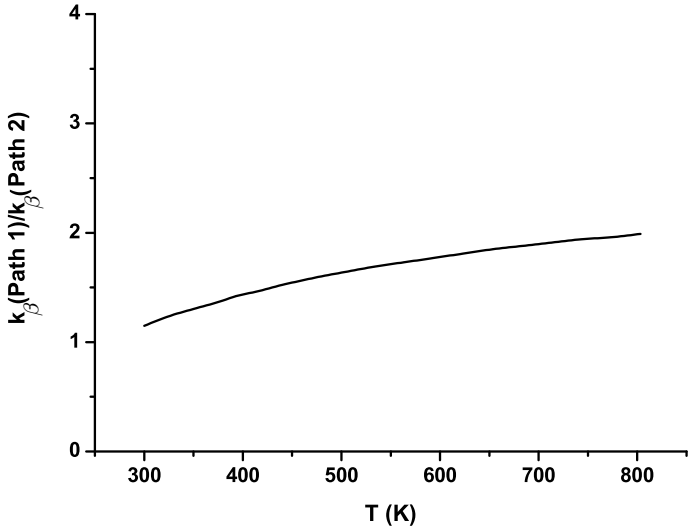

Figure 6.9: The ratio of k_β(path 1)$/k_\beta$(path 2) over the temperature range of 300-800 K with path 1 and path 2 defined as in Figure 6.1.

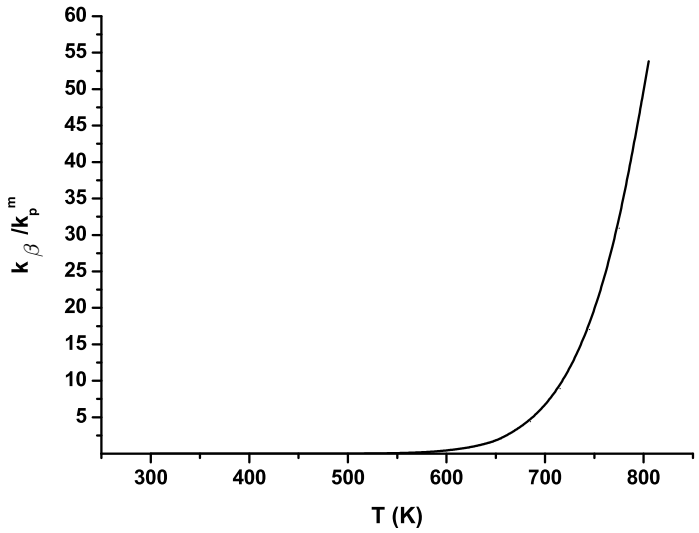

Figure 6.10: The ratio of k_β/k_p^m over the temperature range of 298-800 K.

β-scission and mid-chain propagation are competitive reactions. The ratio of k_β/k_p^m is plotted in Figure 6.10 as a function of temperature, where k_β is the sum of the k_β values for the two different paths. β-scission is negligible compared to mid-chain propagation in the low temperature regime, but due to its higher activation energy, it increases rapidly with increasing temperature and the ratio exceeds one at temperatures greater than 630 K. The ratio of the reaction rates is:

$$\frac{R_\beta}{R_p^m} = \frac{k_\beta[P_m]}{k_p^m[P_m][M]} = \frac{k_\beta}{k_p^m[M]} \tag{6.13}$$

where $[P_m]$ is the total concentration of mid-chain radicals and $[M]$ is the monomer concentration. If the bulk concentration is used for $[M]$ (11.1 L·mol^{-1}), at 230 °C, the two reaction rates become equal. Even for the elevated temperatures proposed for high temperature processing of acrylates, the temperature is typically lower than 180 °C. Thus, β-scission will not be significant compared to mid-chain propagation.

6.4 Conclusion

Four secondary reactions (depropagation, 1,5-hydrogen transfer, mid-chain radical propagation and β-scission) were studied using quantum chemistry and transition state theory based on short chain mimics of methyl acrylate polymeric species. Geometries were optimized using a combination of a conventional gradient-based algorithm and relaxed potential energy scans using UB3LYP/6-31G(d). MPWB1K/6-31G(d,p) was used to calculate the electronic energy values for all reactions. Low frequencies were modeled using a one-dimensional hindered rotation model. The A and E_a values for depropagation were in the range of disparate experimental values for an analogous monomer, butyl methacrylate, and are the first set of values reported for methyl acrylate to our knowledge. Both a trimeric radical and a pentameric radical were used to investigate 1,5-hydrogen transfer of methyl acrylate, and it was found that the units on the backbone not involved in the formation of the six-membered ring in the transition state had a negligible influence. Four different approximations (SCT, Eckart, ZCT and Wigner) were used to calculate the tunneling coefficients. The predicted rate coefficients based on the most rigorous SCT approximation were in reasonably good agreement with experimental data for 1,5-hydrogen transfer of a related monomer, butyl acrylate, and are the first values reported for methyl acrylate. Mid-chain radical propagation was studied using a trimeric mid-chain radical, and it was shown that the rate constant is a factor of 100 to 1000 lower than that for end-chain radical propagation over the temperature range studied. Two possible scission paths for the mid-chain radical were studied based on a hexameric radical, and it was found that the path to form the smaller radical and the longer unsaturated polymer is slightly favored. Comparison of k_β and k_p^m shows that mid-chain radical propagation is preferred within the typical temperature range for high temperature polymerization of acrylates.

Chapter 7

Kinetic Modeling of Polymerization using Kinetic Monte Carlo

7.1 Introduction

In this chapter, kinetic Monte Carlo (KMC) was used to model the homopolymerization of methyl acrylate at various temperatures in a batch reactor. The mechanism of homopolymerization of methyl acrylate includes seven reactions: initiation, propagation, 1,5-hydrogen transfer, mid-chain radical propagation, termination, depropagation and β-scission. The kinetic parameters calculated in the previous chapters were used in the KMC model. Gillespie's algorithm for dynamic Monte Carlo simulation was followed (Gillespie (1977)). The reaction system started with a control volume containing a certain number of monomers and initiators, and a reaction at a specific time was chosen according to its reaction probability. The polymer chain structure was represented using a C++ class including polymer chain length and number of short chain branches as attributes. The data structure "*vector*" was used to store different radicals and polymer. Monomer conversion rate, average molecular weight (M_n, M_w), PDI and average number of branches per polymer chain were tracked. The full molecular weight distribution was recorded at specified time points.

7.2 Elementary Reactions in Methyl Acrylate Homopolymerization

The following reactions and kinetic parameters in methyl acrylate polymerization were included in the KMC model. P_n is used to denote a polymeric radical of length n, and D_n is used to denote a dead species of length n. P_n^m denotes a mid-chain radical, and D_n^m denotes a dead polymer formed from a mid-chain radical.

Initiation:

$$I_2 \xrightarrow{k_d} 2I\cdot \tag{7.1}$$

AIBN was used as the initiator. The initial concentration, $[I_2]_0$, was set as 0.0011 mol·L^{-1}. Kinetic parameters for decomposition of the initiator from the literature were used (Peck and Hutchinson (2004)):

$$\text{A}=6.78\times10^{15}\ \text{s}^{-1},\ E_a=147.2\ \text{kJ·mol}^{-1}$$

Propagation:

The bulk concentration of methyl acrylate, 11.1 mol·L^{-1}, was used as the initial concentration of monomer ($[M]_0$).

$$P_n + M \xrightarrow{k_p} P_{n+1} \tag{7.2}$$

$$\text{A}=6.03\times10^{7}\ \text{L·mol}^{-1}\text{·s}^{-1},\ E_a=21.5\ \text{kJ·mol}^{-1}$$

1,5-Hydrogen Transfer:

$$P_n \xrightarrow{k_{tr}} P_n^m \tag{7.3}$$

$$\text{A}=9.53\times10^{8}\ \text{s}^{-1},\ E_a=41.7\ \text{kJ·mol}^{-1}$$

Mid-chain Radical Propagation:

$$P_n^m + M \xrightarrow{k_p^m} P_{n+1} \tag{7.4}$$

A=1.10 $\times 10^6$ L·mol^{-1}·s^{-1}, E_a=29.8 kJ·mol^{-1}

Depropagation:

$$P_{n+1} \xrightarrow{k_{dp}} P_n + M \tag{7.5}$$

A=9.12$\times 10^{13}$ s^{-1}, E_a=119.0 kJ·mol^{-1}

β-scission 1:

$$P_n^m \xrightarrow{k_{\beta 1}} P_2 + D_{n-2} \tag{7.6}$$

A=9.55$\times 10^{13}$ s^{-1}, E_a=125.5 kJ·mol^{-1}

The structure of the radical generated from β-scission via path 1 is shown in Figure 6.1, which actually has one fewer "-CH_2-" group than a dimeric methyl acrylate radical. Nevertheless, such a simplification does not affect the results dramatically since the mass of a "-CH_2-" group is negligible compared to the weight of the polymer chains produced, and β-scission is an event with low probability.

β-scission 2:

$$P_n^m \xrightarrow{k_{\beta 2}} P_{n-3} + D_3 \tag{7.7}$$

A=3.47$\times 10^{13}$ s^{-1}, E_a=123.3 kJ·mol^{-1}

Termination:

Two radicals can undergo termination through combination and disproportionation.

$$P_n + P_m \xrightarrow{k_{tc}} D_{n+m} \qquad P_n + P_m \xrightarrow{k_{td}} D_n + D_m \tag{7.8}$$

The mode of termination does not influence the reaction rate but only influences the molecular weight distribution. Kinetic parameters measured with SP-PLP were used to specify the rate coefficient for the total rate of termination (Meyer and Keurentjes (2005)).

A=6.00 $\times 10^9$ L·mol^{-1}·s^{-1}, E_a=6.69 kJ·mol^{-1}

k_{tc} and k_{td} were then calculated using the following equations:

$$k_t = k_{tc} + k_{td} \qquad \delta = \frac{k_{td}}{k_{td} + k_{tc}} \tag{7.9}$$

For acrylates, δ is within the range of $0.05 - 0.2$ (Meyer and Keurentjes (2005)). The average value of 0.13 was used. Termination can also happen between an end-chain radical and a mid-chain radical. It was assumed that only termination by combination occurs between these two radicals. Termination between two mid-chain radicals was excluded based on steric arguments.

$$P_n^m + P_m \xrightarrow{k_{tc}} D_{n+m}^m \tag{7.10}$$

7.3 Selection of Control Volume Size

The first step after specifying the mechanism was to determine the effective control volume which still captures the relative concentrations of the species while being computationally affordable. For different reaction systems, the optimum sample volume is determined through comparison of results obtained from various volumes. If the control volume is too small, there is an insufficient number of species with low concentrations, and the results are not accurate. Thus, the control volume is gradually increased until asymptotic results are obtained. In this research, three different sizes of the control volume were examined for methyl acrylate polymerization at 70 °C at a reaction time of 400 s as shown in Figure 7.1. The molecular weight distributions based on the two smallest sample volumes (0.15×10^{-13} L and 0.15×10^{-12} L) are not adequate to obtain a consistent molecular weight distribution. Therefore, the largest sample volume studied, 0.15×10^{-11} L, was used for all subsequent simulations.

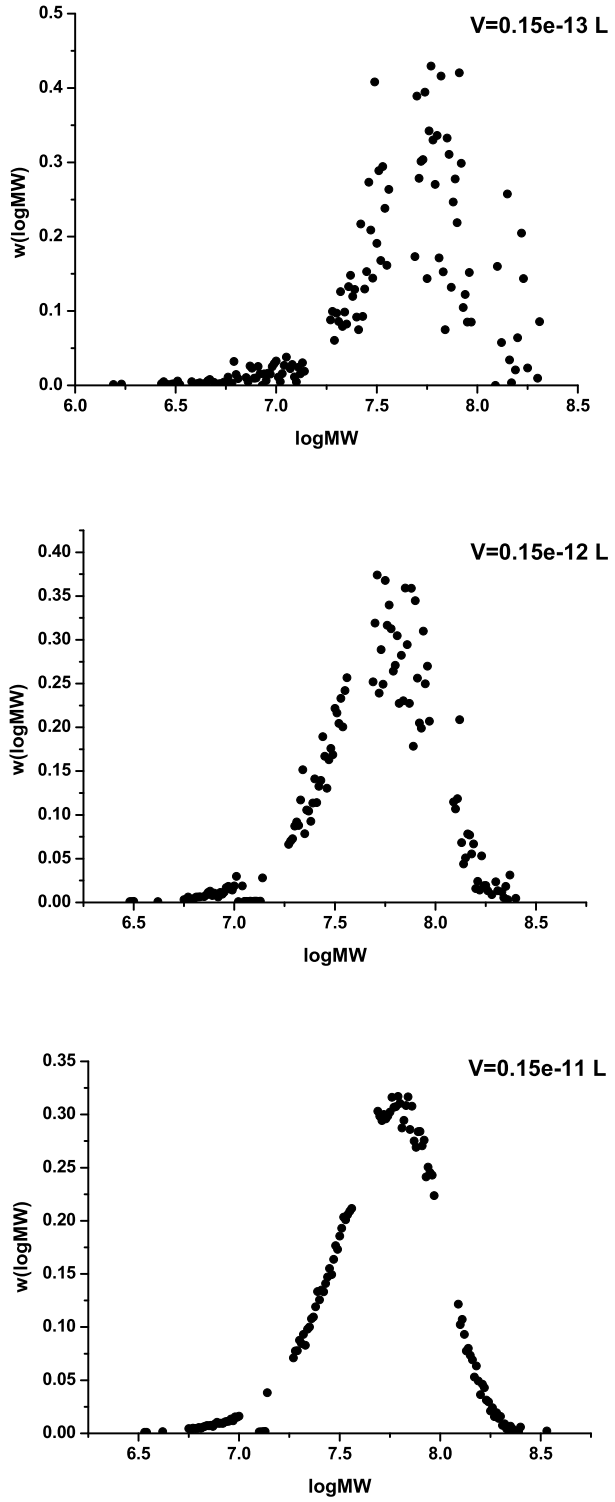

Figure 7.1: Predicted molecular weight distribution of methyl acrylate polymerization at 70 °C using three different sample volumes at a reaction time of 400 s.

7.4 KMC Modeling Results

Bulk polymerization of methyl acrylate at various temperatures was modeled using 0.0011 mol·L^{-1} of AIBN as initiator. The conversion as a function of time of methyl acrylate at 70, 90 and 110 °C is plotted in Figure 7.2. The conversion increases rapidly with increasing temperature. The number average molecular weight (M_n) and weight average molecular weight (M_w) at 90 °C are plotted as a function of conversion in Figure 7.3. The number average molecular weight values as a function of monomer conversion at three different temperatures are shown in Figure 7.4. Increasing temperature results in a decrease of the molecular weight, which is caused by the promotion of secondary reactions. The branching level is defined as Equation 7.11.

$$Branching\% = \frac{Number\ \ of\ \ branches}{Polymerized\ \ monomer\ \ units} \times 100\% \tag{7.11}$$

The branching levels at 60, 70, 90 and 110 °C are plotted in Figure 7.5. The branching level is relatively stable as a function of conversion at a specific reaction temperature, but there is a clear increase as temperature increases. For example, from 60 °C to 110 °C, the branching percentage increases from 0.11 to 0.27. The branching level is an indication of the relative rates of propagation and transfer. At 60 °C, branching occurs about once for every 1000 units polymerized. Plessis et al. used ^{13}C NMR to measure the branching level in butyl acrylate bulk polymerization; at 60 °C, the branching percentage was about 0.47 (Plessis et al. (2003)), which is within a factor of five of the branching level predicted in this model. The predicted molecular weight distributions at 90 °C and 110 °C are shown in Figure 7.6. The temperature increase causes the peak of the molecular weight distribution to shift to the left to lower values.

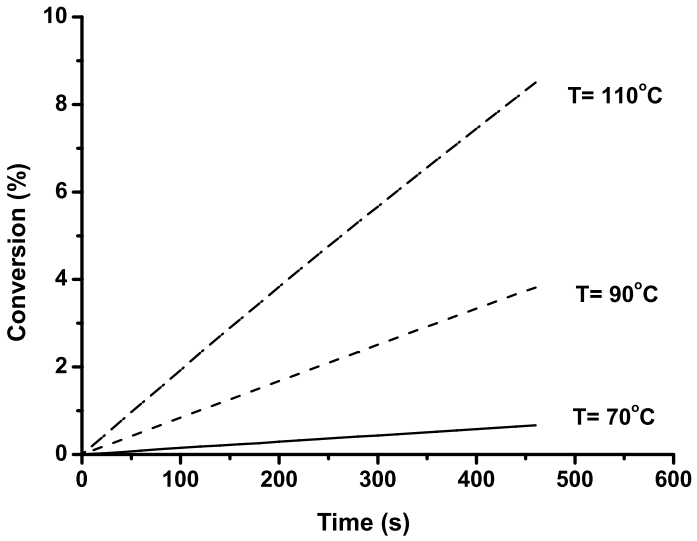

Figure 7.2: Conversion as a function of time for bulk homopolymerization of methyl acrylate at 70 °C (solid line), 90 °C (dashed line) and 110 °C (dashed-dotted line). 0.0011 mol·L^{-1} of AIBN as initiator was used.

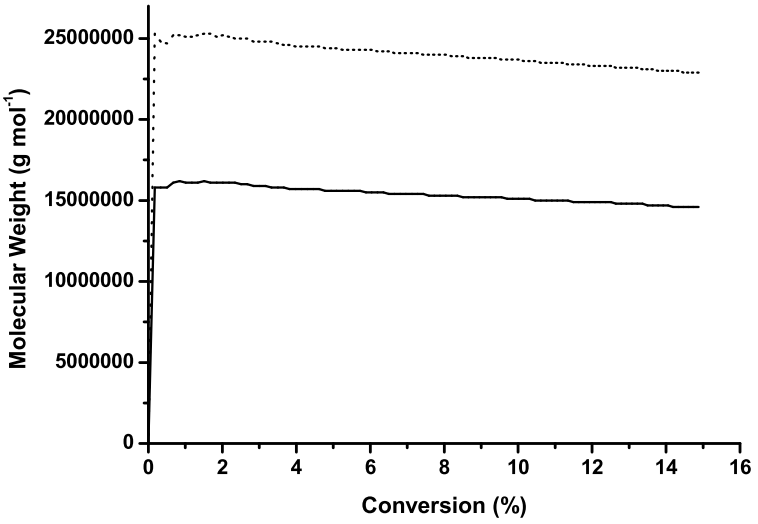

Figure 7.3: Number average molecular weight (M_n, solid line) and weight average molecular weight (M_w, dotted line) as a function of conversion of monomer at 90 °C.

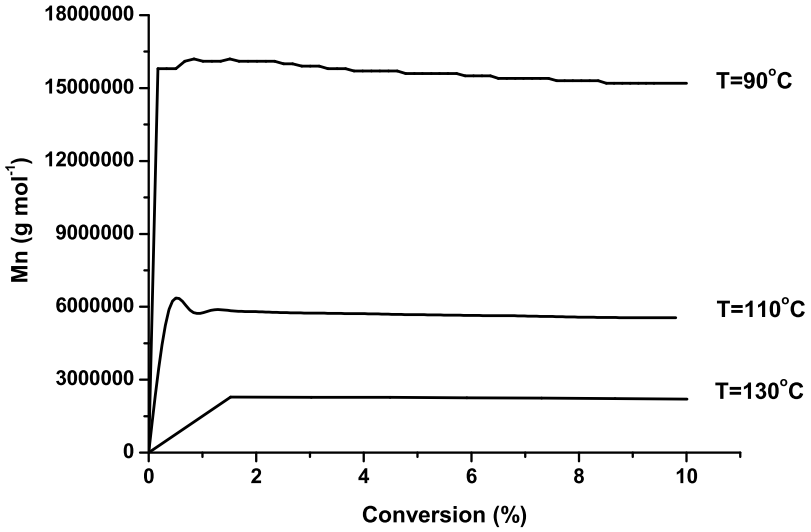

Figure 7.4: Number average molecular weight (M_n) as a function of conversion of monomer at 90 °C, 110 °C, and 130 °C.

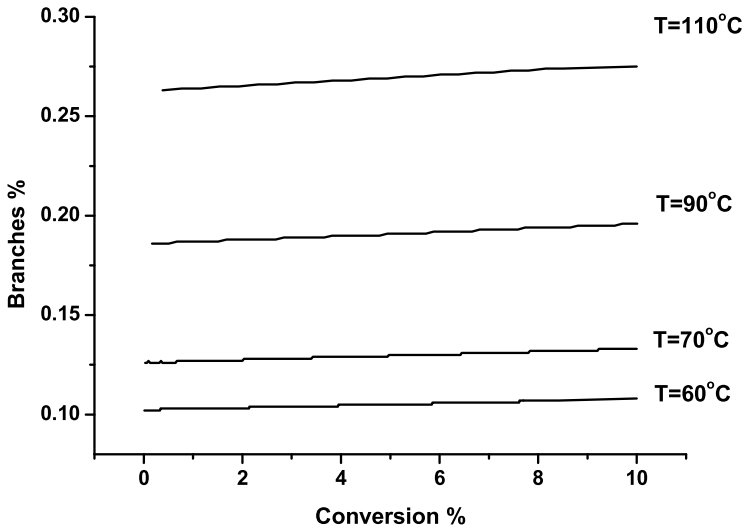

Figure 7.5: Branching level in methyl acrylate polymerization as a function of monomer conversion at 60 °C, 70 °C, 90 °C and 110 °C. With increasing temperature, the branching level increases.

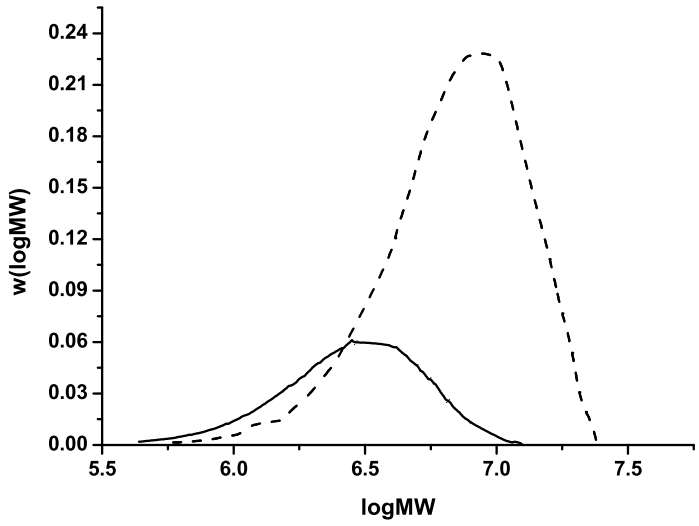

Figure 7.6: Molecular weight distribution at 90 °C (dashed line) and 110 °C (solid line); monomer conversion equals 10%.

7.5 Conclusion

Kinetic Monte Carlo (KMC) was used to model the polymerization of methyl acrylate at various reaction temperatures. It was shown that KMC has the capability to capture detailed characteristics of polymers, including average molecular weight, molecular weight distribution and branching level.

Chapter 8

Conclusion and Recommendations

This chapter provides overall conclusions about the research presented in the previous chapters and also make recommendations for future work.

8.1 Conclusion

A computational methodology based on quantum chemistry and transition state theory has been developed to calculate kinetic parameters for polymerization reactions. The homopolymerization of methyl methacrylate and methyl acrylate was studied first and the accurate kinetic parameters measured with PLP-SEC were used to verify the methodology. The developed methodology was also extended to copolymerization and secondary reactions. The results presented in previous chapters show that the computational methodology can provide kinetic parameters for polymerization reactions which are in good agreement with experimental measurements.

In the development of the methodology based on methyl methacrylate and methyl acrylate propagation reactions, a combination of conventional geometry optimization and relaxed potential scans for each single bond and the bond defining the transition state was used to locate global minimum conformations. Three density functional theory methods with different basis sets were

evaluated for calculating activation energies of methyl methacrylate addition reactions, and the results showed that MPWB1K/6-31G(d,p) provided values that were the closest to and in very good agreement with experimental data. This choice of method and basis set was also verified for methyl acrylate propagation. The addition reactions of monomeric, dimeric and trimeric radicals to monomer were analyzed for both methyl methacrylate and methyl acrylate, and the results showed that addition of a trimeric radical to monomer offered results that were the most consistent with experimental data. Calculations employing a solvation model revealed that the solvent effect was not marked for either methyl methacrylate or methyl acrylate propagation reactions. Two different treatments were used in the calculation of the contribution of low frequencies to the kinetic parameters. The results based on the one-dimensional internal rotation model are closer to experimental data than those based on the harmonic oscillator model.

Methyl methacrylate and methyl acrylate copolymerization reactions were also studied using addition of monomeric, dimeric and trimeric radicals to monomers using quantum chemistry and transition state theory. The use of radicals of different length allowed penultimate and penpenultimate effects to be explored and different models of copolymerization (TM, EPUE and IPUE) to be tested. Unrestricted B3LYP/6-31G(d) was used for geometry optimization and potential energy scans, and the electronic energies were calculated using MPWB1K/6-31G(d,p). Low frequencies were treated using a one-dimensional internal rotor model in the calculation of partition functions for rate constants and thermodynamic properties. It was found that addition reactions involving monomeric or dimeric radicals offered results that were qualitatively consistent with experimental data, but quantitatively accurate monomer and radical reactivity ratios and rate coefficients were not obtained. However, rate coefficients and monomer and radical reactivity ratios for the TM and PUE models which were in good agreement with those fitted from experimental data were obtained when the radical chain length was three. Although the penpenultimate unit had a negligible influence on the activation energy values, its entropic influence was reflected in the frequency factor and thus the rate coefficient. The copolymer compositions predicted using the TM, IPUE and EPUE

models were very close, while the overall rate coefficient ($k_{p,copo}$) predicted based on the EPUE and IPUE models was measurably different from that based on the TM. The reactivity was analyzed based on frontier orbital theory. All reactions studied involved the interaction between the SOMO of the radical and the HOMO of the monomer, indicating electrophilic addition, and a general correlation between the activation energy and the SOMO/HOMO energy gap was observed. Finally, the relationship between the activation energy and the reaction enthalpy for sixteen AD3 reactions was examined, and it was shown that the Evans-Polanyi relationship was obeyed.

Four secondary reactions (depropagation, 1,5-hydrogen transfer, mid-chain radical propagation and β-scission) were studied using quantum chemistry and transition state theory based on short chain mimics of methyl acrylate polymeric species. Geometries were optimized using a combination of a conventional gradient-based algorithm and relaxed potential energy scans using UB3LYP/6-31G(d). MPWB1K/6-31G(d,p) was used to calculate the electronic energy values for all reactions. Low frequencies were modeled using a one-dimensional hindered rotation model. The A and E_a values for depropagation were in the range of disparate experimental values for an analogous monomer, butyl methacrylate, and are the first set of values reported for methyl acrylate. Both a trimeric radical and a pentameric radical were used to investigate 1,5-hydrogen transfer of methyl acrylate, and it was found that the units on the backbone not involved in the formation of the six-membered ring in the transition state had a negligible influence. Four different approximations (SCT, Eckart, ZCT and Wigner) were used to calculate the tunneling coefficients. The predicted rate coefficients based on the most rigorous SCT approximation were in reasonably good agreement with experimental data for 1,5-hydrogen transfer of a related monomer, butyl acrylate, and are the first values reported for methyl acrylate. Mid-chain radical propagation was studied using a trimeric mid-chain radial, and it was shown that the rate constant is a factor of 100 to 1000 lower than that for end-chain radical propagation over the temperature range studied. Two possible scission paths for the mid-chain radical were studied based on a hexameric radical, and it was found that the path to form the smaller radical and the longer unsaturated polymer is slightly

favored. Comparison of k_β and k_p^m shows that propagation of mid-chain radicals is preferred over β-scission within the typical temperature range for high temperature polymerization of acrylates.

Kinetic Monte Carlo (KMC) was used to model the polymerization of methyl acrylate at various reaction temperatures. It was shown that KMC has the capability to capture detailed characteristics of polymers, including average molecular weight, molecular weight distribution and branching level. To our knowledge, this model is the first demonstration of the prediction of complex polymerization kinetics from first principles.

8.2 Recommendations

The present research has focused heavily on methodology development and extensive application of the methodology to model homopolymerization and copolymerization of acrylates. The work performed to date suggests some natural directions for future research.

In optimizing the structures for all reactants, a combined method was used to locate the global minimum. Although this method did overcome energy barriers and locate lower energy conformations, more detailed analysis of the interactions of neighboring groups needs to be addressed in future work. The low frequencies which are mainly composed of torsional motions were treated using a one-dimensional internal rotor model. The interactions between rotors were not incorporated. More elaborate multi-dimensional schemes for treating hindered rotations may improve the accuracy of the predicted rate coefficients even further. A bulk substitution strategy for replacing vibrational frequencies with hindered rotations was employed here. This was a simple approach that allowed the large molecules studied to be handled easily. However, more sophisticated substitution strategies could be warranted and further improve the quantitative prediction of kinetic parameters.

Much effort was devoted to identifying a level of theory that provided quantitatively accurate values of kinetic parameters as verified by comparison against rate coefficients for propagation.

This level of theory was then used to probe secondary reactions. It is possible, however, that there are other quantum chemical methods that would provide enhanced accuracy, especially for secondary reactions. The scarcity of accurate kinetic parameters for individual secondary reactions makes direct comparison infeasible. However, KMC modeling allows the effectiveness of the predictions from quantum chemistry to be verified against experimental data. Thus, it is recommended that an experimental campaign be undertaken to explore methyl acrylate polymerization as a function of temperature to compare predictions from the modeling effort further.

Finally, the methodology was developed based on the polymerization of methyl methacrylate and methyl acrylate. It would be interesting to probe its validity for other acrylate monomers. This would allow the overall research goal of determining kinetic parameters for monomers which cannot be measured experimentally to be realized more fully.

References

Adamsons, K.; Blackman, G.; Gregorovich, B.; Lin, L.; Matheson, R. *Progress in Organic Coatings* **1998**, *34*, 64.

Ahmad, N. M.; Heatley, F.; Lovell, P. A. *Macromolecules* **1998**, *31*, 2822.

Al-Harthi, M.; Soares, J. B.; Simon, L. C. *Macromol. Mater. Eng.* **2006**, *291*, 993.

Ayala, P. Y.; Schlegel, H. B. *J. Chem. Phys.* **1998**, *108(6)*, 2314.

Balint-Kurti, G. G.; Dixon, R. N.; Marston, C. C. *Int. Rev. Phys. Chem.* **1992**, *11 (2)*, 317.

Bebe, S.; Yu, X.; Hutchinson, R. A.; Broadbelt, L. J. *Macromol. Symp.* **2006**, *243*, 179.

Becke, A. D. *J. Chem. Phys.* **1996**, *104*, 1040.

Becke, A. D. *Phys. Rev. A: At.,Mol., Opt. Phys.* **1998**, *38*, 3098.

Beuermann, S.; Buback, M. *Prog. Polym. Sci.* **2002**, *27*, 191.

Beuermann, S.; Buback, M.; Davis, T. *Macromol. Chem. Phys.* **1997**, *198*, 1545.

Beuermann, S.; Buback, M.; Gilbert, R. G. *Macromol. Chem. Phys.* **2000**, *201*, 1355.

Beuermann, S.; Buback, M.; Russell, G. T. *Macromol. Rapid Commun.* **1994**, *15*, 351.

Beuermann, S.; Paquet, J.; McMinn, J. *Macromolecules* **1996**, *29*, 4206.

Brandrup, J.; Immergut, E. H.; Grulke, E. *Polymer Handbook*; Wiley: NewYork; 4th edn., 1999.

Buback, M.; Feldermann, A.; Barner-Kowollik, C. *Macromolecules* **2001**, *34*, 5439.

Buback, M.; Klingbeil, S.; Sandmann, J.; Sderra, M.; Vögele, H.; Wackerbarth, H.; Wittkowski, L. *J. Phys. Chem. (Munich)* **1999**, *210*, S119.

Buback, M.; Kurz, C.; Schmaltz, C. *Macromol. Chem. Phys.* **1998**, *199*, 1721.

Buback, M.; Müller, E. *Macromol. Chem. Phys.* **2007**, *208*, 581.

Cances, E.; Mennucci, B.; Tomasi, J. *J. Chem. Phys.* **1997**, *107*, 3032.

Chiefari, J.; Jeffery, J.; Mayadunne, R.; Rizzardo, G.; E, T. *Macromolecules* **1999**, *32*, 7700.

Chuang, Y.-Y.; Truhlar, D. G. *J. Chem. Phys.* **2000**, *112(3)*, 1221.

Coote, M. L. *J. Phys. Chem. A* **2005**, *109*, 1230.

Coote, M. L.; Davis, T. P. *Prog. Polym. Sci.* **1999**, *24*, 1217.

Coote, M. L.; Johnston, L. P.; Davis, T. *Macromolecules* **1997**a, *30*, 8191.

Coote, M. L.; Michael, D. Z.; Davis, T. P.; Willett, G. D. *Macromolecules* **1997**b, *30*, 8182.

Dotson, N. A.; Galvan, R.; Laurence, R. L.; Tirrell, M. *Polymerization Process Modeling*; Wiley-VCH; 1st edn., 1996.

East, A. L. L.; Radom, L. *J. Chem. Phys.* **1997**, *106(16)*, 6655.

Fischer, H.; Radom, L. *Angew. Chem. Int. Ed.* **2001**, *40*, 1340.

Foresman, J. B. *Exploring Chemistry with Electronic Structure Methods*; Gaussian Inc.: Pittsburgh,PA; 1st edn., 2002.

Frisch, M. J.; Trucks, G. W.; Schlegel, H. B.; Scuseria, G. E.; Robb, M. A.; Cheeseman, J. R.; Montgomery, J. A.; Vreven, J. T.; Kudin, K. N.; Burant, J. C.; Millam, J. M.; Iyengar, S. S.; Tomasi, J.; Barone, V.; Mennucci, B.; Cossi, M.; Scalmani, G.; Rega, N.; Petersson, G. A.; Nakatsuji, H.; Hada, M.; Ehara, M.; Toyota, K.; Fukuda, R.; Hasegawa, J.; Ishida, M.; Nakajima, T.; Honda, Y.; Kitao, O.; Nakai, H.; Klene, M.; Li, X.; Knox, J. E.; Hratchian, H. P.; Cross, J. B.; Adamo, C.; Jaramillo, J.; Gomperts, R.; Stratmann, R. E.; Yazyev, O.; Austin, A. J.; Cammi, R.; Pomelli, C.; Ochterski, J. W.; Ayala, P. Y.; Morokuma, K.; Voth, G. A.; Salvador, P.; Dannenberg, J. J.; Zakrzewski, V. G.; Dapprich, S.; Daniels, A. D.; Strain, M. C.; Farkas, O.; Malick, D. K.; Rabuck, A. D.; Raghavachari, K.; Foresman, J. B.; Ortiz, J. V.; Cui, Q.; Baboul, A. G.; Clifford, S.; Cioslowski, J.; Stefanov, B. B.; Liu, G.; Liashenko, A.; Piskorz, P.; Komaromi, I.; Martin, R. L.; Fox, D. J.; Keith, T.; Al-Laham, M. A.; Peng, C. Y.; Nanayakkara,

A.; Challacombe, M.; Gill, P. M. W.; Johnson, B.; Chen, W.; Wong, M. W.; Gonzalez, C.; Pople, J. A. *Gaussian 03*; Gaussian, Inc.: Wallingford CT; revision c.02 edn., 2004.

Fukuda, T.; Ma, Y.-D.; Inagaki, H. *Macromolecules* **1985**, *18*, 17.

Gaussian Inc. *Gaussian 03 Manual*; Gaussian Inc.: Pittsburgh; 1st edn., 1990.

Gillespie, D. T. *J. Phys. Chem.* **1977**, *81*, 25.

Gomez-Balderas, R.; Coote, M. L.; Henry, D. J.; Fischer, H.; Radom, L. *J. Phys. Chem. A* **2003**, *107*, 6082.

Gonzalez-Lafont, A.; Truong, T. N.; Truhlar, D. G. *J. Chem. Phys.* **1991**, *95(12)*, 8875.

Grady, M. C.; Simonsick, W. J.; Hutchinson, R. A. *Macromol. Symp.* **2002**, *182*, 149.

Hakim, M.; Verhoeven, V.; McManus, N. T.; Debe, M. A.; Penlidis, A. *J. Appl. Poly. Sci.* **2000**, *77*, 1156.

Hehre, W. J.; Radom, L.; Schleyer, P. V. R. *Ab Initio Molecular Orbital Theory*; Wiley: New York; 1st edn., 1986.

Heuts, J. P.; Gilbert, R. G. *Macromolecules* **1995**, *28*, 8771.

Huang, M. D.; Monteiro, J. M.; Gilbert, R. G. *Macromolecules* **1998**, *31*, 5175.

Hulburt, H. M.; Katz, S. *Chem. Engng Sci.* **1964**, *19*, 555.

Hutchinson, R. A.; McMinn, J. H.; Paquet, D. A. *Ind. Eng. Chem. Res.* **1997**, *36*, 1103.

Hutchinson, R. A.; Paquet, D. A.; Beuermann, S.; McMinn, J. H. *Ind. Eng.Chem. Res.* **1998**, *37*, 3567.

Irikura, K. K. *Computational Thermochemistry: Prediction and Estimation of Molecular Thermodynamics*; American Chemical Society: Washington, DC; 1st edn., 1998.

Izgorodina, E. I.; Coote, M. L. *Chem. Phys.* **2006**, *324*, 96.

Kilpatrick, J. E.; Pitzer, K. S. *J. Chem. Phys.* **1949**, *17*, 1064.

Kruse, T. M.; Souleimonova, R.; Cho, A.; Gray, M. K.; Torkelson, J. M.; Broadbelt, L. J. *Macromolecules* **2003**, *36*, 7812.

Kululj, D.; Davis, T. *Macromolecules* **1998**, *31*, 5668.

Leach, A. R. *Molecular Modeling*; Prentice Halls; 2nd edn., 2001.

Levine, S. E.; Broadbelt, L. J. *Polym. Degrad. Stab.* **2008**, *in press*.

Lozano, A. E.; Alonso, A.; Catalina, F.; Peinado, C. *Macromol. Theory Simul.* **1999**, *8*, 93.

Lynch, B. J.; Fast, P. L.; Harris, M.; Truhlar, D. G. *J. Phys. Chem. A* **2000**, *104*, 4811.

Madruga, E.; Fernandez-Garcia, M. *Macromol. Chem. Phys.* **1996**, *197*, 1185.

Masel, R. I. *Chemical Kinetics and Catalysis*; Wiley-Interscience: NewYork; 1st edn., 2001.

McClurg, R. B.; Flagan, R. C.; Goddard, W. A. *J. Comp. Chem.* **1997**, *106(16)*, 6675.

McCord, E. F.; Shaw, W. H.; Hutchinson, R. A. *Macromolecules* **1997**, *30*, 246.

McQuarrie, D. A.; Simon, J. D. *Molecular Thermodynamics*; University Science Books: Sausalito, Califonia; 1st edn., 1999.

Meyer, T.; Keurentjes, J. *Handbook of Polymer Reaction Engineering*; Wiley-VCH; 1st edn., 2005.

Moad, G.; Solomon, D. *The Chemistry of Free Radical Polymerization*; Elsevier Science Inc.: NewYork, 1995.

Moscatelli, D.; Cavallotti, C.; Morbidelli, M. *Macromolecules* **2006**, *39*, 9641.

Nikitin, A. N.; Hutchinson, R. A. *Macromolecules* **2005**, *38*, 1581.

Odian, G. *Principles of Polymerization*; Wiley-Interscience: NewYork; 4th edn., 2004.

Peck, A.; Hutchinson, R.; Grady, M. *Polymer Preprints* **2002**, *43(2)*, 154.

Peck, A. N.; Hutchinson, R. A. *Macromolecules* **2004**, *37*, 5944.

Peng, C.; Avala, P. Y.; Schelegel, H. B. *J. Comp. Chem.* **1996**, *317*, 49.

Pfaendtner, J.; Broadbelt, L. J. *Chemical Engineering Science* **2007**a, *62*, 5232.

Pfaendtner, J.; Broadbelt, L. J. *ChemPhysChem* **2007**b, *8*, 1969.

Pfaendtner, J.; Yu, X.; Broadbelt, L. J. *J. Phys. Chem. A* **2006**, *110*, 10863.

Pfaendtner, J.; Yu, X.; Broadbelt, L. J. *Theo. Chem. Acc.* **2007**, *118*, 881.

Pilar, F. L. *Elementary Quantum Chemistry*; McGraw-Hill: Singapore; 2nd edn., 1990.

Pitzer, K. S. *J. Chem. Phys.* **1946**, *14*, 239.

Pitzer, K. S.; Gwinn, W. D. *J. Chem. Phys.* **1942**, *10*, 428.

Plessis, C.; Arzamendi, G.; Leiza, J. R. *Macromolecules* **2001**, *34*, 5147.

Plessis, C.; Arzamendi, G.; Leiza, J. R.; Schoonbrood, H. A.; Charmot, D.; Asua, J. M. *Macromolecules* **2000**, *33*, 4.

Plessis, C.; Arzamendi, G.; Leiza, J. R.; Van Herk, A. M.; Leiza, J. R.; Asua, J. M. *Macromol. Rapid Commun.* **2003**, *24*, 173.

Pross, A. *Theoretical and Physical Principles of Organic Reactivity*; Wiley: New York; 1st edn., 1995.

Reisch, R. *Chem. Eng. News* **1993**, *71*, 34.

Renaud, P.; Sibi, M. P. *Radicals in Organic Synthesis*; Wiley: Weinheim; 1st edn., 2001.

Schlegel, H. B. *J. Comp. Chem.* **1982**, *3*, 214.

Scott, A. P.; Radom, L. *J. Phys. Chem.* **1996**, *100*, 16502.

Shaik, S. S.; Canadell, E. *J. Am. Chem. Soc.* **1990**, *112*, 1446.

Speight, J. G. *Lange's Handbook of Chemistry*; McGraw-Hill: NewYork; 16th edn., 2004.

Speybroeck, V. V.; Neck, D. V.; Waroquier, M. *J. Phys. Chem. A* **2002**, *106*, 8945.

Speybroeck, V. V.; Neck, D. V.; Waroquier, M.; Wauters, S.; Saeys, M.; Martin, G. B. *J. Phys. Chem. A* **2001**, *105*, 7713.

Speybroeck, V. V.; Vansteenkiste, P.; Neck, D. V.; Waroquier, M. *Chem. Phys. Lett.* **2005**, *402*, 479.

Sumathi, R.; Carstensen, H.; Green, W. H. *J. Phys. Chem.* **2001**, *105*, 6910.

Tobita, H. *Macromol. Theory Simul.* **1996**, *5*, 129.

Tobita, H. *Macromol. Theory Simul.* **2006**, *15*, 23.

Truhlar, D. G. *J. Comp. Chem.* **1991**, *12(2)*, 266.

Truong, T. N.; Duncan, W. T.; Tirtowidjojo, M. *Phys. Chem. Chem. Phys.* **1999**, *1*, 1061.

Van Cauter, K.; Van Speybroeck, V.; Vansteenkiste, P.; Reyniers, M. F.; Waroquier, M. *Chemphyschem* **2006**, *7*, 131.

Vansteenkiste, P.; Speybroeck, V. V.; Pauwels, E.; Waroquier, M. *Chem. Phys.* **2005**, *314*, 109.

Wigner, E. *Z. Phys. Chem.* **1932**, *19*, 203.

Willemse, R. X.; Herk, A. M.; Panchenko, E.; Junkers, T.; Buback, M. *Macromolecules* **2005**, *38*, 5098.

Wong, M. W.; Pross, A.; Radom, L. *J. Am. Chem. Soc.* **1994**, *116*, 11938.

Wong, M. W.; Radom, L. *J. Phys. Chem.* **1995**, *99*, 8582.

Wong, M. W.; Radom, L. *J. Phys. Chem.* **1998**, *102*, 2237.

Yu, X.; Pfendtner, J.; Broadbelt, L. *J. Phys. Chem. A* **2008**, *submitted*.

Zhao, Y.; Lynch, B. J.; Truhlar, D. *J. Phys. Chem. A* **2004**, *108*, 2715.

Zhao, Y.; Schultz, N. E.; Truhlar, D. *J. Chem. Theory Comput.* **2006**, *2*, 364.

Zhao, Y.; Truhlar, D. G. *J. Phys. Chem. A* **2004**, *108*, 6908.